FINITE ELEMENT MODEL OF MASONRY STRUCTURES ON EXPANSIVE SOILS

by

Zandri Smith

A dissertation submitted in fulfilment of the requirements for the degree

Master of Engineering in Civil Engineering

in the

Department of Civil Engineering

in the

Faculty of Engineering, Built Environment, and Information Technology

at the

Central University of Technology, Free State, South Africa

Supervisor: Prof E Theron

Co-supervisor: Dr P Stott

April 2022

DECLARATION

I, the undersigned, declare that the dissertation hereby submitted by me for the degree *Master of Engineering in Civil Engineering* at the Central University of Technology, Free State, is my own independent work and has not been submitted by me to another university and/or faculty in order to obtain a degree. I further cede copyright of this dissertation in favour of the Central University of Technology, Free State.

Zandri Smith

Signature: 

Date: April 2022

Bloemfontein, South Africa

ABSTRACT

The ancient construction of masonry is still a prominent feature in the industry. Masonry is used particularly as a construction material for homes, schools, offices, and industrial buildings. To ensure that masonry structures are safe, they must comply with the Code of Practice for Unreinforced Masonry (SANS 0164-1:1980 as amended in 1986 and 1987), which states the necessary limitations for masonry design work. Therefore, the SANS devised several tests for different material choices. As these tests are mostly performed on physical structures, they are destructive, time-consuming, labour intensive and can be costly. Thus, alternative methods that will provide equivalent information faster, more accurately and less costly will be advantageous.

This study was thus undertaken to design a finite element model to simulate the behaviour of masonry wall panels subjected to soil deformation so that rational material choices can be made to improve the susceptibility of cracking in masonry. In Phase 1, the material properties of five different mortar mixes were analysed in a controlled environment at the Central University of Technology Free State laboratory. In Phase 2, a finite element model was designed with the Prokon software program and refined using the mesh refinement method. The performance of different mortar material properties was analysed using the designed finite element model.

Three experiments were performed on the five different mortar mixes. Three of the mortar mixes were sourced from the SANS 10164-1, and two from the ASTM C270-1T. The experiments performed included the Young's modulus test, determination of the bond strength test, and the application of the deformation test on physical wall panels. After conducting the experimental tests on the five different mortar mixes, an initial finite element model was designed using the finite element method approach based on mesh refinement. The mesh of the initial finite element model was refined to create five different mesh refinement models, each consisting of a different size mesh. The five mesh refinement models were used to design five finite element wall panels. The dimensions of the finite element wall panels were the same throughout, namely 8 × 10 bricks (1 830 × 790 mm). Theoretical parameters were

assigned to each of the five different finite element wall panels to determine which wall panel supplied the most consistent results pertaining to the maximum and minimum stress in a wall panel, as well as the overall flow of stress. One finite element wall panel with a specified mesh refinement was selected from the five finite element wall panels for the analysis on the performance of different mortar material properties and standard cement brick properties. Each of the different mortar material properties and standard cement brick material properties was applied to the selected finite element model with specified mesh refinement. A deformation of 1 mm was applied to each finite element wall panel to determine the magnitude of stress found in a finite element wall panel designed using a specified mortar mix and standard cement brick properties. The tensile stress in each finite element wall panel was compared to the results of the three experiments performed.

The finite element wall panels showed significant similarity to the experimental wall panels built. The stress distribution through each of the finite element wall panels during the mesh refinement process proceeded to illustrate stress differences among the brick and mortar elements. In the finite element wall panel where the mortar material properties with the least amount of strength was implemented the stress distribution in both the brick and mortar elements was remarkably low. In contrast to this result, the finite element wall panel with the higher mortar material properties of higher strength revealed a higher stress distribution in between the brick and mortar elements. The experimental wall panels that were built showed similar comparisons between the mortar with a high strength and a mortar with a lower strength. The experimental wall panel constructed with the higher strength mortar failed at a lower applied deformation than the experimental wall panel constructed with the mortar with lower compressive strength and higher flexibility.

The results of these tests indicated that a mortar with a lower Young's modulus, combined with a brick of higher strength, showed higher flexibility coefficient and lower stress distribution than a mortar with a higher Young's modulus. Therefore, the use of a flexible mortar would reduce the stress in the wall panel and assist in masonry flexibility.

The designed finite element model could make a significant contribution to the masonry industry in the construction of masonry structures on expansive soils. The finite element model could provide some level of confidence on the effect of masonry constructed on heaving soil, and thus determine the choice of adequate materials in such situations.

ACKNOWLEDGEMENTS

A number of special acknowledgements deserve specific mention:

(a) My warmest gratitude to my supervisor, Prof, E, Theron, and co-supervisor, Dr, P, Stott, for inspiring me to broaden my knowledge in the field of Engineering;
(b) Mr Jonathan Steenkamp and his laboratory assistants working at CivilLab@CUT in the laboratory at the Central University of Technology;
(c) CEM Brick Bloemfontein for their assistance and supply of material;
(d) The Rectorate and relevant functionaries from the Central University of Technology, Free State for the opportunity to complete this research;
(e) The Central University of Technology, Free State for their funding;
(f) My family and colleagues, for their patience and understanding throughout this research; and
(g) My husband, James Smith, and our wonderful children, for their love and support.

Acknowledgement above all to my Heavenly Father for setting my feet on a rock and making my steps secure (Ps. 40).

TABLE OF CONTENTS

LIST OF TABLES

Page

Central University of Technology, Free State

LIST OF FIGURES

Page

LIST OF GRAPHS

LIST OF ABBREVIATIONS

%	Percent
°C	Celsius
δ	Bond Strength
AEM	Applied Element Method
ASTM	American Society for Testing and Materials
b	Breadth of Mortar Beam
b	Length of brick
B	Breadth of Solid Finite Element
CAD	Computer-aided Design
COV	Coefficient of Variation
CL90	Hydrated lime mortar
d	Depth of Mortar Beam
d	*Height of Brick*
d_p	Distance from Pivot to Scale Pan
D	Distance from Piot to Scale Pan
DEM	Discreet Element Method
E	Young's Modulus
FEM	Finite Element Method/Model
GPa	Giga Pascal
h	Overall Height of Pier
I	Moment of Inertia
Kg	Kilogram
kPa	Kilopascal
mm	Millimetre
M	Bending Moment
MPa	Mega Pascal
M6	Cement-lime mortar
l	Ratio of Lime to Cement in a Mortar Mix
L	Length of Mortar Beam
L	Length of Solid Finite Element
L_b	Clear Span of Beam

s	Ratio of Sand to Cement in a Mortar Mix
SABS	South African Bureau of Standards
SANS	South African National Standards
W	Width of Solid Finite Element
W	Weight of scale pan
W_1	Self-weight of Pier between Supports
W_2	Mass of Bricks Applied to Break the Beam
x	Flexibility Coefficient
y	Central Deflection of Mortar Beam
Z	Section Modulus

CHAPTER 1: INTRODUCTION OT THE STUDY

1.1 Introduction

The art of masonry has been practised in the building trade for thousands of years. Masonry became a valuable commodity when humankind sought to supplement their rare natural caves with artificial structures to live in (Encyclopaedia Britannica, 1998b). Masonry is one of the oldest manufactured building materials in the world. It evolved from simple circular stone huts to highly versatile and durable complex multilevel forms of construction. Common materials used for masonry are brick and stone, which include marble granite, and limestone. Concrete and glass bricks are also materials used for the construction of masonry.

Brick masonry consists of brick units bonded together with mortar. Brick masonry is constructed by placing arrangements of bricks and mortar systematically to produce a solid mass that can withstand exerted loads (Gumaste, Nanjunda Rao, Venkatarama Reddy, & Jagadish, 2007). The mortar in brick and masonry acts as a binder that fills the joints between the bricks. When constructing masonry structures, such as homes, schools, offices and industrial buildings, knowledge of masonry materials and construction skills is essential for building success. Therefore, factors such as durability, fire resistance, and appearance of the structure should be considered in brick masonry construction (Hendry, 2001; Kunal, 2016; Singh & Munjal, 2017).

In South Africa, the South African Bureau of Standards (SABS) was founded to offer objective benchmarks to ensure minimum safety limits and performance integrity for manufactured products, including building products. The SABS is responsible for compiling and maintaining all the South African National Standards (SANS) that relate to the building and the construction industry and which have to be adhered to by law. This law is the National Building Regulations, known as the National Building Regulations and Building Standards Act, 1977 (Act No. 103 of 1977). The SANS for building and construction are coded with a suffix number, of which the principal one is the SANS 10400. The Code of Practice for Unreinforced Masonry (SANS 10164-

1:1980 as amended in 1986 and 1987) states the necessary limitations to ensure that design work is carried out systematically by providing certain mandatory functions (SANS 0164: Part 1, 1980). Therefore, the SANS devised several tests for unreinforced masonry to test different material choices. However, these tests are mostly performed on physical structures that are time-consuming, labour intensive and possibly costly (Bui, Limam, Sarhosis, & Hjiaj, 2017; Rodič, 2017).

1.2 Problem Statement

In the SANS 10164-1, a clear indication of the potential compressive and shear strength of masonry is provided. However, it does not provide sufficient knowledge for material choices in the event when a wall panel is subjected to soil deformation caused by heaving clay. In the building standards, to select a suitable material, the focus is set more on the strength of the materials subjected to compression than the flexibility of the masonry as a unit. Masonry flexibility goes hand in hand with the shear strength and bond strength of the masonry. Material selection for masonry to be able to flex as the soil deforms differs immensely from that of the material choice for masonry to withstand uniform compression.

1.3 Aim and Objectives

With the latest advances in technology and computer software, several computer simulation programs have been developed to model real phenomena using a set of numerical and mathematical formulas and models. Simulation software is widely used to design specific products so that the outcome will be as close as possible to design specifications without expensive modifications. In the current industry, simulation software programs for testing and analyses on structural design and material properties are still at the start of its development. It is anticipated that these simulation tests would be far less time consuming, non-destructive, less labour intensive and cheaper (Bui et al., 2017; Rodič, 2017). These simulations would also offer a better understanding of material choice and their responses to viable alternatives to physical experiments (Abdulla, Cunningham, & Gillie, 2017).

Therefore, this study was undertaken to design a finite element model that would simulate soil deformation caused by heaving clay, on experimental masonry wall panels to assess the material choices to improve the flexibility of masonry wall panels and their susceptibility to cracking.

To meet this aim, the following objectives were devised:

1. To examine and analyse the material properties of various different mortar mixes;
2. To construct experimental wall panels using the various mortar mixes for the determination of flexibility in brickwork; and
3. To design a finite element model of the experimental wall panels, simulating deformations comparable to those caused by heaving clay.

1.4 Significance of this Study

The design of a finite element model that simulates the performance of masonry wall panels subjected to soil deformation has the potential to make a significant contribution to the light masonry construction industry. Knowledge generated by such simulations could provide information about material choices when constructing light masonry assemblies. Such choices include which SANS-approved brick and mortar combinations should be implemented when designing a particular light masonry assembly subjected to expansive clay.

CHAPTER 2: LITERATURE REVIEW

2.1 Introduction

Masonry is one of the oldest and most widespread structural materials. As building material, masonry is a common and traditional form of construction that has been used globally for thousands of years (Abdulla et al., 2017; Bui et al., 2017; Pirsaheb, Moradi, & Molani, 2020). In the past, the most common materials used in masonry were brick and stone. Some of the most important cultural and historical monuments were masonry structures, such as the Parthenon, the pyramids, and the Colosseum. Early masonry was constructed without mortar and principally designed to resist gravity loads (Bui et al., 2017; Gabor, Ferrier, Jacquelin & Hamelin, 2006). Many of the ancient masonry constructions were on estates or property belonging to a church or other institution (Gabor et al., 2006).

Today, masonry is still used for various construction purposes. It is used as a construction material in a wide variety of structures ranging from large buildings, residential properties, parking structures, bridges, and dams (Thompson, 2008). Because masonry tends to deteriorate over time, there is a continual need to evaluate and repair such structures.

During the past three decades, substantial advancements have been achieved in knowledge of the mechanical behaviour of masonry. This knowledge has been gathered through laboratory tests producing large volumes of experimental data (Parisi & Augenti, 2012). These data are currently used in various modelling approaches of masonry constructions based either on elasto-plastic finite element techniques, or on simplified macro-element approaches.

Since the second decade of the 21st century, masonry unit manufacturing in South Africa has declined. However, despite this decline, major brick manufacturers report increasing demands for residential properties (Research and Markets, 2019). While industry output has remained relatively constant since 2014 at approximately 3.6 billion standard brick equivalents, the industry continues to contract and concentrate. Seasonally adjusted manufacturing production in South Africa decreased by 0,1% in December 2020, compared with November 2020 (Stats SA, 2020).

2.2 History of Masonry

The art and craft of masonry has been practised for thousands of years. After more than 6,000 years, this practice is still in use today (Building Solutions, 2015; Shakir & Mohammed, 2013; Veazey, 2010). This art is one of the oldest of the skilled trades practised on the planet and dates back to the use of sun-baked clay bricks (Hallissey, 2018). People in these early times sought to supplement their rare naturally occurring caves with artificial structures created from piles of stone and earth (Encyclopaedia Britannica, 1998; Fix My Brick, 2018).

In the early days, simple bricks were used for the construction of dwellings to live in. Initially, sun-baked clay bricks were used; however, these bricks tended to crack and distort. To prevent cracking and distortion of the clay shapes, chopped straw, dung or grass were added to the clay mixture and then left to bake in the sun (Colefield, 2018; Veazey, 2010). In Africa and Asia, the oldest masonry was made of stone and earth (Maldonado, Martin, del Sol, & Domizio, 2016). Over time, brick construction became more elaborate and more sophisticated (Veazey, 2010). Around 4,000 BCE, brick production was enhanced by producing bricks of uniform shapes. As time progressed, bricks were cut into specific shapes and later simple moulds were introduced into the production process (Colefield, 2018). Along with the shaping of bricks, around 3,500 BCE firing bricks in kilns began to replace sunbaking as a manufacturing method. Baking improved the durability of the bricks. The production of bricks was no longer dependent on the time of the year when it was warm. At this time, the mobile kilns of the Roman Empire that were used in brickmaking were introduced throughout the ancient world. However, the detailed material properties of which the walls were built were not well known or reliably consistent (Haseltine, 2012). This evolution in brick design made a significant contribution to the development of concrete bricks of modern times.

The brick industry had begun its rise in the late 17th century with the mass production of bricks. Mass production came about when people recognised the strength, durability, and versatility of manufactured bricks (Colefield, 2018). According to record, the earliest manufactured brick was found in Virginia in the Unites States of America (USA). Manufactured bricks are one of the world's oldest manufactured products. One of the first brick mass production facilities was in Albany, New York. Many brick buildings constructed during colonial times are still around today. Examples are the Tyron Palace in North Carolina and the Independence Hall in Philadelphia.

In the early days of masonry construction, naturally occurring materials, as well as manually manufactured units that were joined with fresh mortar were used. Mortar has been used since the prehistoric times (Moayedian & Hejazi, 2021). Some mortars have survived for many thousands of years (Lancaster LimeWorks, 2020). Since the 8th millennium BCE, structural mud-mortars in rubble and adobe masonry, made of earth mixed with water and organic material, were used in Mesopotamia and Babylonia (Pachta et al., 2014). The invention of the use of mortar to fill the gaps between bricks is evident from the buildings of the early Egyptian civilisation to the present day (Haseltine, 2012; The Concrete Center, 2010). Usually, mud-mortars were manufactured near the construction site. Often clay was mixed with organic and inorganic additives to increase mass stability and durability. Organic additives that were used include herbs, roots, straw, and reeds, while sand gravel was added as an inorganic additive.

Over time, buildings constructed of manufactured bricks experienced leaks, which led to the development of cavity walls. Cavity walls consist of at least two single brick walls, with an approximate 5 cm void between the walls (Maas, 2013; Veazey, 2010). Moisture penetrating the first brick wall could thus escape through the void by running down the inside of the outer wall, while the inside wall remained dry. In 1850, these voids between the brick walls became the inspiration for a brick with pre-developed voids (Colefield, 2018; London Damp Company, 2018).

Some of the world's most notable building treasures are masonry constructions. The Egyptian pyramids were built to endure for eternity. A few examples of architectural achievements built with masonry include the Roman stone amphitheatre known as the Colosseum, India's Taj Mahal and the Great Wall of China (Bui et al., 2017; Drougkas et al., 2015; Veazey, 2010; Wahby, 2004). The Colosseum is located just east of the Roman Forum in the centre of the city of Rome. Emperor Vespasian of the Flavian dynasty commissioned this immense stone amphitheatre as a gift to the Roman people around 70 to 72 CE (A & E Television Networks, 2019; Cartwright, 2018). The Taj Mahal is an enormous mausoleum complex commissioned in 1632 by the Mughal emperor Shah Jahan to house the remains of his beloved wife. It was constructed over a period of 20 years on the southern bank of the Yamuna River in Agra, India (UNESCO, n.d.; Walker & Swinney, 2011). The Great Wall of China is in northern China and is an ancient series of walls and fortifications totalling more than 20,000 kilometres. The Great Wall was originally conceived by Emperor Qin Shi Huang in the third century BCE as a means of preventing incursions from barbarian nomads (Mark, 2015; Onion et al., 2019).

2.3 Modern Perspective of Masonry

Over the many years of its existence, masonry has been modified and improved. Unreinforced brick masonry is a composite material that consists of two basic materials. Brick masonry materials consist of masonry units as well as bricks assembled in a specified arrangement and bonded with mortar (Apostolaki et al., 2009; Lakshani et al., 2020; Lourenço, 1998). Structural walls are mainly designed to resist gravity loads; therefore, the strength of brick masonry walls is dependent on the strength of both brick and mortar used for construction (Murthi, Akib, et al., 2021).

Using brick masonry in wall construction has several advantages and can fulfil a number of functions. These functions include providing structure, fire protection, thermal and moisture movement, sound insulation, weather protection and sub-division of space (Hendry, 2001; Kunal, 2016; Singh & Munjal, 2017). Overall, the behaviour of brick masonry is dependent on several factors. The most important of these factors include the specific properties of brick and mortar, the characteristics of the mortar bond between bricks, and the workmanship (Apostolaki et al., 2009; Hendry, 2001; Lawrence et al., 2008). Brick masonry is also a durable material with serviceability that can last for decades and even centuries. The rapid advancements of technological innovations have made significant contributions to the overall quality of brick masonry products (Brick Industry Association, 2006). A better understanding of raw materials and their properties, better control of firing, improved kiln designs and more advanced mechanisation have all contributed to advancing the masonry industry. Despite the displacement of brick masonry application by steel in the 20th century, brick masonry remains of great importance for load-bearing walls in low and medium-rise buildings (Hendry, 2001).

2.3.1 Masonry brick component

Fundamental brick manufacturing has remained largely the same since the rise of the mass production of bricks. Although the basic principles of brick manufacturing are uniform, individual manufacturing plants adapt their production to fit their raw materials for the building operations that they serve (Brick Industry Association, 2006). The composition of raw materials and their specific manufacturing processes affect all properties of bricks (Mineral Economics, 2008; N. Sharma, Telang, & Rath, 2017). The durability of bricks depends upon the achievement of incipient fusion and partial vitrification during firing in manufacturing. Furthermore, important predictors of brick durability in brick specifications include compressive strength, absorption values, firing temperatures and saturation coefficient.

Current manufacturing processes of brick are similar in scope to those used for the past 3,500 years. Brick is the non-elastic building component of masonry, which provides resistance to compressive forces; therefore, the compressive strength of masonry is important (Murthi, Bhavani, et al., 2021; Ventra, 1998). Bricks are produced from various raw materials of which clay, concrete and calcium silicate are the most used (Hendry, 2001). In the masonry industry, several different types of brick are used in construction. Clay is one of the most abundant natural mineral materials on earth. It possesses some specific properties and characteristics that make it a suitable raw material for brick manufacturing. It has plasticity which permits it to be shaped or moulded when mixed with water and it has sufficient wet and air-dried strength to maintain its shape after forming (Brick Industry Association, 2006). Also, after subjection to firing, clay particles fuse to produce a highly durable product. Concrete bricks are made by blending Portland cement, sand, and other aggregates with a small amount of water, then blowing the mixture into moulds (Shakir & Mohammed, 2013). After a set period in a kiln or autoclave to cure, the bricks are removed from the moulds. Calcium silicate bricks are made from a high-grade sand or crushed flint which is mixed with 5 to 8% hydrated lime, containing a high percentage calcium, and water. This mixture is then placed in moulds, after which the moulds are autoclaved under pressure at steam atmosphere for three to eight hours.

Hollow blocks are also becoming a popular product in the masonry world. These blocks have environmentally friendly characteristics because of their low heat dissipation and less raw material usage owing to the presence of cavities in a block (J. Wu, Bai, Zhao, & Li, 2015). The thermal resistance of hollow bricks can be increased by the addition of insulation material, which can either be added to the masonry material brick mix or added as filling insulation material into the holes of masonry bricks (Al-Hadhrami & Ahmad, 2009).

In the Western countries, brick masonry generally consists of bricks which are relatively strong and stiff as compared to the mortar adopted. These bricks have compressive strengths ranging from 15 to 150 MPa with an elastic modulus between 3,500 and 34,000 MPa. In India, studies performed on bricks provided results that showed a relatively lower brick strength ranging from 3 to 20 MPa and an elastic modulus of 300 to 15,000 MPa (Gumaste et al., 2007).

2.3.2 Masonry mortar component

Mortar contributes substantially to the strength and durability characteristics of masonry structures. The earliest mortar types that were used in masonry construction contained lime (Murthi, Akib, et al., 2021). Later, the lime mortar was replaced with cement and thus the usage of lime gradually vanished because cement-based mortar demonstrated greater strength properties than lime mortar (Costigan et al., 2009).

Thereafter, blended cement mortar and masonry mortar containing different amounts of cement were developed for masonry. The strength of the brick-mortar bond is attributed to the mechanical inter-locking of cement hydration products into the surface pores of the bricks.

The quality, strength and durability characteristics of brick masonry mortar is usually determined by its unconfined compressive strength. A study was conducted to evaluate the strength variation of brick masonry using three mortar mixes containing different supplementary cementitious materials applied at 12 and 18 mm thickness (Murthi, Akib, et al., 2021). The supplementary cementitious materials used in this study included dolomite powder and silica fume. In the compressive strength test performed on masonry prisms, it was discovered that the strength of the supplementary cementitious material mortar blend demonstrated a 25% increased strength when compared to the cement mortar. Furthermore, it was also concluded that the shear bond strength of brick masonry is mostly influenced by the brick strength and mortar strength and less by the mortar thickness. In another experiment, the ratio of the mortar thickness was compared to the bond area on a masonry brick; it was found that mortar strengths were equally important to brick strength (J. Wu et al., 2015).

When selecting mortar for a particular construction, the binding properties of the mortar are a major consideration. These binding properties are thus often used to classify different types of mortar. Therefore, each type of mortar has specific characteristics that should be considered for particular construction projects. Mortar can also be categorised by the specific application it is being used for (Cuffari, 2019; Gupta, 2018). Bricklaying mortar is used to bind bricks, stones, and concrete blocks, while finishing mortar is used for construction projects that require plastering, as well as an aesthetically pleasing appearance to the structure. In the application of finishing mortar, binding materials such as lime and/or cement are often included to increase the strength and mobility of the plaster. The inclusion of such binding materials also improves a structure's resistance to damaging environmental conditions, such as extensive rain and wind.

2.4 Brick Masonry Properties

Brick masonry is an assemblage of bricks bonded into an integral mass by mortar. This assemblage of brick and mortar is described as being orthotropic, inelastic and non-homogenous (Asteris & Tzamtzis, 2015; Bui et al., 2019; Singh & Munjal, 2017). The combination of materials of a masonry structure determines the performance of the masonry as a structural element (Costigan, Pavía, & Kinnane, 2015a; F. Wu, Gang, Hong-Nan, & Jin-Qing, 2013). Thus, when considering a brick masonry project, it is important to consider first the properties of the constituent materials and thereafter the behaviour of their combination in the masonry element.

The strength of brick masonry is mainly influenced by the compressive and bond strength of bricks and mortar. Masonry compressive strength is dependent on brick strength, while mortar type influences the bond strength of the brick masonry (Agarwal et al., 2021; Gumaste et al., 2007; Prasad et al., 2014). Brick masonry prism tests have revealed that masonry compressive strength increases as the bond strength between the brick and mortar increases (Costigan et al., 2009; Yang et al., 2019). However, an increase in compressive strength does not lead to an increase in brick masonry compressive strength. The shear strength of mortar joints in unreinforced masonry also plays an important role in the in-plane lateral load resistance of walls (Dizhur et al., 2015; S. Sharma et al., 2021). In tests with prisms constructed of concrete masonry blocks of 11 MPa, it was found that the average compressive strength of the unreinforced concrete block masonry resulted in a compressive strength of 8.25 MPa, whereas the reinforced concrete block masonry prism showed a marginal 3% increase (Agarwal et al., 2021; Nalon et al., 2020).

The reinforcement of brick masonry increases the compressive strength of a masonry structure. For example, when mortar of 1:2:8 cement lime mortar was tested with different shapes of horizontal reinforcements, the mesh reinforcement placed in bed joints increased the compressive strength by 24% in piers built with the limestone brick (Del Zoppo et al., 2020; Oliveira et al., 2018). Reinforced brick masonry is also used in lintels and retaining walls of basements and fences. Such reinforced brick masonry can withstand out-of-plane bending exerted by wind, earthquakes, or earth pressures and eccentric loads or direct loading because of gravity (Lotfy et al., 2015).

The bond strength of brick masonry is a measure of the strength of the bond between masonry units and mortar. This bond determines the potential of brick masonry to resist movement from applied stress caused by lateral or eccentric loads (Bergami & Nuti, 2015; Shadlou et al., 2020). The property of brick masonry to resist movement from applied stress is of particular importance in low-rise domestic and commercial buildings (Association of Australia, 2001; Page, 2012; Singh & Munjal, 2017; Thamboo et al., 2013). Other factors that can also influence the bond strength of brick masonry include the surface texture type of the masonry units, size of pores, porosity, and pore size distribution (Lawrence et al., 2008; Resketi & Toufigh, 2019; Venkatarama Reddy & Uday Vyas, 2008).

When the bond strength between masonry units and mortar is inadequate, it may lead to failure of the structure due to a low shear resistance, which could cause cracking in the masonry structure (Gabor et al., 2006; Thamboo et al., 2013). The expansion of mortar in masonry specimens due to shear tests is known as dilatancy (Andreotti et al., 2019; Parisi & Augenti, 2012). Cracking in masonry is considered as a brittle mode of failure that can cause widespread damage to any masonry structure (Association of Australia, 2001). In a study where the performance of polymer mortar in brick masonry prisms was compared to that of the traditional mortar type, the flexural and shear bond strength of the polymer mortar was consistently higher than that of the traditional masonry (Thamboo et al., 2013). The polymer mortar in the brick masonry prisms presented a flexural tensile strength as high as 50% more than its compressive strength. It was further found in this study that smooth-textured masonry units demonstrated higher bond strength when compared to the rougher surface units. Other factors that also influence the bond strength of brick masonry include interfacial bond strength between brick and mortar, moisture in the brick at the time of laying, thickness of mortar joints, arrangement of bricks, as well as workmanship.

2.5 Computer Simulation in the Building Trade

The Fourth Industrial Revolution (4IR) is evolving at an exponential rate, rather than at a linear rate as was experienced in the prior industrial revolutions. Industrial automation is transforming the ‘what’ and the ‘how’ manufacturers do things (Goossens, 2017). Thus, manufacturers can no longer afford the ‘build it and tweak it’ approach that has been the standard way in many businesses (Rodič, 2017). This revolution has brought about an unstoppable shift from simple digitisation that characterised the Third Industrial Revolution (TIR) to innovation-based combinations of technologies, which characterise the 4IR. This has resulted in complex and multi-disciplinary systems (Goossens, 2017). The most prominent change occurring in the 4IR is the automation of processes across all industries, thereby reshaping production, consumption, transportation and many other systems (Rodič, 2017). In addition, the building trade has been forced to re-examine the way they do business. One of the approaches is to implement simulation modelling to help reduce costs, shorten development cycles, increase the quality of products, and greatly facilitate knowledge management (Rodič, 2017).

Recent advances in computation simulation, as well as the increased capability of modern computers, have brought about the development of a substantial inventory of numerical methods for masonry structure analysis. In masonry computation simulation, the choice of numerical method is dependent on the purpose of the intended structural analysis, the complexity and scale of the structure, as well as the available resources (Saloustros et al., 2017). Available computer simulation software programs have been developed for the precise modelling of masonry structures, while still keeping the use of the software simple enough to be used by professional engineers (Ahmed & Shahzada, 2020). The software program ANSYS (Qfinsoft) was developed by engineers in the 1970’s to develop, market and support engineering simulation software to predict how product designs will behave in the real-world environment (ANSYS, 1970). LS-DYNA is an extension of ANSYS, which is a general-purpose finite element program that is capable of simulating complex real-world problems (LS-DYNA, n.d.).

Abaqus Unified FEA, founded in 1985 (Dassault Systems, 2013), offers a powerful and complete solution for both routine and sophisticated engineering problems covering a vast spectrum of industrial applications ranging from construction to automotive engineering (Dassault Systems, 2013). The Advanced Tool for Engineering Non-linear Analysis software known as ATENA (Cervenka Consulting) was also developed to simulate real-world behaviour of concrete and reinforced concrete structures, including concrete cracking, crushing and reinforcement yielding (Cervenka Consulting, n.d.).

The University of Montpellier developed the open-source software program in the Mechanical and Civil Engineering Laboratory (LMGC), which is dedicated to large object collection interactions and implements the properties of the finite element method (MiMeTICS Engineering, n.d.). Prokon is an analysis software program that was developed in 1989 in South Africa by Eschberger and Pienaar (Eschberger & Pienaar, 1989). This program has the capabilities to simulate a wide variety of components, for example, the structural analysis component, which is one of the 40 design components that is used to determine the effects of loads on physical structures and their components. DIANA FEA BV, previously TNO DIANA BV, was established in 2003 as a spin-off company from the Computational Mechanics department of TNO Building and Construction Research Institute in Delft, the Netherlands. The company provides world-class software products and services in the field of finite element solutions dedicated to civil, geotechnical, earthquake, and petroleum engineering (DIANA FEA BV, 2003).

Today, in simulation modelling, numerical models offer a viable alternative to the physical world and physical experiments. In essence, a numerical model is a theoretic model composed of numbers that is a representation of a real-world system. A real-world situation is described by mathematical formulations which can be analysed by computational methods (Abdulla et al., 2017). Four main numerical methods are employed in numerical models to simulate linear and non-linear behaviour of masonry. These numerical methods are the finite element method (FEM), the discrete element method (DEM), the limit analysis method (LAM) and the applied element method (AEM).

2.5.1 Finite element method

In the finite element method (FEM), finite elements and their connection points, known as nodes, are represented geometrically. These components represent the building blocks of the numerical representation of a model. In contrast to a theoretical model that encompasses complete continuity, the elements in the FEM are a finite number (Dinesh et al., 2015). A modelled object is broken up into a 'meshwork/mesh' that consists of several nodes that are on and in the object. These nodes are connected to form a system of elements. For example, if a brick wall is the network, the bricks are the elements and the four corners where the brick elements meet are the 'nodes.

In masonry, the FEM is based on two main modelling approaches. These approaches are micro-modelling and macro-modelling (Abdulla et al., 2017; Eslami et al., 2012). In the micro-model approach, the simulation details the brick and mortar as continuum elements, while the brick-mortar interfaces are modelled as discontinuum elements (Bui et al., 2017). Because the micro-model is computationally intensive, it is limited to simulating relatively small masonry elements, but does permit a refined analysis (Gabor et al., 2006). The FEM has been successfully applied to the mechanical study of stress and strain in the field of engineering. It is mainly a method for numerical analysis based on material properties (Dinesh et al., 2015). For example, a 2-D finite element based micro-modelling framework was presented for thermo-mechanical response history analysis of solid brick masonry structures subjected to fire (Prakash et al., 2020). It was observed that thermal bowing resulted from a complex interaction between thermal dilation and cracking and crushing in the mortar and brick unit within the masonry structure. In South Africa investigations are currently underway in which the FEM is applied to investigate the performance of low-cost alternative masonry units (AMU's) for their potential to be taken up in the South African construction industry (De Villiers et al., 2019).

In contrast to micro-modelling, the macro-model approach considers the object as homogenous material. In masonry, macro-modelling does not distinguish between brick and mortar (Abdulla et al., 2017). Material properties are obtained from the average properties of the masonry constituents, after which the masonry is modelled as a series of continuum elements. Finite element macro-modelling approaches are widely used for the analysis of large-scale masonry structures (Saloustros et al., 2017). For example, the macro-model approach was used to define the performance of a 500-year-old church in Cusco, Peru under different seismic scenarios (Aguilar et al., 2019). The finite element software program DIANA TNO was used to estimate the global behaviour and possible damage patterns in the church during seismic events.

2.5.2 Discrete element method

The discrete element method (DEM) is a widely used particle scale approach for simulating granular dynamics. This method treats each particle of a granular bed individually by representing the shape and size of each particle and how it interacts with other particles (Luo et al., 2017). The particle interactions are at the heart of the DEM implementation, and they are captured through different user-specified material properties. In masonry the DEM was employed by modelling bricks as a continuum of rigid elements, while the joints were modelled by line interface elements represented by the Mohr-Coulomb law (Bui et al., 2017). After the application of loads, crack development could be successfully demonstrated. The DEM was applied to predict the mechanical behaviour of modern brickwork and concrete block masonry wall panels subjected to in- and out-of-plane loading (Bui et al., 2019). The software program DEC3 facilitated the prediction of the development and propagation of cracks in the wall panels up until collapse. In another example, DEM was used to investigate the dynamic behaviour of non-standard, curvilinear masonry geometries, such as historical and monumental vaults subjected to blast loading. The results of this investigation gave insight into the selection of appropriate numerical methods based on continuum mechanics in the investigation of large masonry structures of non-standard geometries.

2.5.3 Limit analysis method

The limited analysis method is dedicated to structural analysis. The field of limit analysis is based on a set of theorems, referred to as limit theorems. The theorems are based on the law of conservation of energy that states the properties of stresses and strains, lower and upper bound limits for the collapse load and the exact collapse load. The basis of limit analysis rests upon two theorems which can be proved mathematically. The lower bound theorem states that any stress system in which the applied forces are just sufficient to cause yielding is a lower bound, while the upper bound states that any velocity field that can operate under maximum load is known as an upper bound. Kooharian and Heyman (Nodargi & Bisegna, 2020) showed that when attempting to preseve architectural heritage and historical buildings, the structural analysis of masonry structures is a critical challenge and should address accurate structural safety assessments, while considering the necessary repair/strengthening interventions. They achieved this by applying the limit analysis theory under the assumptions of negligible elastic strains, infinite compressive strength, vanishing tensile strength, and no-sliding condition for the masonry material.

2.5.4 Applied element method

The applied element method (AEM) is a relatively new method of analysis that combines traits of both the FEM and the DEM. It is a numerical analysis method that is used for the prediction of the continuum and discrete behaviour of structures. When applying this method, it is possible to simulate the behaviour of structures from zero loading to collapse, as well as modelling large displacements and separations of structural elements (AEM, 2018). The main advantage of the AEM is that it can be used to track the structural collapse behaviour passing through all stages of the application of loads. When applying the AEM, a structural member is divided into virtual elements, which are connected through normal and shear springs representing stresses and strains within the structure (Gohel et al., 2013). In 2018, a portion of the highway connection viaduct over the Polcevera Valley in Genoa, Italy collapsed, resulting in 43 deaths and many injuries. The AEM was applied to evaluate the structural response of the bridge by modelling the progressive reduction of the strength capacity of single macro-components (Domaneschi et al., 2020). The results of the analyses revealed that the stay cable was the most critical element, the failure of which would have triggered the collapse.

2.6 Modelling in FEM

The FEM is a widely used method for solving numerical differential equations in engineering and in mathematical modelling. Engineers and scientists use finite element analysis (FEA) software to build predictive computational models of real-world scenarios (Multiphysics Cyclopedia, 2016). The FEM begin with a computer-aided design (CAD) model that represents the physical parts being simulated, as well as knowledge of the material properties and the applied loads and constraints. This information enables the prediction of real-world behaviour, often with very high levels of accuracy. The FEA software is then used to subdivide the CAD model into smaller parts, called finite elements. The sub-division of the CAD model is achieved through space discretisation by constructing a mesh of the model, which has a finite number of nodes. Discretisation is the first step towards solving the problem and involves transferring continuous functions, models, variables, and equations into the discrete finite elements. Thereafter, a system of algebraic equations is formulated through the FEM method. The FEM then uses numerous methods from the calculus of variations to approximate a solution by minimising an associated error discretisation function. The solution of the FEM is by its nature an approximation and only assures that equilibrium is satisfied, on average, over an element and not over any smaller volume than a complete element (Matthews et al., 2000). If the mesh size is decreased, the equilibrium will be satisfied over smaller and smaller patches. Thus, when using the FEA software in designing a mesh, it should deliver results of acceptable accuracy, but should have a mesh density that is not prohibitively expensive to run. The fineness of the mesh can be important for linear static problems but is especially important for the analysis of non-linear and dynamic problems.

Mesh refinement is an important method for editing finite element meshes to increase the accuracy of a solution to a problem. Refinement is performed in an iterative manner in which a solution is found, error estimates are calculated, and elements in regions of high error are refined (Staten & J, 1997). Several strategies are followed in mesh refinement. Element size reduction is the easiest mesh refinement strategy carried out by reducing element sizes throughout the model (Multiphysics Cyclopaedia, 2016). The advantage of this approach lies in its application simplicity; however, the drawback is that there is no preferential mesh refinement in regions where a locally finer mesh may be needed. Other strategies include the increase of element order, global adaptive mesh refinement, and time-domain and frequency-domain meshing (Multiphysics Cyclopaedia, 2016). In mesh refinement, one strategy may converge much faster than others and is dependent on a particular problem to be solved.

2.7 Code of Practice

Masonry standard code of practice is regulated worldwide by various masonry standards. These masonry standards are instrumental in specifying, testing, and evaluating the basic units and materials used in masonry construction. These standards are also used to guide manufacturers, construction companies, architectural firms, and other producers in the proper use of materials and manufacturing. The standards are for materials such as mortar, tiles, bricks, cement, aggregates, clay, concrete, fibre, and possible mixtures thereof that are used in conjunction with the erection of building structures.

Code of practice for masonry internationally

In the USA, the American Society for Testing and Materials (ASTM) developed an international standard for masonry units for testing and materials. The ASTM C1825-19 standard guide provides general guidance about specifications for masonry units manufactured with constituent materials, manufacturing methods, and combinations thereof. This standard guide was developed in accordance with internationally recognised principles on standardisation established in the Decision on Principles for the Development of International Standards, Guides and Recommendations issued by the World Trade Organisation Technical Barriers to Trade (TBT) Committee. Within the ASTM C1825-19 standard guide, reference is made to 15 different applicable masonry standards developed in America for masonry structures (ASTM C1825-19, n.d.).

In contrast, the standards in Australia are voluntary documents that set out specifications, procedures and guidelines that aim to ensure that products, services, and systems are safe, consistent, and reliable (Australian Standards: BD-004, 2020). There is no requirement for the public to comply with these standards. However, State and Commonwealth governments often refer to Australian Standards® or joint Australian/New Zealand Standards in their legislation. They cover a variety of subjects, including consumer products and services, the environment, construction, energy and water utilities. These standards are also regularly reviewed by Standards Australia technical committees and consist of three categories, namely International Standards, Regional Standards, and the National Standards. For masonry, Australia has developed four different standards. For the member states of the European Division (ED) and European Free Trade Association (EFTA) in Europe, the Eurocodes serve as reference documents for compliance of building and civil engineering works. Eurocode 6 applies to the design of buildings and civil engineering works, or parts thereof, in unreinforced, reinforced, pre-stressed and confined masonry. In Eurocode 6, reference is made to 32 different standards that pertain to masonry constructed in Europe (European Union, 2011).

Code of practice for masonry in South Africa

In South Africa, the South African Bureau of Standards (SABS) is the statutory body which offers objective benchmarks to ensure minimum safety limits and performance integrity for manufactured products, including building. The SABS is responsible for compiling and maintaining a collection of different standards, known as the South African National Standards (SANS) that pertain particularly to the building and the construction industry. These Standards must be adhered to by the National Building Regulations, known as the National Building Regulations and Building Standards Act, 1977 (Act No. 103 of 1977). The SANS for building and construction are coded with a suffix number, of which the principal one is the SANS 10400 (SANS 10400, 1990). The respective standards that relate to building and construction are listed and described in Table 2.1.

Table 2.1: Applicable standards to masonry constructed in South Africa (SANS Edu, 2019)

Standard reference	Standard description
BS 1243	Specification for metal ties for cavity wall construction
SANS 28	Metal ties for cavity walls
SANS 48	Refractory bricks
SANS 227	Burnt clay masonry units
SANS 285	Calcium silicate masonry units
SANS 523	Limes for use in building
SANS 1090	Sand for plaster and mortar
SANS 1215	Concrete masonry units
SANS 0100	Structural use of concrete Part 2: Materials and execution of work
SANS 0137	The installation of glazing materials in buildings
SANS 0145	Concrete masonry construction
SANS 0160	General procedures and loadings to be adopted for the design of buildings
SANS 0161	The design of foundations for buildings
SANS 0162	The structural use of steel
SANS 0163	The design of timber structures
SANS 0164	The structural use of masonry
SANS 10400-B	The application of the National Building Regulations, Structural design
SANS 10400-K	The application of the National Building Regulations, Walls
SANS 50771-3	Aggregate concrete masonry units (dense and light-weight aggregates)
SANS 50771-4	Autoclaved aerated concrete masonry units
SANS 51996-1	Design of masonry structures, general rules for reinforced and unreinforced masonry structures
SANS 51996-2	Design of masonry structures, design considerations, selection of materials and execution of masonry
SANS 51996-3	Design of masonry structures, simplified calculation methods for unreinforced masonry structures

In the regulation to maintain safety in masonry construction, several tests need to be performed. Three of the masonry standards describe several tests specified by the National Standards for masonry for brick masonry and brick masonry components. These tests relate to unreinforced masonry, concrete masonry and burnt clay masonry. Table 2.2 lists the standards mostly applicable to brick masonry and brick masonry components and the number of tests described in each of the standards.

Table 2.2: South African Standards that relate to tests for brick masonry and brick masonry components

Standard reference	Standard description	Scope	Number of tests
SANS 10164: Part 1-1980	Unreinforced masonry walling	This part of the code of practice covers recommendations and requirements for the design of unreinforced loadbearing masonry walling erected din areas other than those where earthquakes may be encountered.	9
SANS 1215:2008	Concrete masonry units	This specification covers precast solid and precast hollow concrete masonry units for use in walling.	4
SANS 227:2007	Burnt clay masonry units	This specification covers clay masonry units for use in walling.	6
SANS 285:2010	Calcium silicate masonry units	This specification covers calcium silicate masonry units for use in walling	5

The SANS 10164-1 specifies several tests for unreinforced masonry to ensure safe and optimal masonry structures. Unreinforced masonry relates to an arrangement of bricks, bonded together with mortar without the use of reinforcement in the bed joints. Table 2.3 lists and describes the various tests specified by SANS 10164-1 for unreinforced masonry.

Table 2.3: Description of South African tests for unreinforced masonry walling which are part of the SANS 10164: Part 1-1980

Test	General instructions for test
1. Preliminary (laboratory) mortar tests	At least six weeks before the commencement of construction work on site, determine (in the laboratory) the strength of the mortar for each class proposed for use on the project, using materials from the sources from which the site will be supplied.
2. Works mortar tests	Prior to commencement of construction agreement must be reached between the testing authority and the contractor as to the frequency of sampling and testing and the number of cubes to be made and tested, which should not be less than three for any particular sample.
3. Determination of characteristic compressive strength of masonry	Obtain the characteristic compressive strength for masonry (f_k) from the ultimate strength of a brickwork or blockwork panel tested to destruction in accordance with this section. Modifications to the test results may be necessary, depending on the compressive strength of the structural units and of the mortar used for the test panel.

Test	General instructions for test
4. Determination of characteristic flexural strength of masonry	As an alternative to or in the absence of characteristic flexural strength data as given, characteristic values for the two orthogonal directions may be determined by the testing of wallettes built of the requisite bricks or blocks and mortar.
5. Determination of water absorption of clay bricks	The water absorption in clay bricks is determined through two alternative standard methods.
6. Determination of initial rate of absorption	The initial rate at which a brick absorbs moisture is determined.
7. Determination of bond strength of brickwork	Check the bond strength between bricks and mortar by means of a bending test carried out on piers tested as beams supported at the two ends and loaded at the centre.
8. Determination of flexural bond strength of damp-proof courses	Flexural strength at the damp-proof (d.p.c.) course should only be considered reliable if the material of the d.p.c. has a proven ability to transmit tension between the courses above and below it. The following is a method to verify such property.
9. Determination of short-term shear strength at damp-proof courses	The short-term shear at a damp-proof course varies considerably depending on the material used. The following is a means of determining the short-term shear strength of brickwork at the damp-proof course.

2.8 Masonry in South Africa

2.8.1 Background

Masonry is an accepted, and one of the most traditional forms of light masonry construction in South Africa. After the Second World War, the demand for small low-cost light masonry structures in South Africa became eminent. These structures would have had to be constructed on limited financial resources, but still have all the important structural performance aspects such as strength, stability, robustness, durability, and serviceability. Unfortunately, in the construction of these small light masonry structures where minimum structural performance criteria were established, the engineers' tendency to structurally over-design with wasteful expenditure or overlooking local materials with unknown performance characteristics started to rise (Crofts & Lane, 2000).

The South African Institution of Civil Engineering (SAICE) developed a series of National Standards, SANS 1200 (Standardised Specifications for Civil Engineering Construction) and SANS 0120 (Code of Practice for use with Standardised

Specifications for Civil Engineering and Contract Documents), in the late 1970s and early 1980s. The SANS 1200 and SANS 0120 was handed over to the SABS to publish and maintain. These two series stagnated and were not further developed to keep up with the current technological advanced practices, procedures, materials and methods since their publications (Watermeyer, 2016). The SANS 1200 was then withdrawn and replaced with the SANS 2001. The current SANS 2001 family of standards provides technical descriptions of the standard of materials and workmanship, but do not refer to the actions of those responsible for executing the works or the parties to a contract.

South Africa is known as one of the semi-arid areas in the world, consisting of a dry sub-humid weather environment. Soils found in semi-arid areas have a shrinkage and swelling potential that can cause damage to buildings, utility services, and transportation links in towns and cities (Ozer et al., 2012; Vorwerk et al., 2015). The primary cause for shrinkage and swelling potential in soil in semi-arid areas is due to the intense seasonal rainfall and lengthy intervals of drought (P. Stott & Theron, 2015). Figure 2.1 shows a layout of the distribution of expansive clay found in South Africa where a high concentration is in the central region of South Africa.

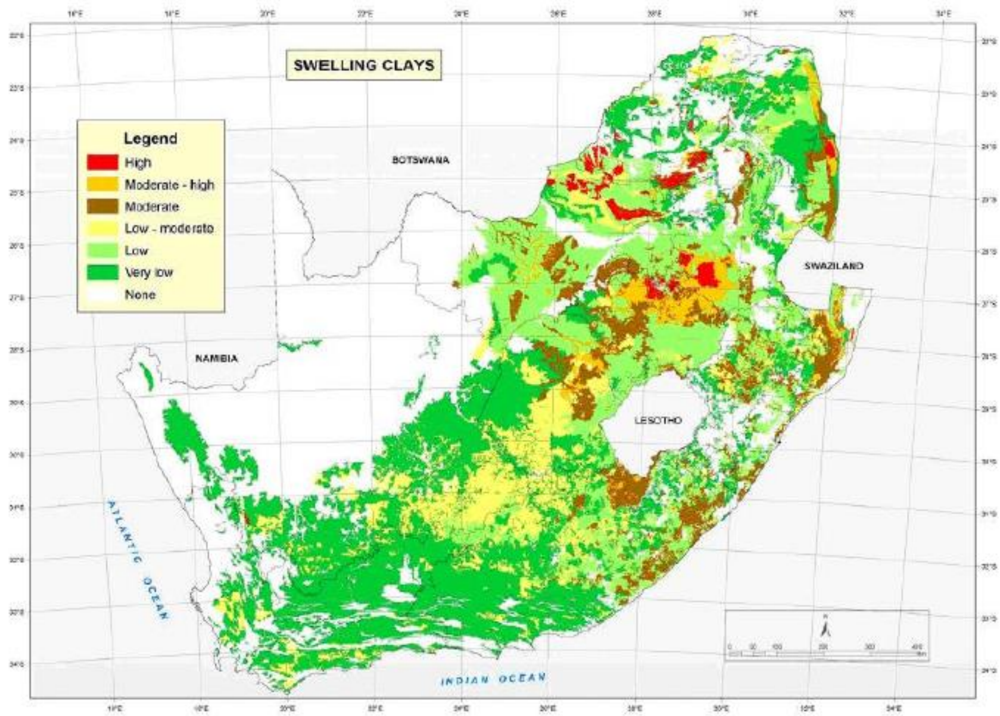

Figure 2.1: Distribution of expansive clay in South Africa (Turner & Paige-Green, 2007)

Soil, in any area of the world, is used as a structural support for building foundations as well as a construction material in commercial and residential projects (Aneke et al., 2019; Bester, 2017). In the construction of light masonry structures on expansive clays, various geotechnical tests have to be conducted to determine the severity of shrinkage or swelling potential of the clay in that particular area. The results of the geotechnical tests would then assist to determine the correct masonry material and foundation choices for a successful structure to last past its potential lifespan.

In the rise of demand for low-cost light masonry structures, the magnitude of geotechnical testing samples sent to commercial laboratories rose as well. (P. Stott & Theron, 2015) raised concern in the importance of proper geotechnical sample analyses for structures found on expansive clays. This concern was brought forward due to the large number of failures that occurred in the construction of small light masonry structures before reaching their expected lifespan (P. R. Stott, 2017). P. Stott and Theron (2015) also noted that the clients of the commercial laboratories are often under both time and economic pressures resulting in tests being inadequately prepared and tests rushed, producing inadequate results for highly plastic materials found in expansive clays.

P. R. Stott (2017) explained that there are mainly two reasons why small masonry structures tend to fail on expansive clays. Firstly, the expansive potential of clay depends on the suction against which the clay can draw in water. The clay can then only swell if the suction potential is greater than the pressure of the foundation above it. The pressure that a light masonry structure applies to the soil beneath it, even clays with very limited suction potential, can cause heave. Then secondly, the masonry currently used in South Africa is very brittle. Pigeon (1980) examined design methods for alleviation of heave damage from various countries including Australia, the U.S.A and South Africa. He noted widely differing values assumed by various methods for the distortions (deflection/length) that masonry can sustain without cracking. Some values were as low as 1 in 360, others as high as 1 in 3500. He noted that the lower values are “unlikely to guarantee a satisfactory level of serviceability”. Currently, in South Africa 1 in 3500 is often considered a suitable estimate of distortion for the probable onset of cracking in masonry panels due to soil heave underneath foundations. The reason for the wide range of flexibilities found by Pigeon is almost certainly due to the mortar specified (and complied with) in the standards of the various countries.

2.8.2 Mortar specifications and comparisons

According to the SANS 10164-1, mortar specifications are categorised into three classes (SANS 0164: Part 1, 1980). The first class, or Class I as specified by the SANS 10164-1, is for highly stressed masonry incorporating high strength structural units such as multi-storey load bearing buildings. Class II is for normal loadbearing applications such as parapets, balustrades, retaining structures, and freestanding and garden walls, as well as other walls exposed to possible dampness. The last class, Class III, mortar is for lightly stressed, i.e., single storey bearing walls, where exposure to dampness is not severe. Table 2.4 illustrates the limiting proportions of material for each mortar class.

Table 2.4: Limiting proportions for mortar as per SANS 10164-1

Mortar class	**Portland cement**	**Lime**	**Sand (Measured loose and damp)**	**Masonry cement : Sand or Portland cement with mortar: Sand plasticizer**	
	kg	***l***	***l*, max.**	**kg**	***l*, max.**
I	50	0-10	130	50	100
II	50	0-40	200	50	170
III	50	0-80	300	50	200

The American Standards for Testing and Materials uses other limiting proportions in their mortar mixes (ASTM C270-51T). Table 2.5 shows the limiting proportions of the mortar mixes as per the ASTM C270-51T. The American specification deals with volume for the ratio of cement:lime:sand, whereas the South African specification deals with mass for the cement and volume for the sand and lime.

Table 2.5: Limiting proportions for mortar as per ASTM C270-51T

Mortar class type	Portland cement	Lime	Sand
M	1	$\frac{1}{4}$	$3\frac{1}{2}$
S	1	$\frac{1}{2}$	$4\frac{1}{2}$
N	1	1	6
O	1	2	9
K	1	3	12

Comparing the limiting proportions of the SANS 10164-1 against the ASTM C270-51T, the mass of cement used in the SANS had to be converted to volume. Table 2.6 illustrates the adjusted limiting proportions of the SANS 10164-1 converted to volume. A 50 kg bag of cement packed at the factory, has an approximate volume of 33 litres. The SANS Class I mortar is between the ASTM Type M and Type S. Class II has close correspondence to Type N. Class III with the maximum permitted quantities of sand and lime has close correspondence to Type O.

Table 2.6: Adjusted limiting proportions of the SANS 10164-1

SANS 10164-1 Mortar Class	Cement	Lime	Sand (Max)
I	1	0-0.3	4
II	1	0-1.2	6
III	1	0-2.4	6

2.8.3 Mortar flexibility

Mortar flexibility is dependent on several factors including the cement content. It has an inverse, non-linear relationship to the Portland cement content. Before the use of cement in mortar around 1930, lime was the primary ingredient in mortar for most buildings throughout Europe and America and many structures in South Africa including churches, the Union Building and the Castle of Good Hope. Lime mortar has high flexibility, but low compressive strength (Costigan et al., 2009).

In 2015, Costigan et al. conducted several experiments on the mechanical properties and behaviour of masonry using three types of mortar mixes. The mortars under consideration included hydrated lime (CL90s), natural hydraulic lime (NHL), and a cement-lime mortar (M6) (Costigan et al., 2015a). The purpose of this experimental study was to understand the characteristics of lime-mortar versus cement mortar. The knowledge of masonry strength and deformation characteristics is important as they determine the masonry performance over time and allowable stress and stiffness in the design of new buildings. After conducting the experiments, Costigan et al. (2015) found that as the hydraulic grade of the mortar increased, the stiffness of the masonry compressive strength decreased. The results also showed that the properties of the mortar have a strong impact on the deformation of the masonry, resulting that the stress-strain relationship becomes increasingly non-linear as mortar strength decreases. Table 2.7 shows the strength results of the compressive strength, flexural strength, and the mortar elasticity results Costigan et al. (2015) obtained using the different compositions of mortar after 28 days. The mortar mixing ratio for the hydraulic lime mortars were the same where no cement was added. Similar compressive results were visible for the hydraulic lime mortars except for NHL2. The mortar containing hydrated lime showed a considerably lower compressive strength. The mortar containing Portland cement had the highest compressive strength. This pattern followed for the flexural and elastic modulus results where the mortar containing Portland cement had greater strength values compared to those without any cement. The mortar containing hydrated lime resulted to be the mortar with the lowest strength.

Table 2.7: Mortar compressive, flexural, and elasticity strength results of Costigan et al. (2015)

Mortar Cement:lime:sand		**Mortar compressive strength (N/mm^2)**	**Mortar flexural strength (N/mm^2)**	**Mortar elastic modulus (N/mm^2)**
NHL5 *5 N/mm^2 Hydraulic lime*	0:1:3	3.9	1.2	278
NHL3.5 *3.5 N/mm^2Hydraulic lime*	0:1:3	3.9	0.6	184
NHL2 *2 N/mm^2 Hydraulic lime*	0:1:3	1.9	2.7	130
CL90 *Hydrated lime*	0:1:3	0.6	0.2	70
M6 *Portland cement-lime*	1:0.5:4	11.2	3	927

2.9 Environmental Considerations in the Building Trade

The consumption of natural resources and energy has been increasing at an alarming rate worldwide. The consumption of these resources is increasing proportionally to the world's population growth and subsequent development of economic sectors (Alonso-Santurde et al., 2012; CIDB, 2007). As a result, the increased demand and consumption of already scarce resources are impacting the environment extensively (Alonso-Santurde et al., 2012; Silva et al., 2016). Natural resources are mined from riverbeds and hillsides for earth-based materials such as clay, shale, and sand in brick production. This has resulted in resource depletion, environmental degradation, and energy consumption (Shakir & Mohammed, 2013). Environmental degradation through these mining activities also causes widespread air pollution that remains after the mines cease operations, leaving scars on the landscape.

With the advancement in concrete technology in recent years, environmental considerations have become a necessity. The worldwide production of billions of tons of concrete, energy and water consumption, as well as the generation of construction and demolition waste are not compatible with the demands of sustainable construction in the building trade (Kunal, 2016). It has been estimated that the worldwide cement industry generates about 7% of all carbon dioxide emissions and other greenhouse gases (GHGs), where one ton of cement releases about one ton of carbon dioxide and other GHGs into the atmosphere (Geyer, 2012; Kunal & Rajor, 2012; Milling et al., 2020; Sugo et al., 2004). The amount of waste resulting from construction and demolition activities amounted to 34% of the total amount of 2.5 billion tonnes of waste generated in 2012 in the European Union (Silva et al., 2016).

Because of the rapid growth in the construction industry and the vast amounts of waste generated by the industry, civil engineers are searching for more efficient and durable alternatives to conventional brick production. For example, alternative formulations of material use in the production of ceramic bricks have reduced the use of core foundry sand when mixed with green sand, originating from the breakdown of moulds, and core sand (Alonso-Santurde et al., 2012). Green sand is mainly composed of silica, bentonite, bituminous coal, and water, while core sand is composed of silica, organic binders, and catalysts. Recycled aggregates (RAs) from treated construction and demolition wastes have also been used to replace natural aggregates in the production of new construction products. The use of these RAs creates new market opportunities which are also favourable to the environment (Silva et al., 2016).

Another study showed that when new clay bricks do not meet the manufacturer's standards, they can be recycled by regrounding through an inexpensive crushing process, after which new quality bricks can be manufactured (Ventra, 1998). The excessive extraction of clay and the removal of topsoil have resulted in the depletion of the virgin clay (Shakir & Mohammed, 2013). Therefore, recycling wastes in clay brick could reduce the over-exploitation of virgin clay and environmental contamination of waste, thereby contributing to the sustainable use of environmental resources. In China, building and industrial wastes are used as raw materials to manufacture fired hollow blocks with 29-row holes, which improve insulation, and reduce energy consumption and the weight of the hollow blocks (J. Wu et al., 2015).

Several non-building and construction type of waste materials have been used in brick production. The harbour sediments of the German harbour basin of Bremen are dredged annually to maintain a certain water level. The availability, homogeneity and mineralogical, petrographic, and chemical composition of these harbour sediments make this a suitable raw material for brick production (Hamer & Karius, 2002). In Brazil, granite sawing wastes are collected from companies as alternative ceramic raw materials in the production of ceramic bricks and tiles (Menezes et al., 2005). The bricks and tiles containing the granite wastes have physical and mineralogical characteristics that are similar to those of conventional ceramic bricks and tiles. In Turkey, earthquake-resistant fibrous waste material with high compressive strength has been investigated for its potential as raw material in mud brick production (Binici et al., 2005). It was found that the presence of these fibres increased the elasticity of the mud bricks. In another study in Turkey, the long cellulose fibres which are produced from wood, straw and reeds in Kraft pulp production were included in the material formulation of clay bricks. The inclusion of these pulp residues does not create any extrusion problems but increases the plasticity through the addition of increased water content (Demir et al., 2005). The slag of welding flux has also been tested as substitute for sand in the production of multiple-use mortars and clay for ceramic bricks (Viana et al., 2009). This substitute material reduces the extraction of natural sand and clay, thereby contributing to the reduction of the risk of groundwater contamination due to the inadequate disposal of slag and welding flux.

Currently, unusual alternative waste materials are constantly under investigation, for example, the use of cigarette butts in the production of clay bricks. Trillions of cigarette butts are produced worldwide annually, leading to many thousands of kilograms of toxic waste (Kadir et al., 2009). By sourcing these waste products and recycling them into fired clay bricks, the thermal conductivity performance of the bricks was improved by 51 and 58% with the addition of 5 and 10% cigarette butts. In another study conducted in Mexico, cellular concrete bricks were produced from lightweight mortar containing recycled expanded polystyrene aggregate instead of sandy materials (Hernández-Zaragoza et al., 2013). The resulting cellular concrete bricks still met the Mexican standard requirements. These bricks were also lighter than their commercial competitors, less permeable and more flexible, making them less vulnerable to cracking.

2.10 Discussion

Although masonry is one of the oldest and most widespread structural materials, it is currently still a common and traditional form of construction. Because masonry is so widely used, it is necessary to streamline production processes continually to meet the ever-changing business world and environmental conditions. Furthermore, considering specific regulations and standards, regular testing must take place when new materials and products are introduced into the market to ensure minimum safety limits. The possibility of performing destructive tests is often not feasible and may be prohibitively expensive. It is thus important to develop and apply computational tools to predict the behaviour of masonry structures under specific conditions with sufficient reliability.

CHAPTER 3: STUDY DESIGN

3.1 Introduction

In the building trade, material choices are one of the most important aspects to ensure that buildings are constructed according to standard specifications. For example, selecting a mortar class with inadequate material properties for a particular building project could affect the overall behaviour of the entire brickwork. Therefore, it is standard procedure to conduct physical tests to ascertain which material choices are best for certain projects. Several tests have been devised by the South African National Standards to facilitate these material choices in the building trade (SANS 0164: Part 1, 1980). Some of these tests include determining the compressive and bond strength of masonry. However, these tests are time consuming, labour intensive, costly and not always specified for a soil-sensitive project. Therefore, this study was undertaken to design a finite element model that would simulate deformation caused by heaving clay on experimental masonry wall panels to assess the material choices to improve the susceptibility of cracking in masonry.

3.2 Study Design

A finite element model was designed to assess the performance of various mortar material properties in a masonry wall panel. The study was therefore divided into two phases for the analysis of the material properties and the design of the finite element model (Figure 3.1). In the first phase, five different mortar mixes from two National Standards, the SANS 10164-1 and ASTM C270-51T, were selected for this study. Three experiments were performed on each of the five different mortar mixes to analyse their material properties and effects. In Phase 2, a finite element model was designed and refined using a finite element analysis software package to design five mesh refinement models. The five mesh refinement models were used to analyse two sets of finite element wall panels for the purpose of assessing the performance of the various mortar mixes when one millimetre of deformation was applied in a dome form to the bottom row of elements.

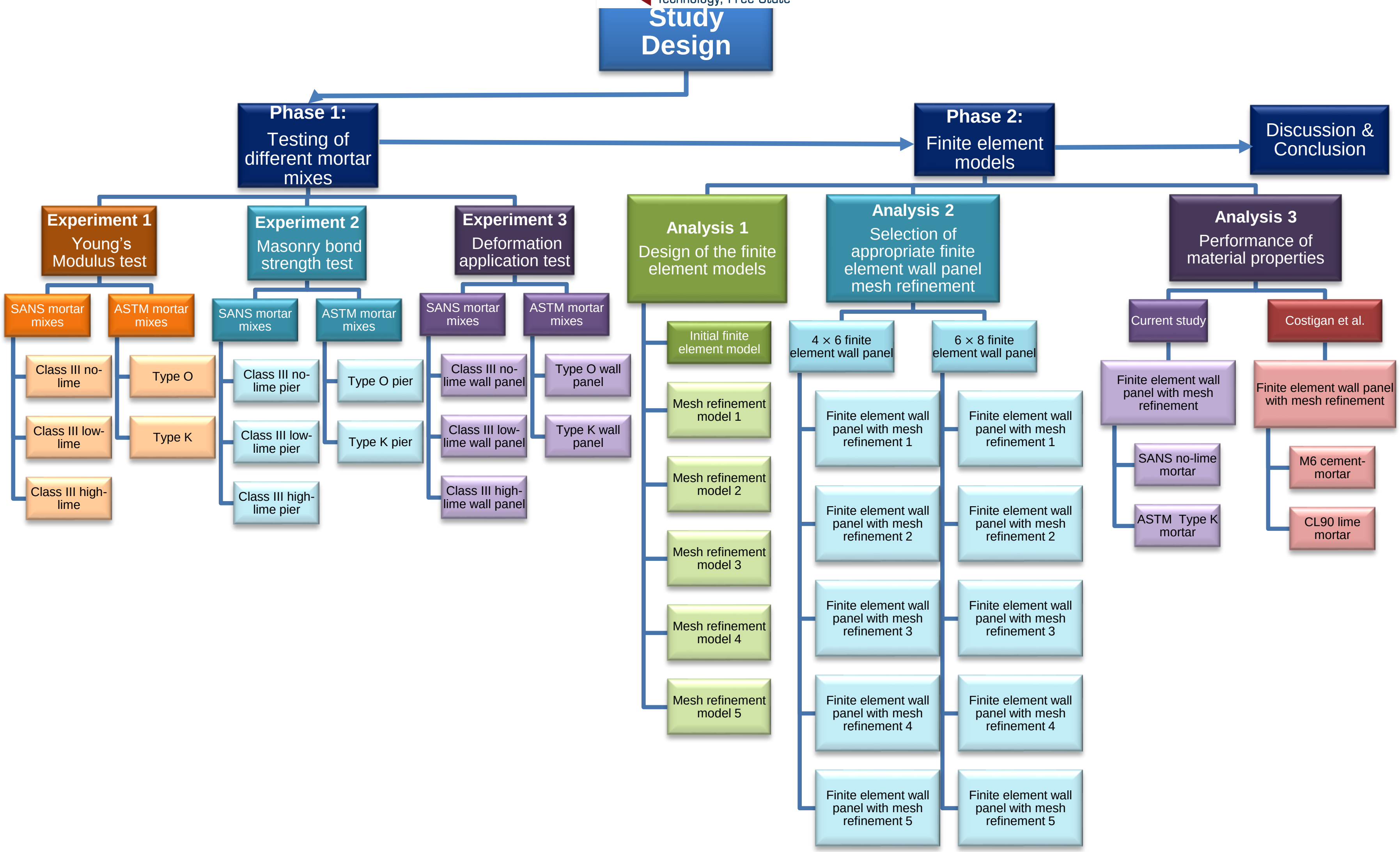

Figure 3.1: Flow diagram of the study design

3.2.1 Phase 1: Testing of different mortar mixes

In Phase 1, five different mortar mixes were selected from two National Standards to be analysed. Three of the mortar mixes were from the SANS 10164-1 and the other two from the ASTM C270-51T. Three experiments were performed on the five different mortar mixes to analyse the material properties of each mortar mix. The experiments performed on the mortar mixes are tabulated in Table 3.1:

Table 3.1: Aim and brief description of the experiments performed in Phase 1

Test	Aim of test	Brief description of test
Experiment 1: Young's Modulus test	The aim of Experiment 1 was to determine the elastic properties of the different mortar mixes by performing a Young's modulus test.	A sample of each of the different mortar mixes were cast into small beams with size of 150 × 12 × 12 mm. These cast mortar beams were then subjected to a bending test that would allow a performance of larger deflection in each beam with the application of smaller forces and simpler measurements. Small weights were then added to the centre of each mortar beam in 5-second intervals for 2 minutes. The magnitude and the deflection at 5-second intervals were used to determine the Young's modulus of each of the five mortar beams. This process was repeated for each of the five different mortar mixes.
Experiment 2: Bond strength test	The aim of Experiment 2 was to determine the bond strength between the bricks and mortar by performing a bond strength test.	The determination of the bond strength between the standard brick combined with each of the five different mortar mixes were performed according to the SANS 10164-1.
Experiment 3: Deformation application test	The aim of Experiment 3 was to determine the magnitude of deformation that a masonry wall panel could absorb before failure occurred.	Five experimental wall panels each with dimensions of 1 830 × 760 mm were constructed using each of the five different mortar mixes and the standard cement brick. Three of the mortar mixes originated from the SANS 10164-1 and two from the ASTM C270-51T. The Type O mortar from the ASTM showed remarkable similar mixing ratio of the Class III SANS mortar mix. Type K from the ASTM contained a more lime and sand and was used for comparison reasons. A steady deformation was applied to the centre bottom area of each experimental wall panel until failure occurred. (The wall panel sizes were adapted to the limited testing area availability at the Central University of Technology)

3.2.2 Phase 2: Design of the finite element models

In Phase 2, an initial finite element model was designed using a finite element analysis software package. The initial finite element model was used to design five mesh refinement models. A 4 × 6 and 6 × 8 finite element wall panel was then designed using the five mesh refinements. The performance of the finite element wall panels was analysed using a set of theoretical parameters to ascertain which mesh refinement showed the most consistent results. A selected finite element wall panel with mesh refinement was then used to analyse the performance of four different mortar mixes, including two mortar mixes from Costigan et al. (2015). Because Costigan et al. (2015) conducted compressive, flexural, and elastic strength experiments on various mortar types, two of the mortar mixes stood out. The CL90 (hydrated lime mortar) and the M6 (Portland cement-lime mortar). The CL90 with the hydrated lime had the least amount of strength and the M6 mortar the most. Analysing the stress pattern in the wall panels with the SANS 10164-1 Class III no-lime mortar and high-lime mortar with the CL90 and M6, showed remarkable results of flexibility when a mortar contains a higher amount of cement.

3.3 Conclusion

This study consisted of two phases in which the material properties of five different mortar mixes were tested and analysed using a finite element model and experimental wall panels. Through the application of several physical tests, the material properties of the five different mortar mixes were analysed in ten (10) finite element wall panels. A finite element wall panel with specified mesh refinement was then selected for further performance analysis. The selected finite element wall panel with specified mesh refinement would give an understanding of the stress patterns found in wall panels resulting from applied deformation using a range of different material properties.

CHAPTER 4: MORTAR MATERIAL PROPERTIES

4.1 Introduction

In this study, a series of experiments was performed using five different mortar mixes to determine what effects material composition has on masonry subjected to deformation caused by expansive clay. Three of the mortar mixes were formulated according to the SANS 10164-1, while two were formulated according to the ASTM C270-51T. Each of the mortar mixes differed from the others in the ratio of their material composition. One mortar mix contained only cement and sand, while the other mortar mixes contained a mixture of cement, lime, and sand. Two mortar mixes consisted of a high-lime ratio and two of a low-lime ratio to the cement. Three experiments were performed on each different mortar mix to analyse the material properties of the different mixes. In Experiment 1, Young's modulus was determined to ascertain the flexibility of each mortar mix. In Experiment 2, the masonry bond strength between a standard cement brick and each mortar mix was determined. In Experiment 3, the maximum deformation an experimental wall panel could absorb before failure occurred was determined. Figure 4.1 shows the layout of Phase 1, indicating the various experiments that were performed.

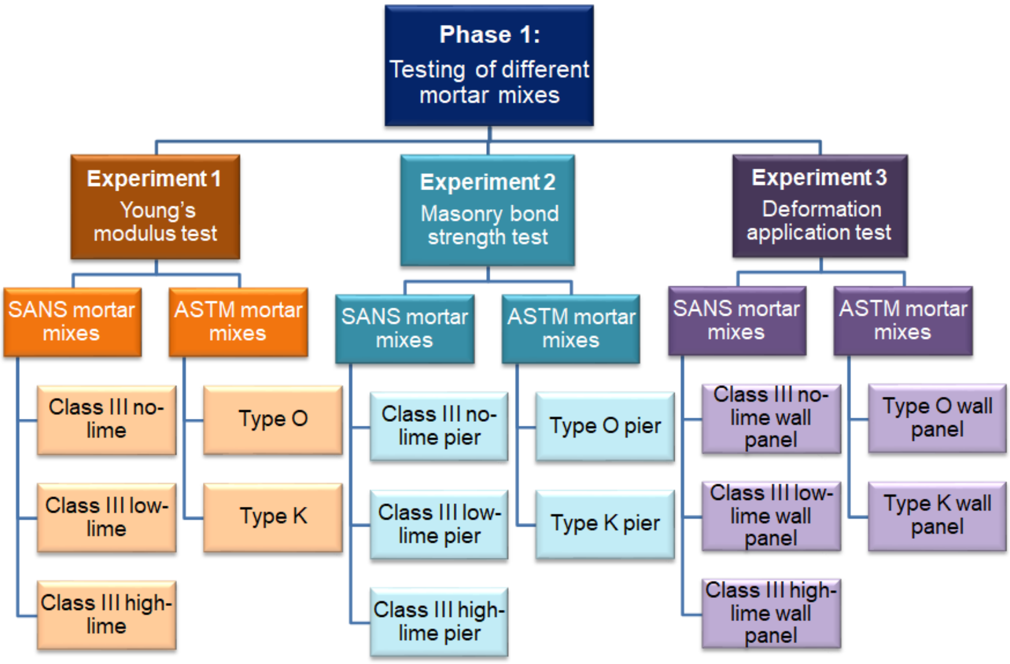

Figure 4.1: Layout of Phase 1 showing the three experiments performed with the different mortar mixes

4.2 Materials and Methods

4.2.1 Materials and experiments

The material properties of the five different mortar mixes were analysed in three experiments. These mortar mixes consisted of different mortar mix ratios of cement, lime, and sand. Table 4.1 lists the mortar mix ratios of the different mortar mixes:

Table 4.1: Mortar mix ratios

Mortar mix	Cement	Lime	Sand
SANS Class III no-lime	1	0	6
SANS Class III low-lime	1	1	6
SANS Class III high-lime	1	1.6	6
ASTM Type O	1	2	9
ASTM Type K	1	3	12

Three experiments were performed to determine the material properties of the different mortar mixes. In Experiment 1, five tests were performed, one on each of the different mortar mixes. Similarly, five tests were performed to determine the bond strength and finally the maximum deformation an experimental wall panel could absorb. Table 4.2 lists the experimental series and sub-experiments conducted on the mortar mixes:

Table 4.2: Experimental series and sub-experiments conducted with the different mortar mixes

Experiments	Description	Materials	Tests in series
1. Young's modulus test	In this test, the flexibility of the five different mortar mixes was determined.	SANS Class III no-lime mortar	1.1 SANS Class III no-lime mortar beam
		SANS Class III low-lime mortar	1.2 SANS Class III low-lime mortar beam
		SANS Class III high-lime mortar	1.3 SANS Class III high-lime mortar beam
		ASTM Type O mortar	1.4 ASTM Type O mortar beam
		ASTM Type K mortar	1.5 ASTM Type K mortar beam
2. Masonry bond	In this test, the bond strength between a standard cement	Standard cement brick with SANS Class III no lime mortar	2.1 SANS Class III no-lime pier

Experiments	Description	Materials	Tests in series
strength test	brick and each of the five different mortar mixes were determined.	Standard cement brick with SANS Class III low-lime mortar	2.2 SANS Class III low-lime pier
		Standard cement brick with SANS Class III high-lime mortar	2.3 SANS Class III high-lime pier
		Standard cement brick with ASTM Type O mortar	2.4 ASTM Type O pier
		Standard cement brick with ASTM Type K mortar	2.5 ASTM Type K pier
3. Deformation application test	In this test, deformation was applied to five experimental wall panels built using the five different mortar mixes and the standard cement brick.	Standard cement brick with SANS Class III no-lime mortar	3.1 SANS Class III no-lime wall panel
		Standard cement brick with SANS Class III low-lime mortar	3.2 SANS Class III low-lime wall panel
		Standard cement brick with SANS Class III high-lime mortar	3.3 SANS Class III high-lime wall panel
		Standard cement brick with ASTM Type O mortar	3.4 ASTM Type O wall panel
		Standard cement brick with ASTM Type K mortar	3.5 ASTM Type K wall panel

4.2.2 Experiment 1: Determination of the Young's modulus

In Experiment 1, the material flexibility was determined for each mortar mix. Each sample of mortar mix was used to perform the Young's modulus test. The method used to conduct the Young's modulus test is not specified in the SANS 10164-1 and thus motivated as follows:

a. The testing method meant to give a measurement of a wide enough range to give a meaningful plot of results;
b. A bending test, instead of a pulling test was performed that allowed for a large deflection in the sample with the application of small forces and simple measurement recording;
c. A suitable apparatus was used for investigating the deformation of billets of clay at high suction. This apparatus was now used and found to give accurate results for high suction in clay billets;

d. This suitable apparatus needed minimum modification to test mortar billets of suitable size; and
e. An equation for deriving the Young's modulus was derived from elementary strength of materials and checked as being in agreement with equation 13.6, p. 217 in 'Strength of Materials' (Case et al., 1964)

A series of steps were followed to perform the Young's modulus test:

1. Each mortar mix was prepared according to the selected mortar mixing ratios specified in the SANS 10164-1 and ASTM C270-51T. Enough mixture was prepared to cast five beams per mortar mix.

2. The prepared mixtures for each mortar mix were then poured into a mould of five beams. The dimensions of each beam were 150 × 12 × 12 mm. Figure 4.2 shows five mortar beams in a mould made out of perspex material:

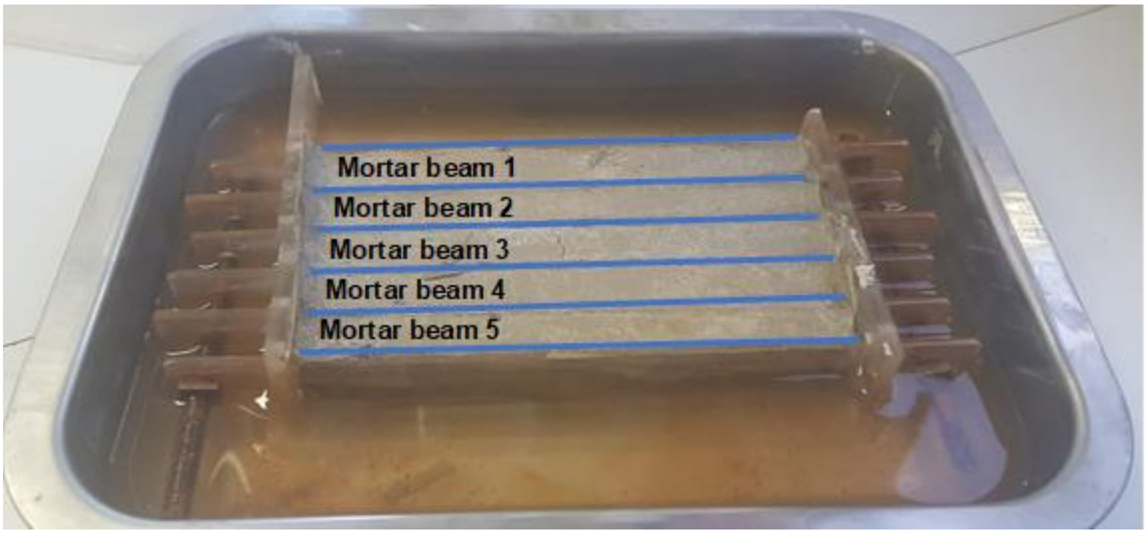

Figure 4.2: Five mortar beams in a mould

3. The mould with cast beams was left at room temperature for 24 hours. Thereafter, the mould was placed inside a temperature-controlled water bath with a temperature of approximately 26 °C for seven days to cure.

4. After curing, the mould containing the cured beams was carefully removed from the water bath. Each mortar beam was then carefully extracted from the mould

and dried off using a paper towel. A dried mortar beam was then placed onto two supports (wooden blocks) approximately 130 mm apart on either side of the apparatus.

5. A suitable apparatus was used to determine the flexibility in each mortar beam. The apparatus was initially used in the study to determine bending tension in soil samples, and then modified to determine bending in mortar samples. Figure 4.3 illustrates a layout of the top and side view of the apparatus that was modified to use for the determination of the Young's modulus.

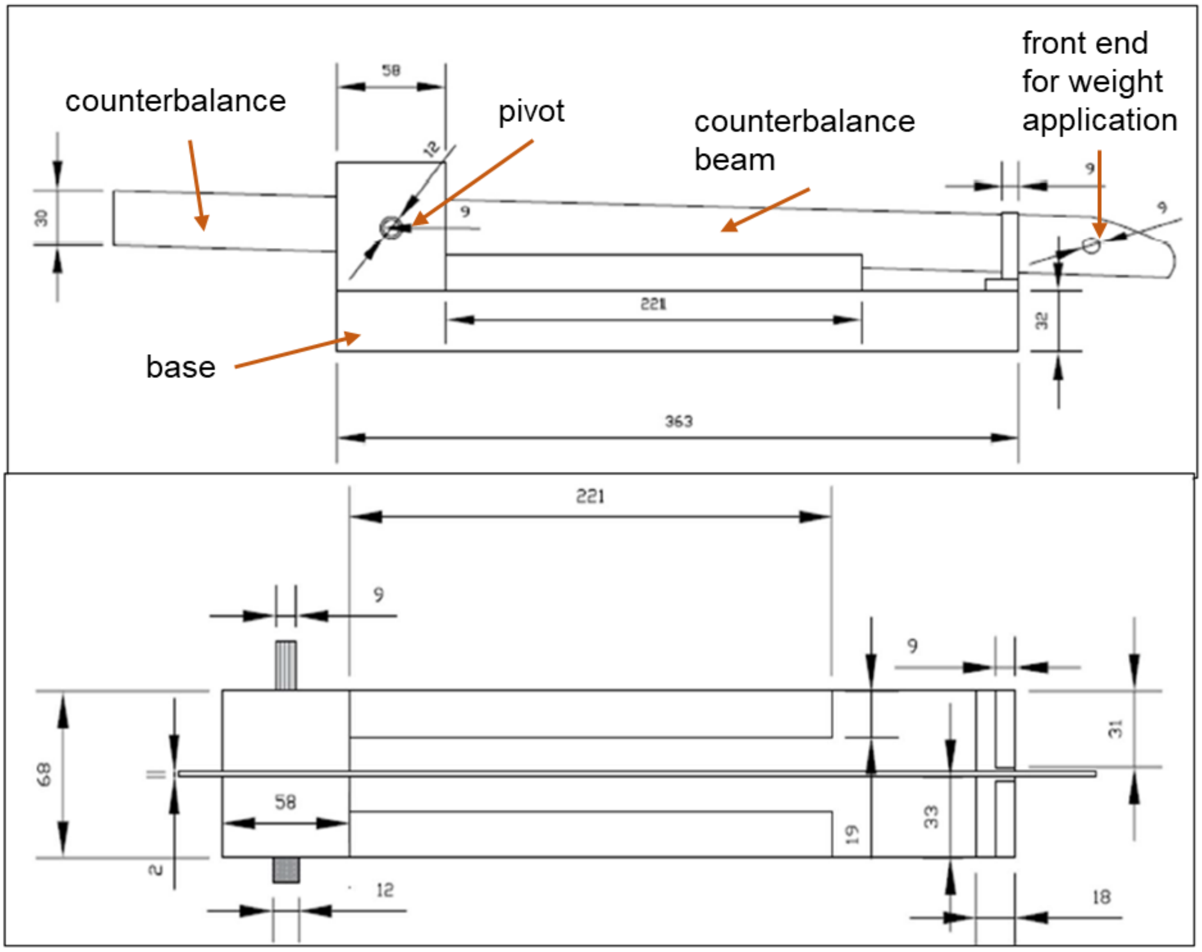

Figure 4.3: Front and side view of apparatus modified for the determination of the Young's modulus

6. On the centre of each mortar beam, a weightless counterbalanced beam was placed to which weights were added.

7. The counterbalanced beam was then loaded with weights of approximately 14 g each at five-second intervals. Weights were added to the mortar sample for a total of two minutes, resulting in a final weight of 350 g. The deflection of the mortar beam was measured with a dial gauge as each weight was loaded every five seconds. (Figure 4.3).

a. **b.**

Figure 4.4: Modified Young's modulus apparatus **a.** Mortar beam simply supported on two supports with the counterbalanced beam and dial gauge attached, **b.** Weights that were added to the counterbalanced beam.

8. The recorded data was now used to determine the Young's modulus of each mortar beam.

9. To determine the Young's modulus (E, MPa), the moment of inertia (I, mm^4) was first calculated:

$$I = \frac{b \times d^3}{12} \tag{4.1}$$

Where:

b = breadth of mortar beam (mm)

d = depth of mortar beam (mm)

10. The Young's modulus in MPa was then calculated for each mortar beam:

$$E = \frac{L^3 \times WD}{48 I d_p y} \tag{4.2}$$

Where:

W = weight of scale pan (N)

D = distance from pivot to scale pan (mm)

d_p = distance from pivot to test specimen (mm)

L = length of mortar beam between supports (mm)

I = moment or inertia of mortar beam (mm^4)

y = central deflection of mortar beam (mm)

E = Young's modulus (N/mm^2 = MPa)

4.2.3 Experiment 2: Determination of the masonry bond strength

In Experiment 2, the masonry bond strength between a standard cement brick and each of the different mortar mixes was determined. This test is in section 6.7 of the SANS 0164-1:1980. A view of the bond strength test per the SANS 10164-1 Standards is illustrated in Figure 4.4:

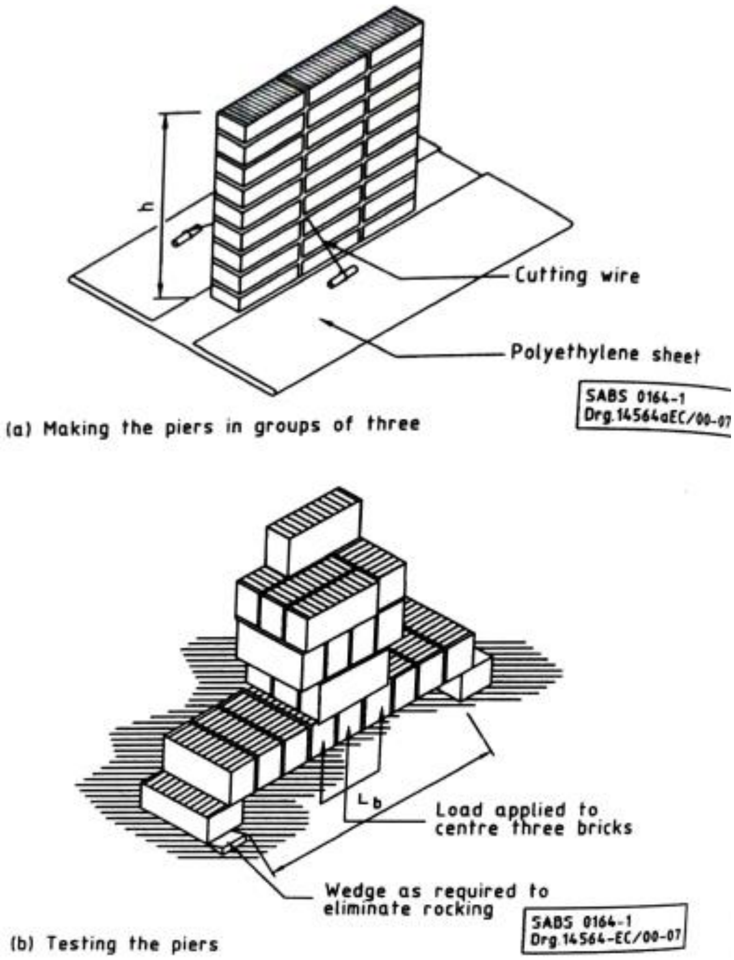

Figure 4.5: View of the bond strength test as per the SANS 10164-1

For each test in the series, the masonry bond strength was performed on three piers consisting of a brick structure made up of nine stacked standard cement bricks with a 10 mm layer of mortar between each brick. In total, 15 tests were performed in this series. The following steps were followed to determine the masonry bond strength between the mortar and the brick:

1. For each mortar mix, three piers were constructed simultaneously on a level surface.

2. These piers were then wrapped in plastic sheeting and left to cure for seven days.

3. After curing, each pier was weighed to the nearest 0.1 kg.

4. The piers were then horizontally repositioned on two symmetrically placed supports at each end with clear span L_b (mm), and with the stretcher face of the bricks facing the ground to form a beam.

5. Standard cement bricks were carefully loaded, one brick at a time, to the centre of the beam until the beam broke.

6. After the beam had broken, the loaded bricks (representing the applied load) were weighed (W_2) together to the nearest 0.1 kg.

7. After the loaded bricks had been weighed, the self-weight of the pier between the supports, bending moment (M) and the section modulus (Z) were calculated. Their values were used to determine the bond strength (δ) of the pier.

    a. The self-weight of the pier between the supports was calculated by first weighing the pier and then multiplying the weight by a factor obtained from the following equation. The result of this calculation was labelled W_1:

    $$W_1 = Weight\ of\ pier \times \frac{L_b}{h} \quad (4.3)$$

    Where:

    L_b = clear span of beam (mm)

    h = overall height of pier (mm)

b. The M in Nmm was calculated to obtain the bending effect caused by the load added to the beam. The following formula was used to calculate the bending moment (M):

$$M = \frac{W_1 L_b}{8} + \frac{5W_2 L_b}{24} \quad (4.4)$$

Where:

W_1 = self-weight of pier between supports (kg)

W_2 = mass of bricks applied to break the beam (kg)

L_b = clear span of the beam between the supports (mm)

c. The Z in mm^3 was calculated to obtain the ratio of the section modulus of the beam. The following formula was used:

$$Z = \frac{bd^2}{6} \quad (4.5)$$

Where:

b = length of the brick (mm)

d = height of the brick (mm)

d. The bond strength (δ) was now calculated in N/mm^2 using the following formula:

$$\delta = \frac{M}{Z} \quad (4.6)$$

Figure 4.5 provides photographs of the three stages of the determination of the masonry bond strength test:

a. b. c.

Figure 4.6: Three stages of the masonry bond strength test **a.** Three piers, **b.** Beam, and **c.** Broken beam

4.2.4 Experiment 3: Determination of maximum deformation absorbed by a masonry wall panel

In Experiment 3, the maximum deformation an experimental wall panel could absorb before failure occurred was determined for each of the different mortar mixes. Due to limitations of space, full size wall panels usually the size of a single storey masonry building (2,000 × 6,000 mm), were not constructed. However, smaller wall panels were constructed that would fit the current apparatus available at the Central University of Technology, Bloemfontein campus. With full size wall panels, the self-weight of the wall panel would be sufficient in the event where a dome deformation would be placed directly to the bottom row of bricks. This could however not be executed, and a smaller wall panel had to be constructed. The self-weight of the smaller wall panel was, however, not sufficient when a deformation was applied and the whole wall panel lifted. An experimental wall panel with dimensions of 1,830 × 790 mm (8 × 10 bricks) was built using standard cement bricks and a 10 mm layer of mortar mix between each brick joint. To still proceed in testing the deformation of the wall panel, several necessary restraints were added to the smaller wall panel. A series steps were followed to determine the maximum deformation each wall panel could absorb before failure of the mortar between the bricks occurred:

1. A steel frame with an opening of 1,900 × 1,000 mm was used to house the experimental wall panel.

2. A group of specialised industrial levelling jacks, of approximately 40 mm in height, was placed and equally spaced over the base of the opening of the steel frame. A steel plate of 3 mm thickness was placed over the length of the base on top of all the jacks.

3. The experimental wall panel could now be built using standard cement bricks and a specified mortar mix. The first row of bricks of the experimental wall panel was placed so that the mortar joint in the middle of the bottom row of bricks was positioned exactly over the middle industrial levelling jack, leaving enough space at the ends of the experimental wall panel for horizontal movement.

4. The constructed experimental wall panel was now wrapped in plastic sheeting and left to cure for seven days.

5. On the seventh day, the plastic sheeting was removed, and safety bars were placed at the two open sides of the steel frame housing the experimental wall panel.

6. Four of the seven industrial levelling jacks at the base of the frame were removed and placed at the two top corners of the experimental wall panel between the wall panel and the steel frame. These jacks restrained the experimental wall panel from any movement at the top corners. The three remaining industrial levelling jacks were kept underneath the experimental wall panel: one in the middle and two at each end of the wall panel.

7. A dial gauge was placed on the centre of the top brick of the experimental wall panel to measure the deformation applied to the wall panel via the central industrial levelling jack below.

8. After the wall panel had been safely secured, the centre industrial levelling jack at the bottom of the experimental wall panel was used to apply an upward movement at a steady rate.

9. The deformation applied to the experimental wall panel until failure occurred was recorded for further analysis. Figure 4.6 shows an experimental wall panel inside the steel frame before failure occurred.

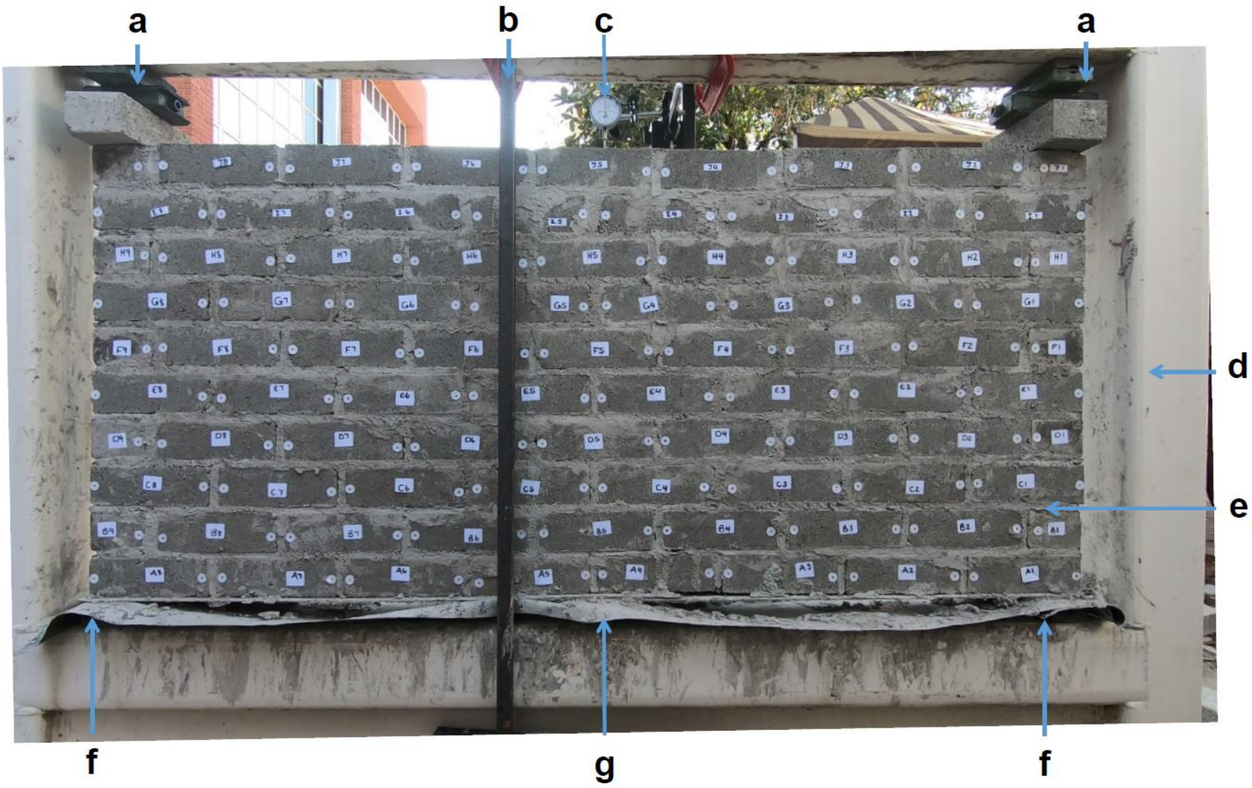

Figure 4.7: Experimental wall panel inside the steel frame **a.** Top industrial levelling jacks, **b.** A safety beam, **c.** Dial gauge, **d.** Steel frame, **e.** Experimental wall panel, **f.** Bottom corner industrial levelling jacks, **g.** Bottom middle industrial levelling jack

4.3 Results: Experiment 1 – Young's Modulus Test

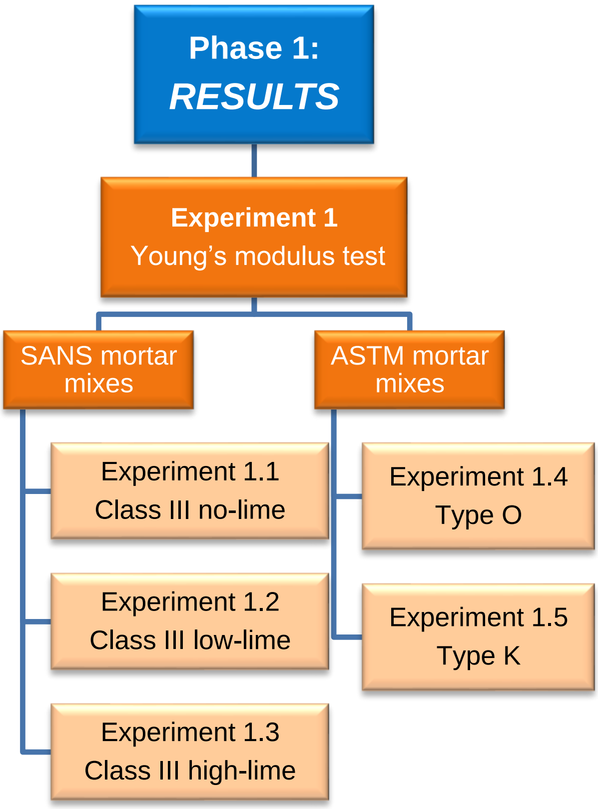

Figure 4.8: Layout of Phase 1 showing the results of the first experiment performed with the different mortar mixes

4.3.1 Experiment 1.1: SANS Class III, no-lime mortar beam

In Experiment 1.1, the SANS Class III no-lime mortar beams were used to conduct the Young's modulus test. The mortar mix consisted of 1 part cement and 6 parts sand. An average Young's modulus of about 2.3 GPa was determined by first calculating the individual Young's modulus values of each mortar beam sample using the sourced equation from (Case et al., 1964) for beam deflections, and then the average of the five samples was calculated. All the average Young's modulus for each of the five mortar mixed were determined using this method. None of the five mortar beams broke during this test and the beams illustrated a linear-like behaviour when graphed. Graph 4.1 shows the results of the Young's modulus for the SANS Class III no-lime mortar mix:

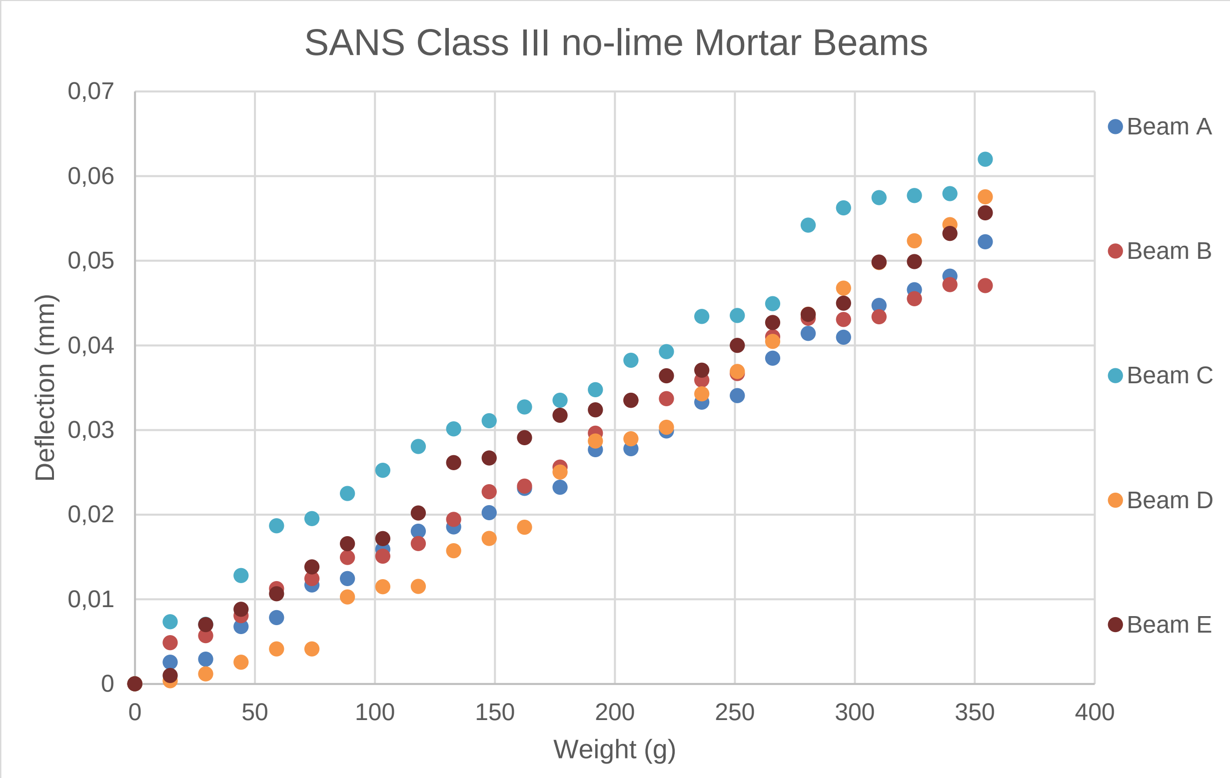

Graph 4.1: Results of the Young's modulus for SANS Class III no-lime mortar beams

4.3.2 Experiment 1.2: SANS Class III low-lime mortar beam

For Experiment 1.2, the SANS Class III low-lime mortar beams were used for the Young's modulus test. This mortar mix consisted of 1 part cement, 1 part lime and 6 parts sand. Similarly, an average of the Young's modulus was determined, and resulted in just over 1.7 GPa. None of the mortar beams had broken during testing. The beams had a delayed reaction of deflection but still portrayed a linear-like behaviour. Graph 4.2 shows the results of the SANS Class III low-lime mortar beams:

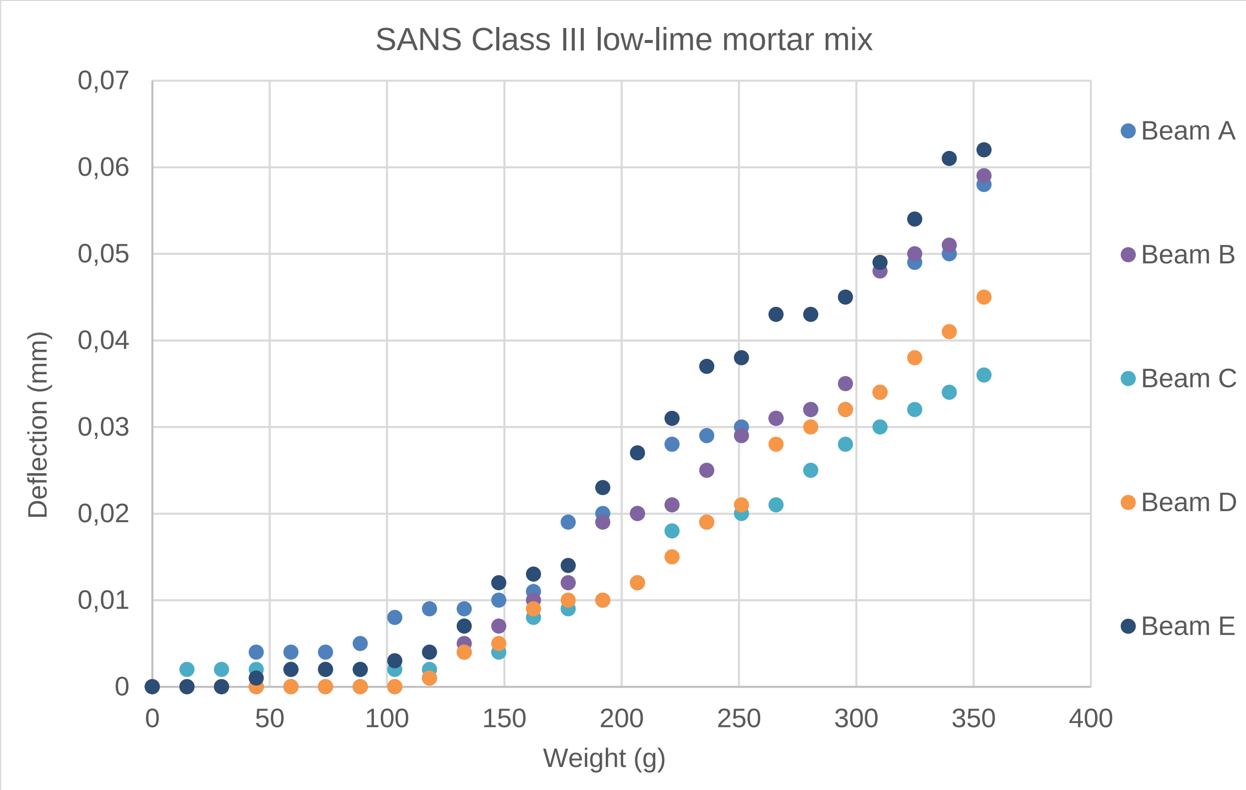

Graph 4.2: Results of the Young's modulus for SANS Class III low-lime mortar beams

Experiment 1.3: SANS Class III high-lime mortar beam

In Experiment 1.3, the SANS Class III high-lime mortar beams were used in the Young's modulus test. This mortar mix contained a higher amount of lime compared to the previous SANS mortar mixes. This mortar consisted of 1 part cement, 1.6 parts lime and 6 parts sand. The average Young's modulus for this mortar mix was determined as approximately 1.3 GPa. Zero mortar beams broke during the test. The results of the recorded deflection indicated a linear-like behaviour for all five beams. Graph 4.3 shows results of the Young's modulus for the SANS Class III high-lime mortar beams.

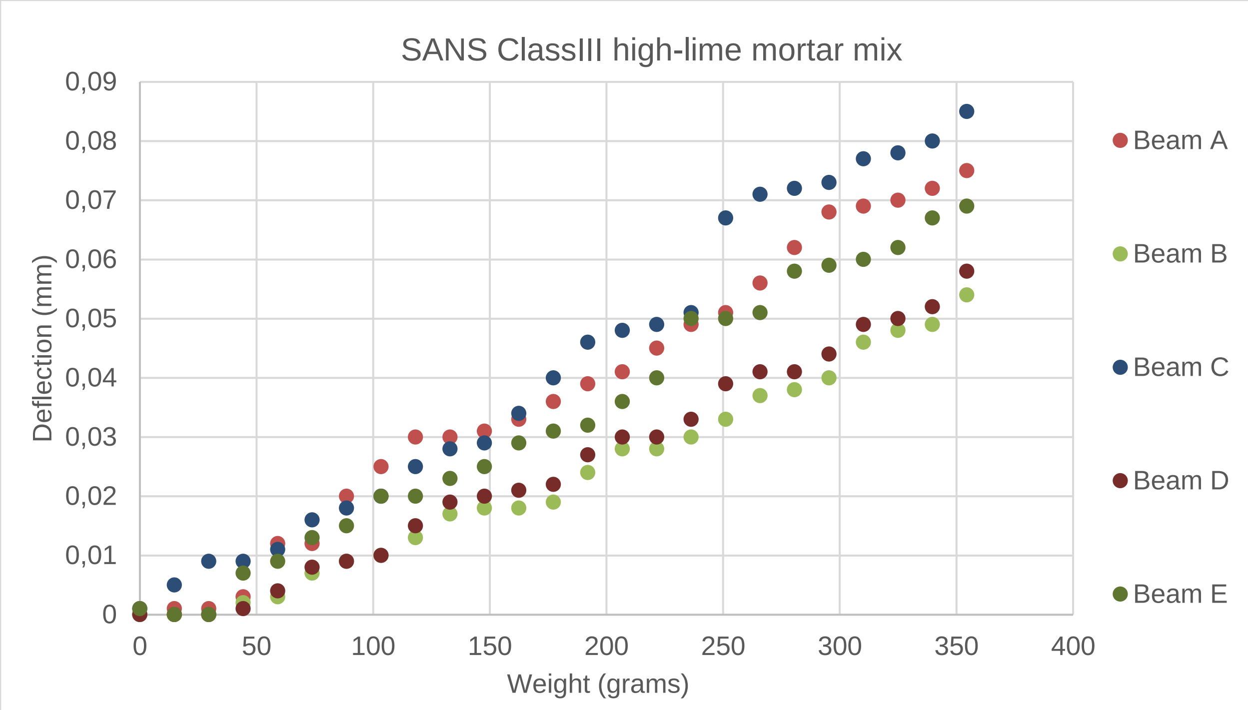

Graph 4.3: Results of the Young’s Modulus for SANS Class III high-lime mortar beams

4.3.3 Experiment 1.4: ASTM Type O mortar beam

In Experiment 1.4, the ASTM Type O mortar mix from the American Standard was used in the Young’s modulus test. This mortar mix contained 1 part cement, 2 parts lime and 9 parts sand. After the test had been conducted, an average Young’s modulus in the region of 1.2 GPa was ascertained. This showed a much lower Young’s modulus compared to the SANS. None of the beams had broken during this test and illustrated a linear-like behaviour when the results were graphed. Graph 4.4 shows the results of the Young’s modulus for ASTM Type O mortar mix beams:

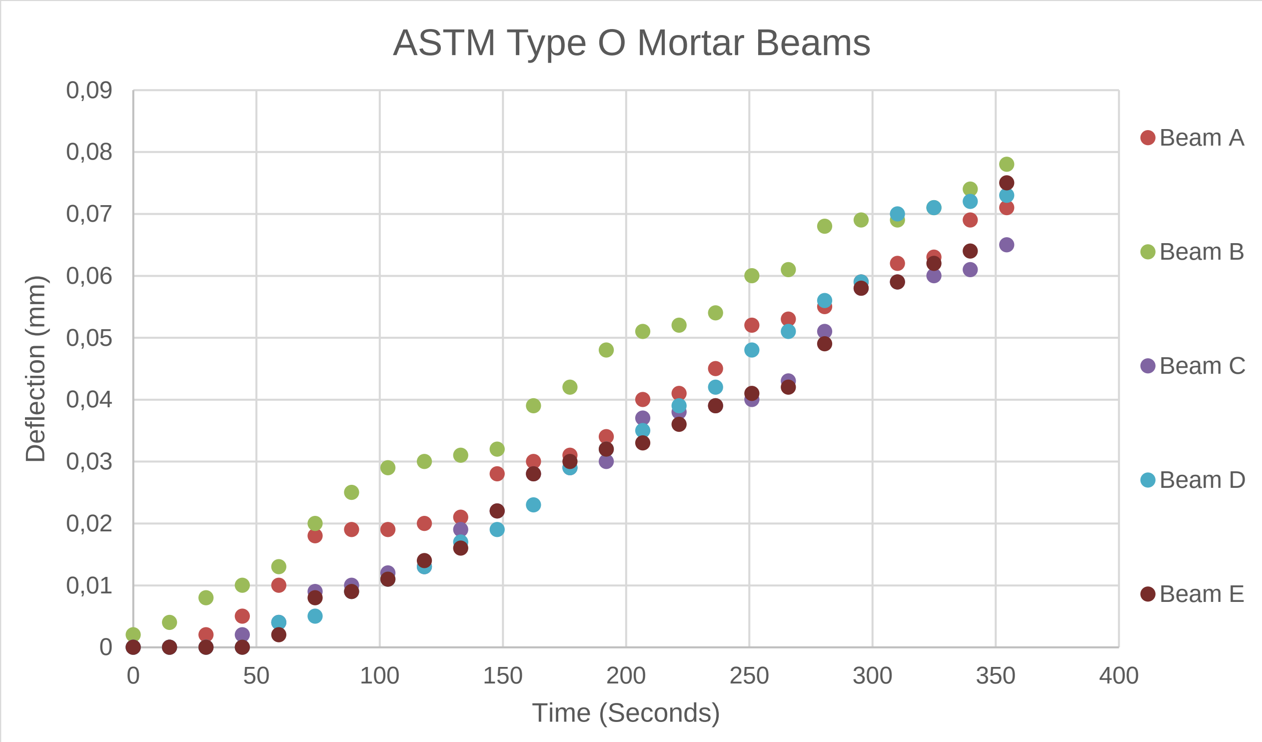

Graph 4.4: Results of the Young's Modulus for ASTM Type O mortar beams

Experiment 1.5: ASTM Type K mortar beam

For Experiment 1.5, the ASTM Type K mortar mix was used to conduct the Young's modulus test. This mortar mix contained a mixture of the most lime and sand in a mortar mix for the ASTM National Standards. This mortar mix consisted of 1 part cement, 3 parts lime and 12 parts sand. The recorded Young's modulus after conducting the test was just over 0.8 GPa. During the test, one of the mortar beams failed before the two-minute limit had been reached. The graphed results showed similar linear-like behaviour to that of the ASTM Type O mortar mix. Graph 4.5 shows the Young's modulus results of the ASTM Type K mortar beams:

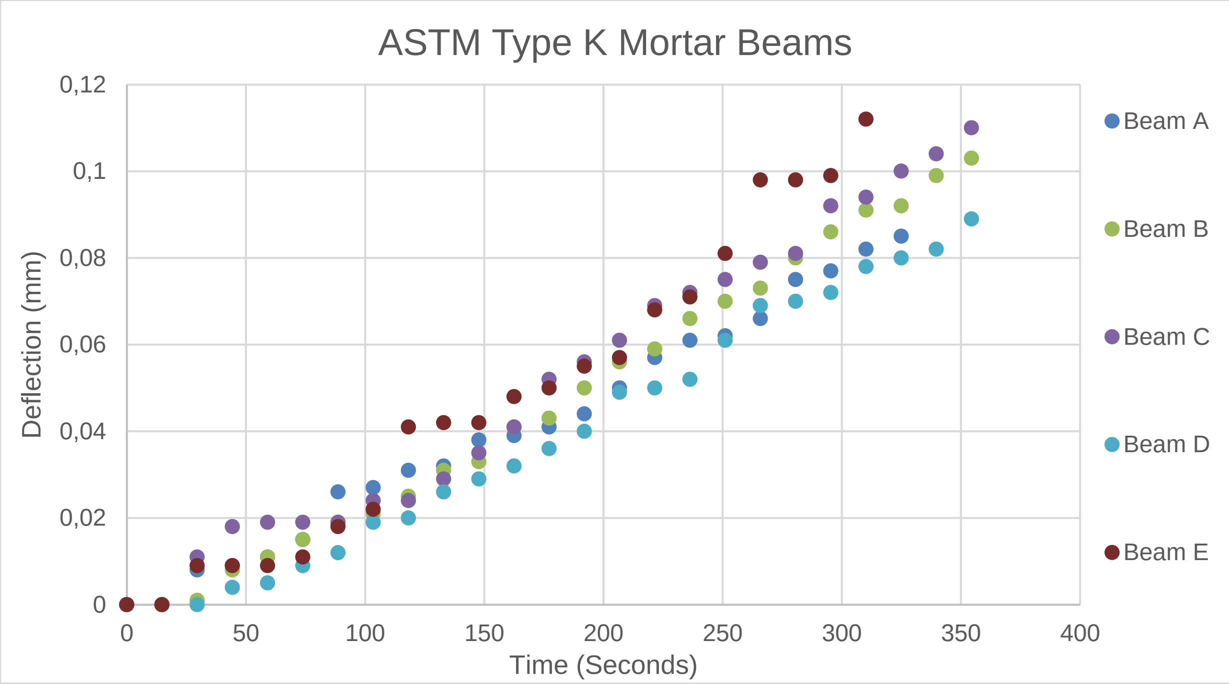

Graph 4.5: Results of Young's Modulus for ASTM Type K mortar beams

4.3.4 Comparative Young's modulus results

After conducting the Young's modulus test on all five different mortar mixes, a series of results were ascertained. The SANS Class III no-lime mortar mix had no added lime to the mix and had the lowest deflection. During the second test using the SANS Class III low-lime mortar mix, the Young's modulus slightly reduced, compared to that of the SANS Class III no-lime, and the deflection remained approximately the same. With the SANS Class III high-lime mortar mix, a higher content of lime was added and resulted in the Young's modulus decreasing further. The decrease in the Young's modulus caused the deflection in the mortar beams to increase. In the Young's modulus tests using the ASTM mortar mixes, a higher content of lime and sand was used. The ASTM Type O mortar mix beams had overall much lower Young's modulus values with rather higher deflections, compared to the SANS mortar mixes. During the last test, the ASTM Type K mortar mix beams were tested and the Young's modulus was found to be the lowest. This mortar mix was shown to have the highest deflection which resulted from its low Young's modulus value. Table 4.3 shows the comparative results of the Young's modulus tests for the three SANS mortar mixes and the two ASTM mortar mixes:

Table 4.3: Comparative results of the Young's modulus tests for the SANS and ASTM mortar mixes

Mortar Mix	Beam	Maximum Deflection (mm)	Young's Modulus (MPa)
SANS Class III No-lime	A	0.052	2,355.072
	B	0.047	2,530.365
	C	0.062	2,222.617
	D	0.058	2,102.283
	E	0.056	2,123.537
	Average	*0.055*	*2,266.775*
	COV (%)	*9.342*	*0.628*
SANS Class III Low-lime	A	0.058	1,610.958
	B	0.059	1,361.172
	C	0.036	1,961.766
	D	0.045	2,194.669
	E	0.059	1,535.082
	Average	*0.051*	*1,733.329*
	COV (%)	*18.192*	*0.330*
SANS Class III High-lime	A	0.075	1,103.358
	B	0.046	1,477.495
	C	0.085	1,256.412
	D	0.058	1,768.679
	E	0.069	1,424.711
	Average	*0.066*	*1,389.806*
	COV (%)	*20.292*	*0.446*
ASTM Type O	A	0.071	1,153.575
	B	0.078	1,049.521
	C	0.065	1,369.576
	D	0.073	1,117.738
	E	0.075	1,412.076
	Average	*0.072*	*1,220.497*
	COV (%)	*6.027*	*0.696*
ASTM Type K	A	0.085	969.881
	B	0.103	801.815
	C	0.110	824.520
	D	0.089	920.485
	E	0.112	742.422
	Average	*0.099*	*851.825*
	COV (%)	*10.965*	*1.215*

4.4 Results: Experiment 2 – Masonry Bond Strength

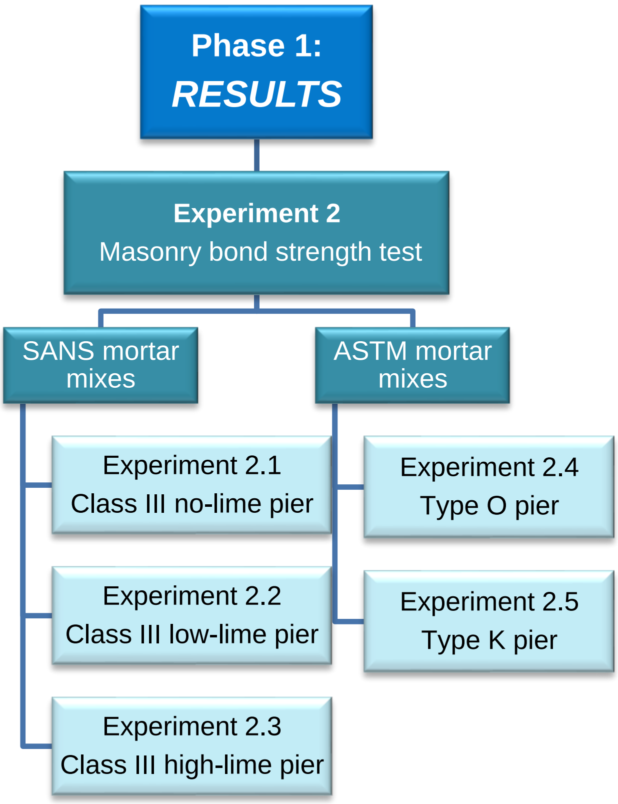

Figure 4.9: Layout of Phase 1 showing the results of the second experiment performed with the different mortar mixes

4.4.1 Experiment 2.1: SANS Class III no-lime mortar pier

In Experiment 2.1, the masonry bond strength between the standard cement bricks and the SANS Class III no-lime mortar mix was determined. The length, pier weight and self-weight of the three piers were almost the same. The concentrated load applied to the three piers differed by approximately 10 kg (approximately 3 bricks). The average concentrated load recorded was close to 38 kg. The final average bond strength was 362 kPa for this mortar mix. Table 4.4 shows the bond strength results of the SANS Class III no-lime mortar mix piers and standard cement bricks:

Table 4.4: Results of the bond strength test for the standard cement brick and SANS Class III no-lime piers

Pier	Pier length	Clear span (L_b)	Pier weight	Self-weight (W_1)	Concentrated load (W_2)	Number of bricks loaded	Bending moment (M)	Section modulus (Z)	Bond strength (δ)
	mm	mm	kg	kg	kg		N.mm	$\times 10^3$ mm^3	kPa
1	640	570	33.9	30.2	40.2	12	48,923.4	179,666.7	377.79
2	640	570	33.8	30.1	43.5	13	52,816.5	179,666.7	398.99
3	640	570	33.8	30.1	30.0	9	37,093.0	179,666.7	311.63
Average			*33.9*	*30.1*	*37.9*	*11*	*46,277.6*	*179,666.7*	*362.80*

4.4.2 Experiment 2.2: SANS Class III low-lime mortar pier

In Experiment 2.2, the standard cement bricks and SANS Class III low-lime mortar mix were used to conduct the masonry bond strength test. The three piers had similar length, weight and self-weight results. The average concentrated load recorded for this mortar mix was pushing 40 kg (12 bricks), resulting in a bond strength just over 417 kPa. Table 4.5 shows the results of the standard cement bricks and SANS Class III low-lime mortar piers:

Table 4.5: Results of the bond strength test for the standard cement brick and SANS Class III low-lime piers

Pier	Pier length	Clear span (L_b)	Pier weight	Self-weight (W_1)	Concentrated load (W_2)	Number of bricks loaded	Bending moment (M)	Section modulus (Z)	Bond strength (δ)
	mm	mm	kg	kg	kg		N.mm	$\times 10^3$ mm^3	kPa
1	705	635	32.9	29.6	22.8	7	31,938.0	179,666.7	292.93
2	705	635	32.6	29.4	84.5	26	111,993.2	179,666.7	737.63
3	705	635	32.6	29.4	13.2	4	19,396.5	179,666.7	222.24
Average			*32.7*	*29.5*	*40.2*	*12*	*54,442.6*	*179,666.7*	*417.60*

4.4.3 Experiment 2.3: SANS Class III high-lime mortar pier

With Experiment 2.3, the test of the masonry bond strength was conducted using the SANS Class III high-lime mortar and standard cement bricks. During this test, one pier broke under its own self-weight and no concentrated load could be placed on that pier. The bond strength of the pier that broke under its own self-weight was not included to determine the average bond strength for the SANS Class III high-lime mortar. This resulted in an average concentrated load of 20 kg between the remaining two piers. The average bond strength of the three piers resulted in just under 344 kPa. Table 4.6 shows the results of the standard cement bricks and the SANS Class III high-lime mortar piers:

Table 4.6: Results of the bond strength test for the standard cement brick and SANS Class III high-lime piers

Pier	**Pier length**	**Clear span** (L_b)	**Pier weight**	**Self-weight** (W_1)	**Concentrated load** (W_2)	**Number of bricks loaded**	**Bending moment** (M)	**Section modulus** (Z)	**Bond strength** (δ)
	mm	**mm**	**kg**	**kg**	**kg**		**Nmm**	**mm^3**	**kPa**
1	720	650	32.7	29.5	0	0	2,398.6	179,666.7	-
2	718	648	33.1	29.9	35.4	11	49,235.5	179,666.7	392.69
3	720	650	32.9	29.7	22.4	7	32,166.6	179,666.7	297.19
Average			*32.9*	*29.7*	*19.3*	*6*	*27,933.5*	*179,666.7*	*344.940*

4.4.4 Experiment 2.4: ASTM Type O mortar pier

In Experiment 2.4, the ASTM Type O mortar mix with the standard cement brick was used in the masonry bond strength test. The concentrated loads applied to all three piers were similar and resulted in an average load of 22 kg (7 bricks). The average bond strength recorded for this mortar mix was higher than those of the SANS high-lime mortar mix and averaged at 290 kPa. Table 4.7 shows the results of the standard cement bricks and the ASTM Type O mortar mix piers:

Table 4.7: Results of the bond test for the ASTM Type O low-lime mortar piers

Pier	Pier length	Clear span (L_b)	Pier weight	Self-weight (W_1)	Concentrated load (W_2)	Number of bricks loaded	Bending moment (M)	Section modulus (Z)	Bond strength (δ)
	mm	mm	kg	kg	kg		Nmm	mm³	kPa
1	705	635	32.4	29.1	16.1	5	23,142.2	179,666.7	242.22
2	710	640	32.6	29.4	25.6	8	35,835.7	179,666.7	314.73
3	713	643	32.3	29.1	25.6	8	35,983.0	179,666.7	315.08
Average			*32.4*	*29.2*	*22.4*	*7*	*31,563.6*	*179,666.7*	*290.68*

4.4.5 Experiment 2.5: ASTM Type K mortar pier

In Experiment 2.5, the masonry bond strength test was conducted on the standard cement bricks and the ASTM Type K mortar mix. The concentrated loads applied to these piers were almost half that of the ASTM Type O mortar mix piers. The bond strength for this mortar mix and standard cement brick resulted in the range of 222 kPa. Table 4.8 shows the results of the standard cement bricks and the ASTM Type K mortar mix piers:

Table 4.8: Results of the bond test for the ASTM Type K mortar piers

Pier	Pier length	Clear span (L_b)	Pier weight	Self-weight (W_1)	Concentrated load (W_2)	Number of bricks loaded	Bending moment (M)	Section modulus (Z)	Bond strength (δ)
	mm	mm	kg	kg	kg		Nmm	mm³	kPa
1	742	672	32.9	29.8	3.2	1	6,894.0	179,666.7	160.91
2	742	672	33.1	29.9	19.3	6	29,020.9	179,666.7	284.82
3	742	672	33.0	29.8	0	0	2,506.7	179,666.7	-
Average			*33.0*	*29.8*	*7.5*	*2*	*12,807.2*	*179,666.7*	*222.865*

4.4.6 Comparative masonry bond strength results

In the masonry bond strength test, the five different mortar mixes were used with the standard cement brick and tested. In the piers built using the SANS Class III no-lime mortar, the workability of the mix was poor owing to an absence of lime in the mix, resulting in a less than perfect bond between the mortar and the brick. In the masonry bond strength test using the SANS Class III low-lime mortar mix, the mix contained half the maximum amount of lime allowed by the SANS National Standards. This gave better workability characteristics, resulting in a better bond between the mortar and the brick. This resulted in a better average bond strength compared to the mortar mix without lime. From here, the SANS Class III high-lime mortar had a higher amount of lime, resulting in the average bond strength gradually declining as the lime increased. With the ASTM Type O mortar mix, the amount of lime in the mix increased as well as the amount of sand. This caused slightly better workability conditions. The bond area between the mortar and brick may have increased slightly, increasing the workability and bond strength. The average bond strength for the ASTM Type O mortar mix was still less than the SANS Class III low-lime mortar mix. With the ASTM Type K mortar mix piers, the highest content of lime and sand was used, and this resulted in the lowest bond strength of the five mortar mixes. Table 4.9 shows the comparative results of the masonry bond strength tests for the SANS and ASTM mortar mixes:

Table 4.9: Comparative results of the masonry bond strength tests for the SANS and ASTM mortar mixes

Pier Material Composition	Average Bond strength (kPa)
SANS Class III no-lime mortar and standard cement brick	362.80
SANS Class III low-lime mortar and standard cement brick	417.60
SANS Class III high-lime mortar and standard cement brick	344.940
ASTM Type O mortar and standard cement brick	290.68
ASTM Type K mortar and standard cement brick	222.865

4.5 Results: Experiment 3 – Deformation Application Test

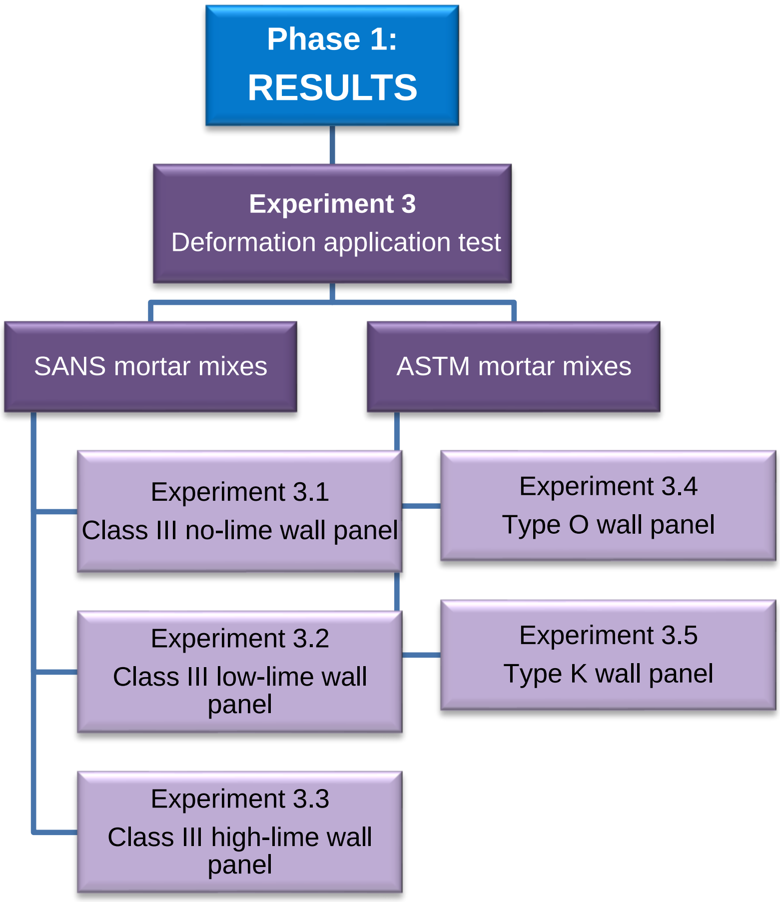

Figure 4.10: Layout of Phase 1 showing the results of the third experiment performed with the different mortar mixes

In Experiment 3, deformation was applied to each of the experimental wall panels which were built using the five different mortar mixes and standard cement brick. For each wall panel a gradual deformation was applied at a steady rate to determine the maximum deformation a wall panel could absorb before failure occurred. The dial gauge placed at the top of each experimental wall panel recorded all deformation applied. As the deformation was applied at a steady rate, the needle of the dial gauge would also move at a steady pace. Once the needle of the gauge would have a sudden jump in movement, it would indicate that failure in the experimental wall pane has occurred. A definition of this failure is an appearance of a crack showing either in the mortar or brick of the wall panel.

In the wall panel built using the standard cement brick and SANS Class III no-lime mortar mix, the failure occurred suddenly, and bricks were broken as the failure crack went straight down without following mortar joints, as was the case with the other walls. In the experimental wall panel built using the SANS Class III low-lime mortar mix and standard cement brick, the failure was less sudden and the crack smaller. In the experimental wall panel built using the standard cement brick and SANS Class III high-lime mortar, the initial crack formed in the vertical joint in the row second from the top. The experimental wall panels built using the ASTM mortar mixes and standard cement bricks failed very quietly. The initial cracks for both the mortar mixes were small and were only detected upon close investigation. The failures for both the ASTM mortar mixes were very quiet and subtle. Table 4.10 shows the results of the experimental wall panels upon initial failure:

Table 4.10: Comparative results of the experimental wall panels upon initial failure

Experimental wall panel materials	**View of experimental wall panel when failure occurred**
Experiment 3.1 Standard cement brick with SANS Class III no-lime mortar mix	

Experimental wall panel materials	View of experimental wall panel when failure occurred
Experiment 3.2 Standard cement brick with SANS Class III low-lime mortar mix	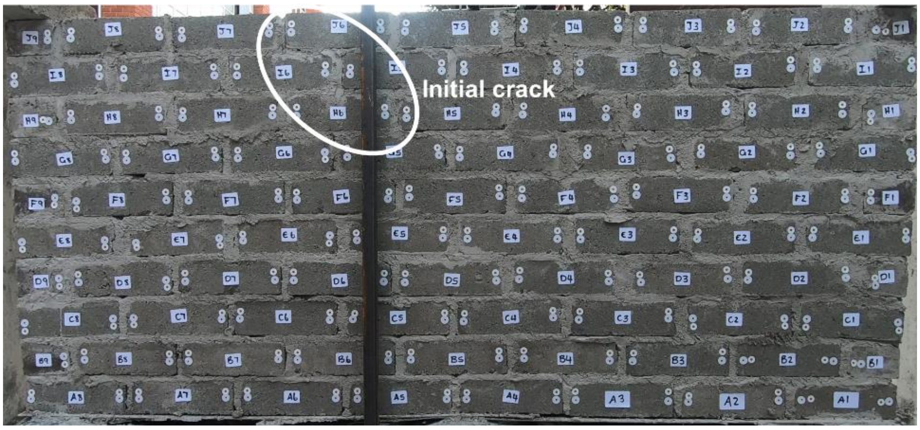
Experiment 3.3 Standard cement brick with SANS Class III high-lime mortar mix	
Experiment 3.4 Standard cement brick with ASTM Type O mortar mix	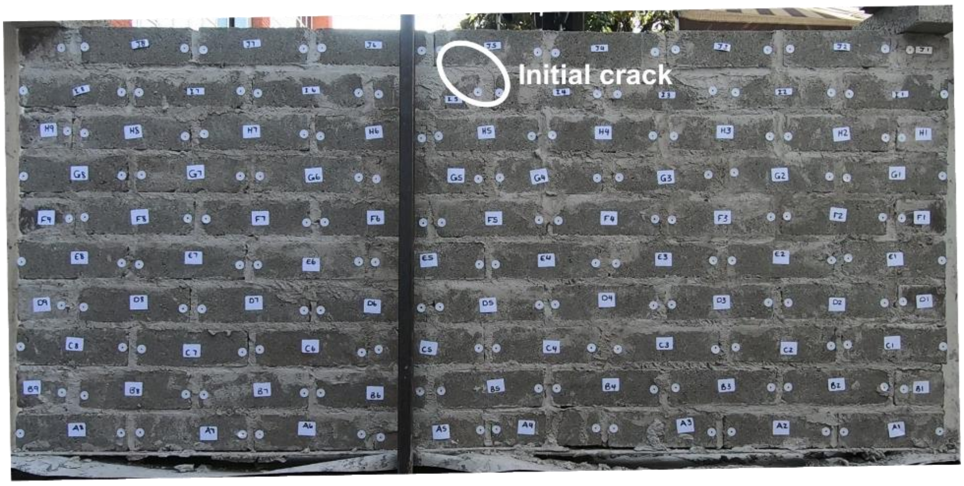

Experimental wall panel materials	View of experimental wall panel when failure occurred
Experiment 3.5 Standard cement brick with ASTM Type K mortar mix	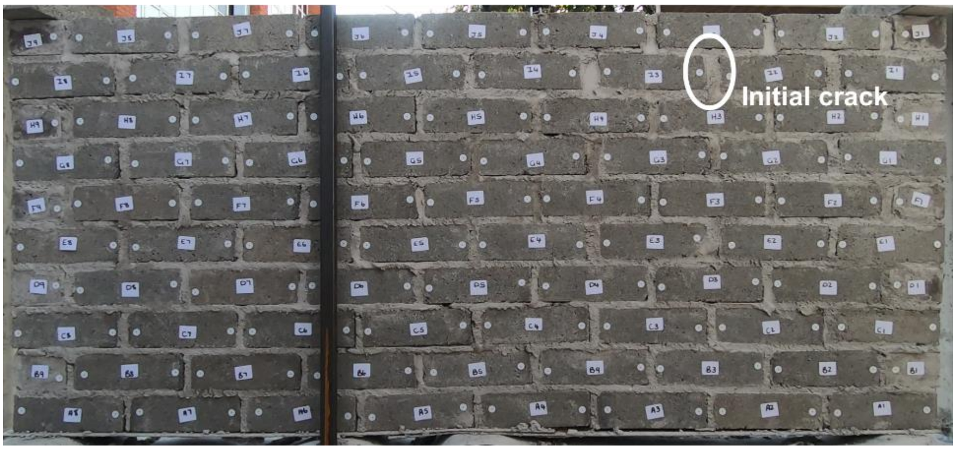

When the failure point had been reached for each experimental wall panel built using the five different mortar mixes, the magnitude of deformation was recorded. The experimental wall panel built using the SANS Class III no-lime mortar mix absorbed the least amount of deformation applied. The SANS Class III low-lime absorbed twice as much deformation as that of the SANS no-lime mortar, whereas the high-lime content of the SANS Class III mortar absorbed a little more. The experimental wall panels built using the ASTM mortar mixes showed the ability of absorbing greater deformations. The experimental wall panel built using the ASTM Type K mortar mix and standard cement brick absorbed the most deformation applied. Table 4.11 shows the comparative results of the deformation each wall panel could absorb before failure occurred:

Table 4.11: Comparative results of the deformation each experimental wall panel absorbed before failure occurred

Mortar Mix Wall Panel	Applied Deformation (mm)
SANS Class III no-lime	0.35
SANS Class III low-lime	0.70
SANS Class III high-lime	0.75
ASTM Type O	0.85
ASTM Type K	1.15

Flexibility Coefficient

In Experiment 3, only the lime content in each of the three SANS mortar mixes differed, whereas the lime and sand content in the two ASTM mortar mixes differed. The addition of lime and sand content to the different mortar mixes resulted in the absorbed deformation of each experimental wall panel increasing before failure occurred. This led to an understanding that as the lime and sand content in each mortar mix increased, the flexibility of the mortar in the wall increased and the strength decreased. The absence of lime content in the SANS Class III no-lime mortar mix resulted in the mortar having the least amount of flexibility and the highest strength, causing the masonry to be brittle. The ASTM Type K mortar with the standard cement brick contained the highest content of lime and sand and resulted in the wall panel with the highest flexibility and the least amount of strength.

Graph 4.6 depicts a comparison of the flexibility of the experimental wall panels built with the different mortar mixes. The content of cement in each mortar mixed remained the same, whereas the lime and sand content of the different mortar mixes differed. Thus, the lime and sand ratios of the different mortar mixes were used to create a formula to determine a proposed flexibility coefficient of the different mortar mixes. This coefficient shows that when no lime is present in a mortar mix, the deformation would be at a minimum. As the sand and lime content rises in a particular mortar mix, the flexibility coefficient rises as well, resulting in a higher ability of deformation absorption before failure will occur.

$$x = 0.7(l) + 0.1(s) \tag{4.7}$$

Where:

x = flexibility coefficient

l = ratio of lime to cement in the mortar mix

s = ratio of sand to cement in the mortar mix

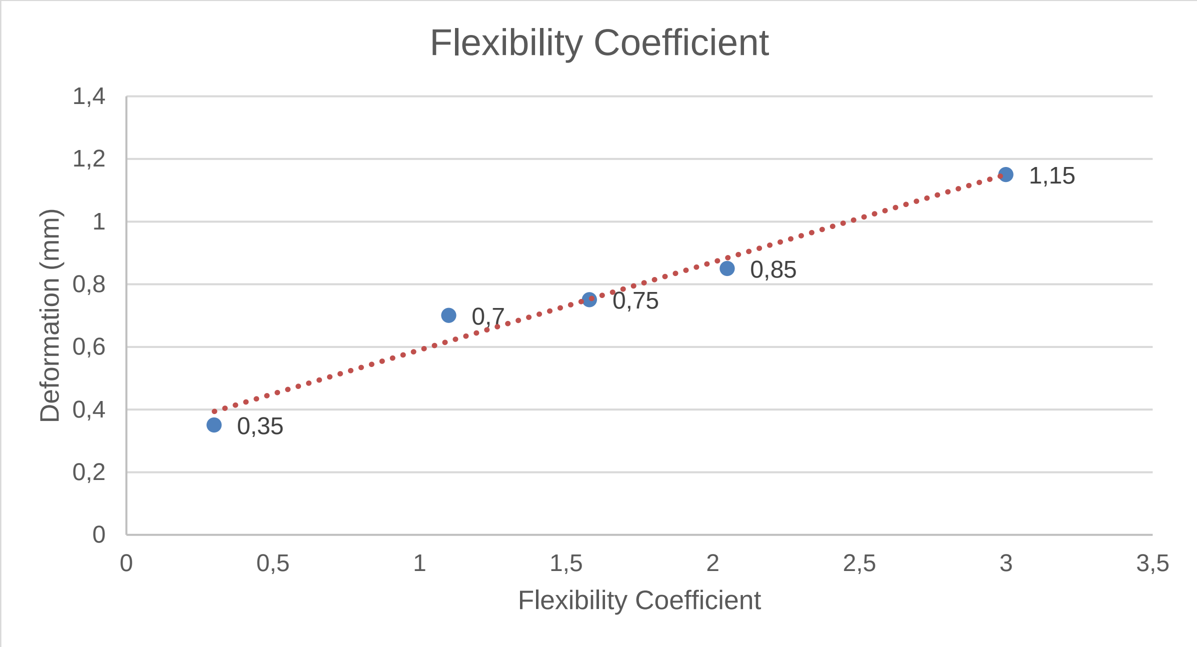

Graph 4.6: Flexibility coefficient comparison of the different mortar mixes in the experimental wall panels

4.6 Conclusion

The experiments conducted in Phase 1 showed the performance of different mortar mixes. The results determined in Experiment 1 indicated that the higher the content of lime and sand in a mortar mix, the more the material will absorb deformation before failure occurs, thus being more flexible. Experiment 2 indicated that the content of lime influenced the workability of the mortar and bond strength between the mortar and brick. In the final experiment, Experiment 3, the flexibility of the experimental wall panels depended on the content of lime and sand in a mortar mix. The lower the lime and sand content in a mortar mix, the more brittle the mortar higher the strength of the masonry with little to no flexibility. The higher the lime and sand content in a mortar mix, the higher the flexibility of the masonry and lower the strength.

CHAPTER 5: FINITE ELEMENT MODELS

5.1 Introduction

In Chapter 5, three analyses were performed using a software package locally available at the Central University of Technology, Bloemfontein campus to determine the difference in stress patterns found in the brick and mortar because of applied deformation to a wall panel. In Analysis 1, an initial finite element model was designed, and the mesh of the initial finite element model refined to create four mesh refined models using the mesh refinement method. The mesh refinement models were then used to create five finite element wall panels. In the second analysis, the performance of the five finite element wall panels was analysed to determine the appropriate mesh refinement for further performance analysis of mortar material properties. In Analysis 3, one of the five finite element wall panels was used to analyse the performance of the material properties of four different mortar mixes, two from the SANS 10164-1 and two from Costigan et al. (2015), alongside the material properties of the standard cement brick. Figure 5.1 shows the layout of Phase 2 and the analyses that were performed:

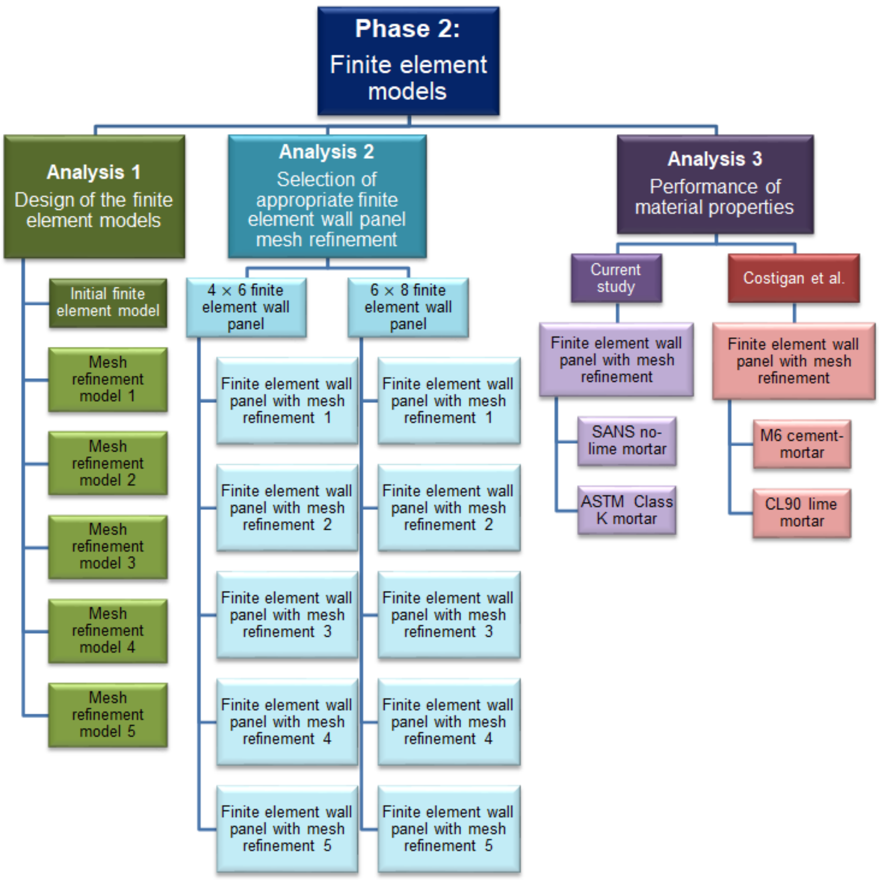

Figure 5.1: Layout of Phase 2 showing the three analyses performed

5.2 Materials and Methods

5.2.1 Materials and analyses

In Phase 2, three analyses were performed using a finite element analysis software package locally available to students and staff at the Central University of Technology. The software package, Prokon, was used in the analysis of various finite element designs.

The software package, Prokon, consists of three types of elements for frame analyses (Prokon Software Consultants, 2010). The first being the beam element where element forces can be placed directly onto a beam element in a positive or negative vertical direction. The second element type is the shell element. Shell elements can be used alongside normal beam elements. For this purpose, Prokon uses four-node quadrilateral and three-node triangular isoparametric shell elements with plate bending and membrane behaviour. Both the quadrilateral and triangular elements yield accurate stiffness modelling. However, stress recovery from the triangular elements is not as accurate as in the case for quadrilateral elements. Therefore, deflections using triangular elements are generally quite accurate, but moments may be less accurate. The shell element is particularly used in the design of flat slabs supported on columns or walls. Solid elements are the third type of finite element. In solid elements, there are 8-noded hexahedral and 4-noded tetrahedral elements. These elements have three rotational degrees of freedom per node and are generally more accurate than more commonly used solid elements that do not have rotational degrees of freedom. Both the hexahedral and tetrahedral elements yield accurate stiffness modelling. However, stress recovery from the tetrahedral elements is not as accurate as is the case for hexahedral elements. That said, the deflections calculated using tetrahedral elements are generally quite accurate, but stresses may be less accurate. In this study, the third type of finite element, the solid finite element, was used in the design of the finite element model.

To analyse a finite element, a set of material parameter had to be added to the material database of the software program and be assigned to a specified element. Not all material parameter inputs are the same as Prokon categorises the material database into five categories: Steel, Concrete, Timber, Aluminium, and Other. For this study, the category of 'Other' was used to add the specified materials to the database. Under this category, the following set of material parameters were required: Young's modulus (kN/m^2), Poisson's ratio, Density of material (kN/m^3), Expansion coefficient, and specified compression Stress/Strain values of each material type. Table 5.1 provides the values of the Prokon material properties.

Table 5.1: Prokon material properties input

Material	Young's modulus, *E* (kN/m^2)	Poisson's ratio	Density (kN/m^3)	Expansion coefficient	Stress/Strain values	
					Strain	**Stress (MPa)**
Cement brick	$15\,000 \times 10^3$	0.2	25	10×10^{-6}	-3.5×10^{-3}	-1.0
					0.0	0.0
					110.0×10^{-6}	2.6
					210.0×10^{-6}	5.0
					320.0×10^{-6}	7.2
					430.0×10^{-6}	9.1
					540.0×10^{-6}	10.7
					640.0×10^{-6}	12.1
					750.0×10^{-6}	13.2
					860.0×10^{-6}	14.1
					970.0×10^{-6}	14.7
					1.07×10^{-3}	15.1
					3.5×10^{-3}	15.8
SANS No-lime	$2\,200 \times 10^3$	0.2	25	10×10^{-6}	4.4×10^{-7}	0.97×10^{-3}
					1.3×10^{-6}	2.91×10^{-3}
					2.2×10^{-6}	4.85×10^{-3}
					3.1×10^{-6}	6.78×10^{-3}
					3.9×10^{-6}	8.72×10^{-3}
					4.9×10^{-6}	10.66×10^{-3}
					5.7×10^{-6}	12.60×10^{-3}
					6.6×10^{-6}	14.54×10^{-3}
					7.5×10^{-6}	16.47×10^{-3}
					8.4×10^{-6}	18.41×10^{-3}

Material	Young's modulus, *E* (kN/m^2)	Poisson's ratio	Density (kN/m^3)	Expansion coefficient	Stress/Strain values: Strain	Stress/Strain values: Stress (MPa)
					9.3×10^{-6}	20.35×10^{-3}
					1.01×10^{-5}	22.29×10^{-3}
					1.06×10^{-5}	23.26×10^{-3}
SANS Low-lime	$1\,700 \times 10^{3}$	0.2	25	10×10^{-6}	5.06×10^{-7}	0.86×10^{-3}
					1.5×10^{-6}	2.58×10^{-3}
					2.5×10^{-6}	4.30×10^{-3}
					3.5×10^{-6}	6.03×10^{-3}
					4.6×10^{-6}	7.75×10^{-3}
					5.6×10^{-6}	9.47×10^{-3}
					6.6×10^{-6}	11.19×10^{-3}
					7.6×10^{-6}	12.91×10^{-3}
					8.6×10^{-6}	14.63×10^{-3}
					9.6×10^{-6}	16.36×10^{-3}
					1.06×10^{-5}	18.08×10^{-3}
					1.2×10^{-5}	19.80×10^{-3}
					1.2×10^{-5}	20.66×10^{-3}
SANS High-lime	$1\,300 \times 10^{3}$	0.2	25	10×10^{-6}	7.04×10^{-7}	0.91×10^{-3}
					2.1×10^{-6}	2.74×10^{-3}
					3.5×10^{-6}	4.57×10^{-3}
					4.9×10^{-6}	6.40×10^{-3}
					6.3×10^{-6}	8.23×10^{-3}
					7.7×10^{-6}	10.06×10^{-3}
					9.2×10^{-6}	11.89×10^{-3}
					1.06×10^{-5}	13.72×10^{-3}
					1.2×10^{-5}	15.55×10^{-3}
					1.3×10^{-5}	17.38×10^{-3}
					1.5×10^{-5}	19.21×10^{-3}
					1.6×10^{-5}	21.04×10^{-3}
					1.7×10^{-5}	21.96×10^{-3}
ASTM Type O	$1\,200 \times 10^{3}$	0.2	25	10×10^{-6}	7.06×10^{-7}	0.85×10^{-3}
					2.1×10^{-6}	2.54×10^{-3}
					3.5×10^{-6}	4.24×10^{-3}
					4.9×10^{-6}	5.93×10^{-3}
					6.3×10^{-6}	7.62×10^{-3}
					7.7×10^{-6}	9.32×10^{-3}
					9.2×10^{-6}	11.02×10^{-3}

Material	Young's modulus, *E* (kN/m²)	Poisson's ratio	Density (kN/m³)	Expansion coefficient	Stress/Strain values	
					Strain	Stress (MPa)
					1.06×10^{-5}	12.72×10^{-3}
					1.2×10^{-5}	14.41×10^{-3}
					1.3×10^{-5}	16.11×10^{-3}
					1.5×10^{-5}	17.80×10^{-3}
					1.6×10^{-5}	19.50×10^{-3}
					1.7×10^{-5}	20.34×10^{-3}
ASTM Type K	850×10^{3}	0.2	25	10×10^{-6}	9.3×10^{-7}	0.79×10^{-3}
					2.8×10^{-6}	2.38×10^{-3}
					4.7×10^{-6}	3.96×10^{-3}
					6.5×10^{-6}	5.54×10^{-3}
					8.4×10^{-6}	7.13×10^{-3}
					1.02×10^{-5}	8.73×10^{-3}
					1.2×10^{-5}	10.29×10^{-3}
					1.4×10^{-5}	11.88×10^{-3}
					1.6×10^{-5}	13.46×10^{-3}
					1.8×10^{-5}	15.05×10^{-3}
					1.9×10^{-5}	16.63×10^{-3}
					2.1×10^{-5}	18.21×10^{-3}
					2.2×10^{-5}	19.00×10^{-3}

The material properties of the five different mortar mixes and standard cement brick was added to the Prokon material database for further analysis. A second-order analysis was performed during the analysis process, as masonry can range from a linear to a non-linear material. (Costigan et al., 2015a) explains that as the strength of a mortar decreases, the stress-strain relationship becomes more non-linear. Therefore, a stronger mortar will have a more linear stress-strain relationship. The second-order analysis considers the linear and non-linear stress-strain relationship of these materials ranging from a strong to a weaker mortar mix.

In Analysis 1, an initial finite element model was designed, and the mesh of the model refined to create five other mesh refinement models. The five mesh refinement models were used to design five finite element wall panels. In Analysis 2, the performance of the five finite element wall panels was analysed to ascertain which of the finite element wall panel(s) with selected mesh refinement had the potential of illustrating the most consistent results concerning the maximum and minimum stress within a wall panel compared to the other finite element wall panels. The finite element wall panels illustrating the most consistent results were selected for further performance analysis and subsequent practical experimentation. In Analysis 3, a finite element wall panel with selected mesh refinement was used to analyse the performance of four specified mortar mixes including those of Costigan et al. (2015). Table 5.2 shows the series of analyses performed in Phase 2:

Table 5.2: Series of analyses performed in Phase 2

Analysis	Description	Models	
1. Design of initial finite element model and mesh refinements	During this analysis, an initial finite element model was designed, and the mesh of that model refined to create five mesh refinements. Five 4 × 6 brick element wall panels were then designed using the five mesh refinements.	Mesh refinement model 1	Finite element wall panel with mesh refinement 1
		Mesh refinement model 2	Finite element wall panel with mesh refinement 2
		Mesh refinement model 3	Finite element wall panel with mesh refinement 3
		Mesh refinement model 4	Finite element wall panel with mesh refinement 4
		Mesh refinement model 5	Finite element wall panel with mesh refinement 5
2. Selection of appropriate finite element wall panel mesh refinement	During this analysis, the performance of two different finite element wall panels and refinements were analysed	Ten finite element wall panels designed using the five mesh refinements. Each finite element wall panel was assigned the material properties of the standard cement brick and SANS no-lime mortar mix.	
3. Performance of material properties using a selected finite element wall panel	The performance of the standard cement brick and four different mortar material properties were analysed using a selected finite element wall panel.	Selected finite element wall panel with Standard cement brick and SANS no-lime mortar material properties	
		Selected finite element wall panel with Standard cement brick and ASTM Type K mortar material properties	
		Selected finite element wall panel with Standard cement brick and cement-lime (M6) mortar material properties	
		Selected finite element wall panel with Standard cement brick and hydrated lime (CL90) mortar material properties	

5.2.2 Software package used for the design of the Finite Element Model

In this study, the software package Prokon, was used for the design of the different finite element models. Prokon is a structural design computer package that was created in 1989 by South Africans Karl Eschberger and Jacques Pienaar (Eschberger & Pienaar, 1989). Prokon is a modular system that includes frame and finite element analysis, steel member and connection design, concrete design and detailing, and several other analyses. The software supports a comprehensive array of design codes including the codes of Europe, the United States, Canada, India, Australia, and South Africa. Prokon was selected for this study because it is available to staff and students at the Central University of Technology, Free State, where the study was conducted.

The Prokon software consists of various components that were used in the design process of the initial finite element model in this study. These design components are accessible from the top ribbon of the Prokon software user interface, showing each component in a different tab (Figure 5.2). Each design component is used for a different type of material analysis and consists of several specific sub-components. The *Analysis* tab provides the sub-components to design and analyse structural elements, while the sub-components in the *Steel* tab are used for the design and analysis of steel members and combinations of steel members. In the *Concrete* tab, sub-components are found for the design and analysis of various concrete beams, footings, slabs, piles, and other concrete elements. The sub-components in the *Timber & Masonry* tab are used for the design and analysis of timber sections and masonry sections. The *General* tab contains sub-components used for the design of gutters and analysis of wind. The sub-components of the *Geotechnical* tab are used for the design and analysis of soil and rock conditions. The material database of the Prokon software can be found in the *General* component tab. In this study, the finite element model was designed using the *Frame* analysis sub-component in the *Analysis* component.

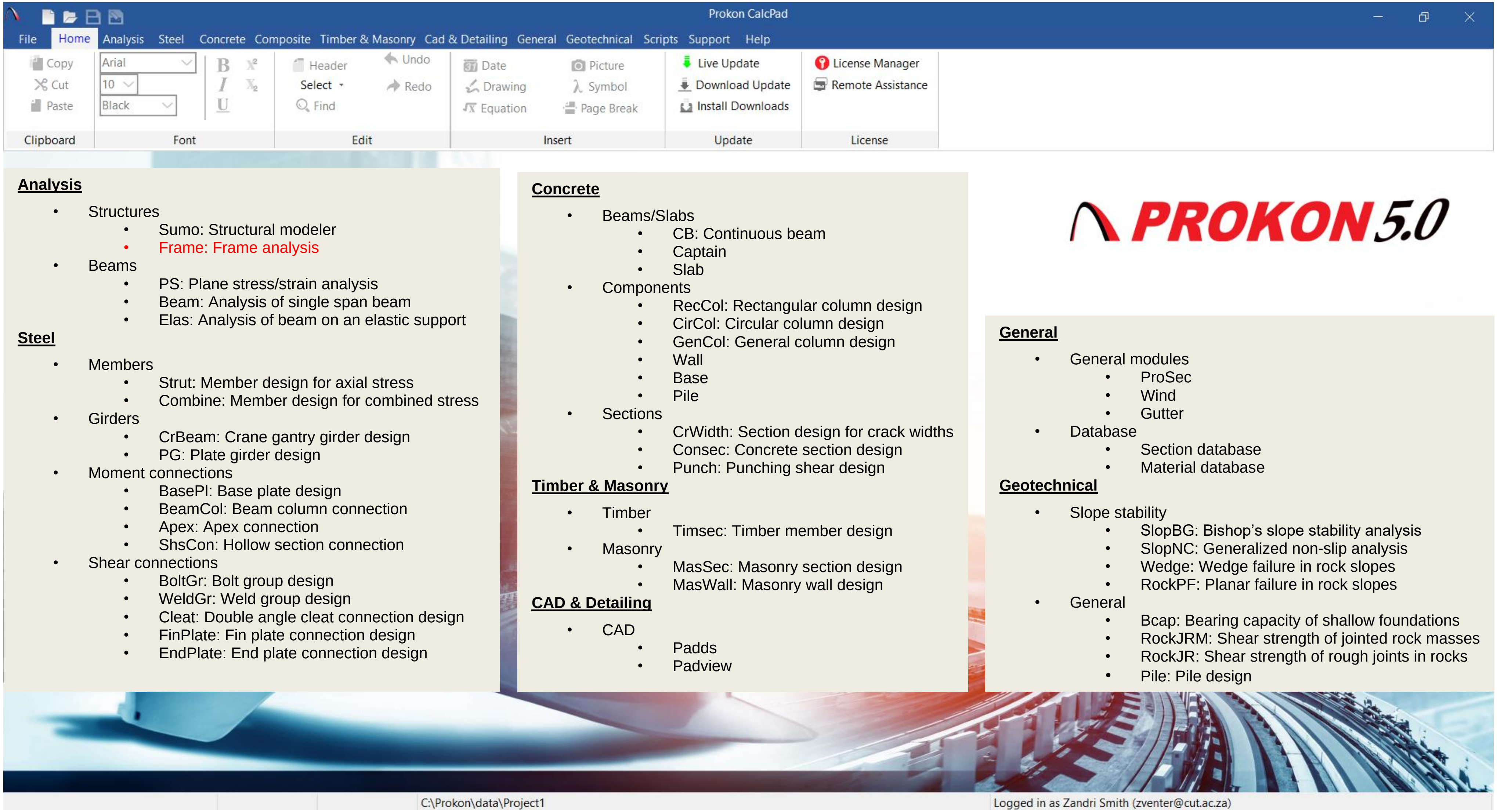

Figure 5.2: User interface showing the components and sub-components of Prokon

5.3 Analysis 1: Design of the Finite Element Models

In the Prokon environment, an initial finite element model was designed using the frame analysis sub-component of the Analysis component. The model was designed using a series of nodes, determining the outer boundaries of the model, after which a solid element was used to fill the space between the nodes. The initial finite element model consisted of a single brick solid element and a mortar solid element. Figure 5.3 shows the initial finite element model designed:

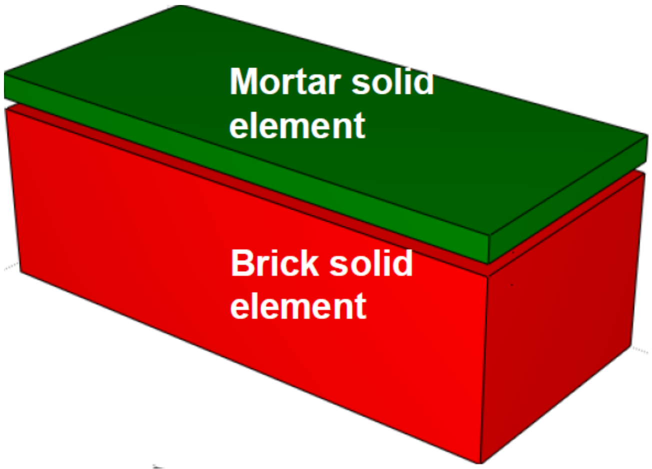

Figure 5.3: View of the initial finite element model with a brick and mortar solid elements

A finite element wall was designed using the brick solid elements of the initial model and mortar solid elements placed vertically and horizontally to join the components. The finite element wall panel had dimensions of 4 × 6 bricks (910 × 480 mm) where four bricks were placed horizontally, and six courses high. The size and placement of the nodes at the corners of each brick and mortar solid element limited the arrangement of the elements to a stack bond pattern. Figure 5.4 illustrates the finite element wall panel designed using the initial model in a stack bond pattern:

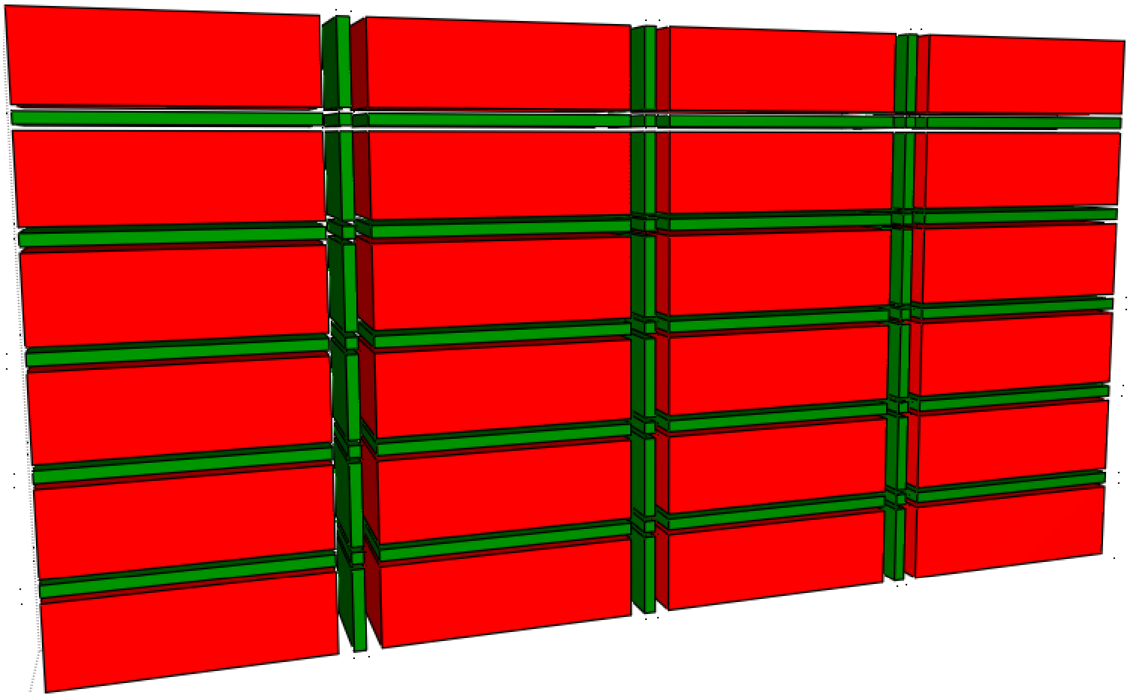

Figure 5.4: Finite element wall panel of initial model in a stack bond pattern

The brick and mortar solid elements in a stack bond arrangement are not a pattern used in the construction of light masonry structures, but rather the stretcher bond arrangement of bricks. To accomplish the stretcher bond pattern, the brick solid elements must be re-arranged so that a brick solid element is placed perpendicularly above a vertical mortar solid element. The arrangement of the elements in a stretcher bond pattern resulted in the brick and mortar solid elements being inadequate for analysis owing to nodal arrangements' not complying with analysis protocols. A refinement of the brick and mortar solid elements of the initial finite element model had to be considered. To be able to use the nodes of the vertical mortar solid element in the middle of the brick solid element above, the brick solid element had to have the same size element in the middle. This allowed for a refinement where the brick solid element was divided into three smaller solid elements. Two of the solid elements were bigger, flanking a smaller brick solid element in the middle that was situated directly above a vertical mortar solid element. Figure 5.5 shows the first mesh refinement of the initial finite element model:

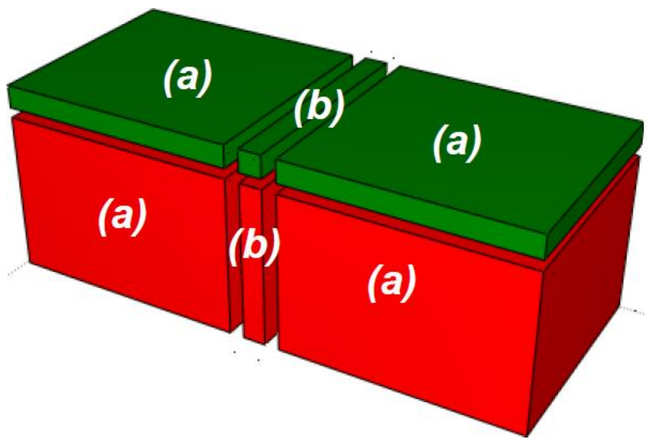

Figure 5.5: View of the first mesh refinement model **a.** bigger solid elements shouldering the **b.** smaller solid elements

The first mesh refinement of the initial finite element model was implemented to design a finite element wall panel with dimensions of 4 × 6 bricks (910 × 480 mm). The arrangement of the brick and mortar solid elements in the stretcher bond pattern was implemented where a brick solid element was placed directly above a vertical mortar solid element. Figure 5.6 shows the finite element wall panel designed using the first mesh refinement model:

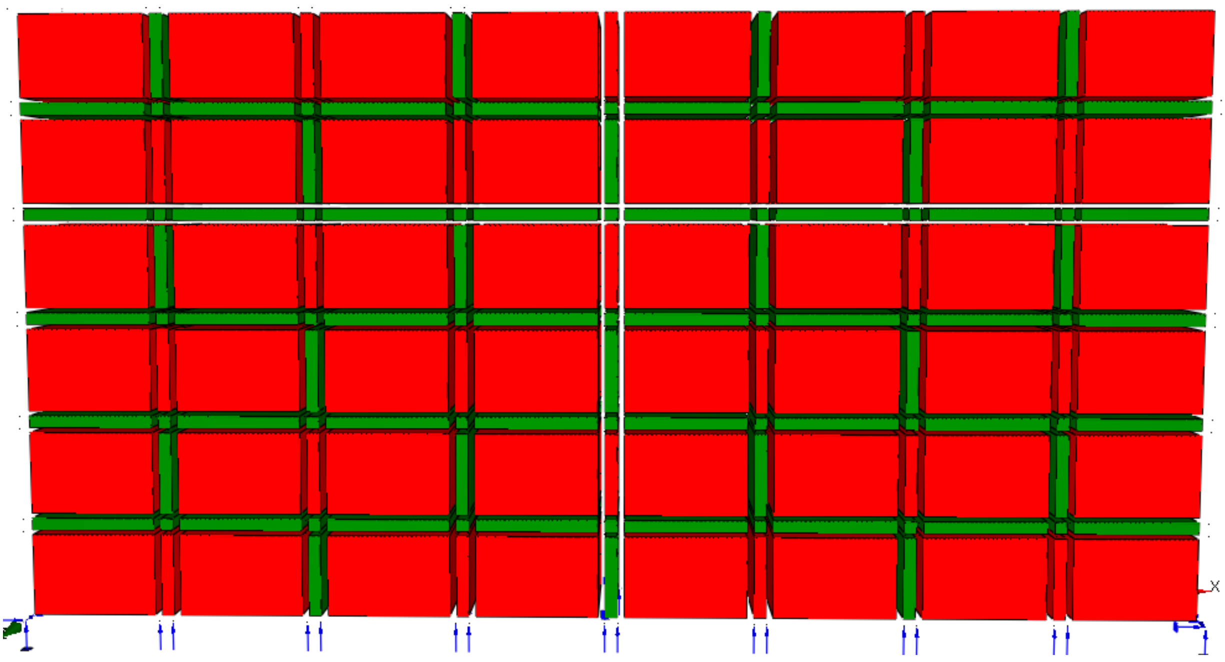

Figure 5.6: Finite element wall panel designed using the first mesh refinement

Following the same mesh refinement process as the design of the first mesh refinement model, four mesh refinements were designed, each consisting of a smaller mesh size than the previous mesh refinement model. Table 5.3 shows the initial model and the five mesh refinement models along with their different brick and mortar element mesh sizes and number of elements:

Table 5.3: View of the initial finite element model and five mesh refinement models

Model name	**View of model**	**Number of elements per element size and type**	**Size per element L × B × W (mm)**
Initial finite element model	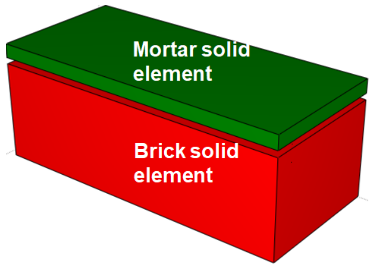	Mortar: 1	Mortar: 220 × 98 × 10
		Brick: 1	Brick: 220 × 98 × 70
Mesh refinement model 1	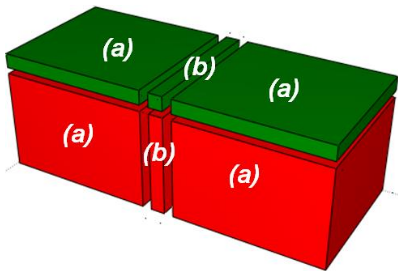	Mortar: 2 *(a)* 1 *(b)*	Mortar: 105 × 98 × 10 *(a)* 10×98×10 *(b)*
		Brick: 2 *(a)* 1 *(b)*	Brick: 105 × 98 × 70 *(a)* 10 × 98 × 70 *(b)*
Mesh refinement model 2	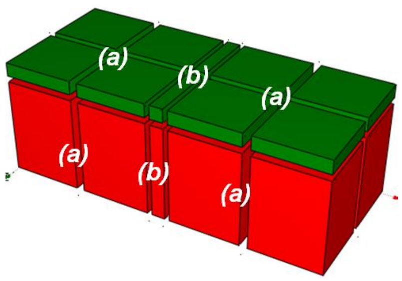	Mortar: 8 *(a)* 2 *(b)*	Mortar: 52.5 × 49 × 10 *(a)* 10 × 49 × 10 *(b)*
		Brick: 8 *(a)* 2 *(b)*	Brick: 52.5 × 49 × 70 *(a)* 10 × 49 × 70 *(b)*
Mesh refinement model 3		Mortar: 9 *(a)* 3 *(b)*	Mortar: 35 × 32.67 × 10 *(a)* 10 × 32.67 × 10 *(b)*

Model name	View of model	Number of elements per element size and type	Size per element L × B × W (mm)
	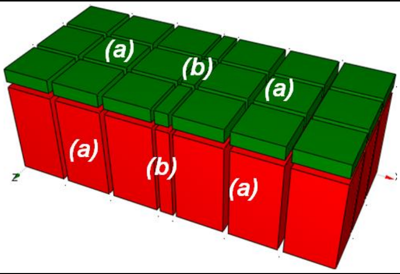	Brick: 9 *(a)* 3 *(b)*	Brick: 35 × 32.67 × 70 *(a)* 10 × 32.67 × 70 *(b)*
Mesh refinement model 4	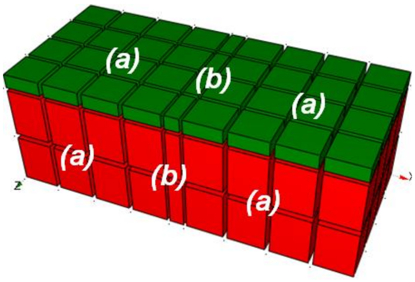	Mortar: 32 *(a)* 8 *(b)*	Mortar: 26.2 × 24.5 × 10 *(a)* 10 × 24.5 × 10 *(b)*
		Brick: 64 *(a)* 8 *(b)*	Brick: 26.2 × 24.5 × 35 *(a)* 10 × 24.5 × 35 *(b)*
Mesh refinement model 5	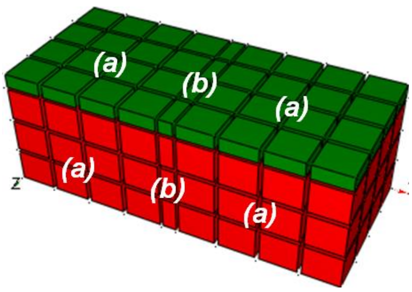	Mortar: 32 *(a)* 8 *(b)*	Mortar: 26.2 × 24.5 × 10 *(a)* 10 × 24.5 × 10 *(b)*
		Brick: 96 *(a)* 8 *(b)*	Brick: 26.2 × 24.5 × 23.3 *(a)* 10 × 24.5 × 23.3 *(b)*

Each of the five mesh refinement models was used to analyse five finite element wall panels. Each finite element wall panel had dimensions of 4 × 6 bricks. A view of the five finite element wall panels using the five mesh refinements is tabulated in Table 5.4.

Table 5.4: View of the five finite element models using the five mesh refinements

Mesh refinement model	**View of the finite element wall panel**
1	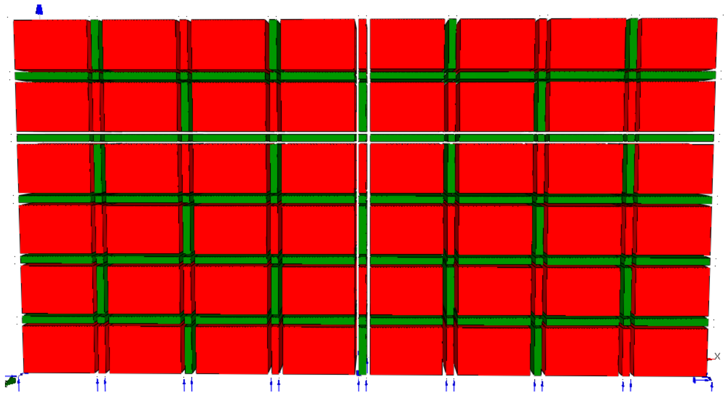
2	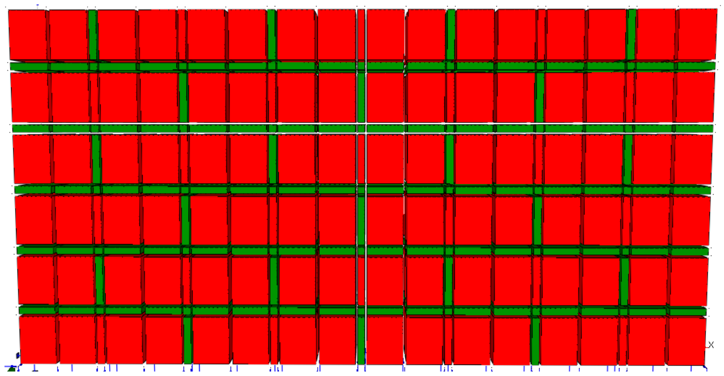
3	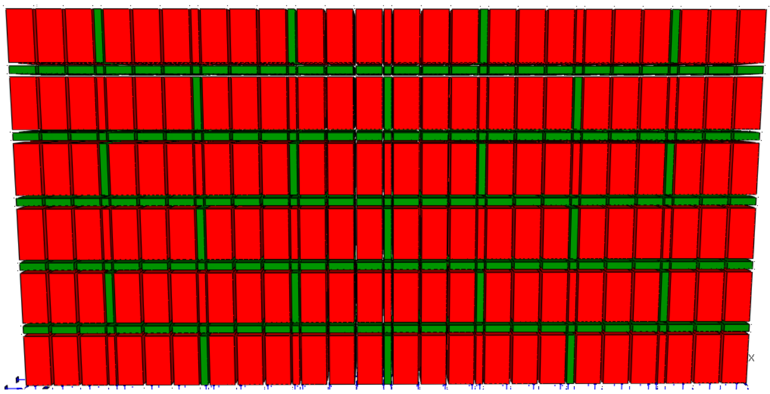
4	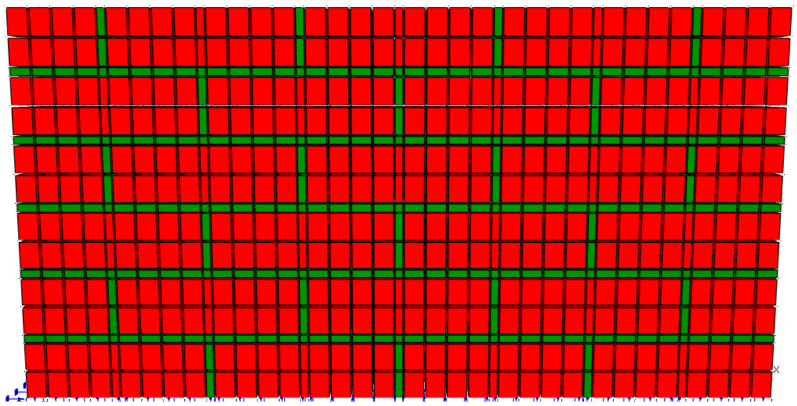

Mesh refinement model	View of the finite element wall panel
5	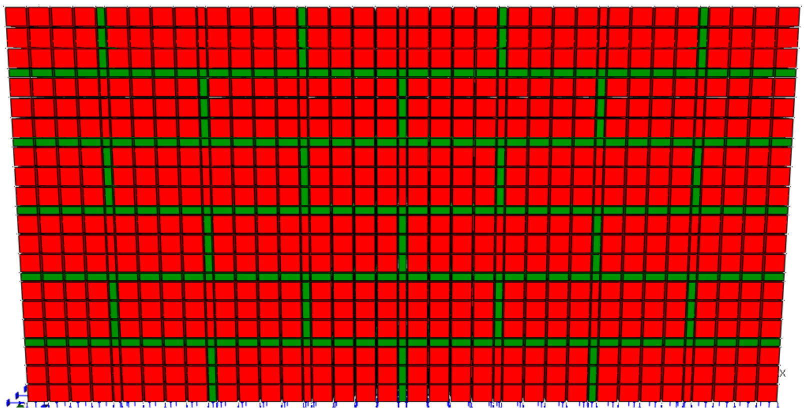

5.4 Analysis 2: Selection of appropriate mesh refinement

The performance of the finite element wall panel was analysed using a set of parameters. The brick solid elements in each of the wall panels had the material properties of a standard cement brick and the material properties of two different types of mortar mixes. The material properties of the SANS no-lime mortar mix with an approximate 2 GPa Young's modulus and ASTM Type K with Young's modulus of just over 0.8 GPa were used, as the SANS no-lime mortar mix illustrated to have the highest strength with lowest flexibility and the ASTM Type K mortar mix the opposite of low strength and high flexibility. Two different sized finite element wall panels with dimensions of 4 × 6 and 6 × 8 were analysed. Each of the two different finite element wall panels was fully restrained from movement at one bottom corner of the wall panel to keep the panel from lifting and falling over.

The flexibility of masonry is currently at a ratio of 1:3500, meaning that for every 3,500 mm wall panel in length, a 1 mm deformation applied could possibly cause damage to a normal non-flexible mortar. The size of the experimental wall panel used in this study is of a ratio of approximately 1:1800, where for every wall panel with length of 1,800 mm, a deformation of approximately 1 mm was applied. A 1 mm dome displacement was thus applied over the bottom area of each wall panel. Figure 5.7 shows the outline of a finite element wall panel in black, with the dome displacement in red applied to each wall panel. A maximum displacement of 1 mm is located at the central bottom area of the wall panel, and gradually becoming less at it reaches the two bottom ends. After the addition of the dome displacement, the performance of the in-plane stresses between the differing brick and mortar materials properties, was analysed. The application of the dome displacement applied to the finite element model replicates the displacement expansive clay exercises on a physical masonry wall panel.

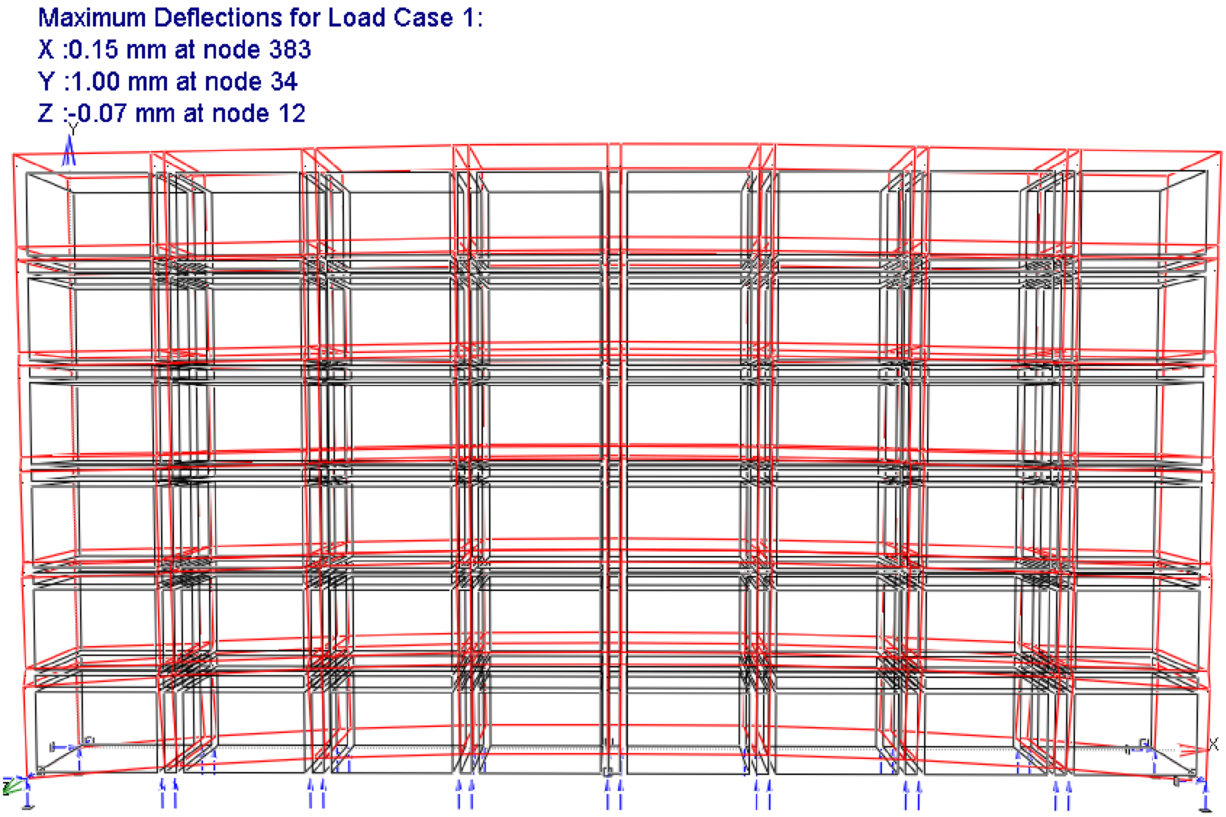

Figure 5.7: Outline of finite element wall panel with displacement added

5.4.1 4 × 6 Finite element wall panel

In the 4 × 6 finite element wall panel with the first mesh refinement and the SANS no-lime mortar material properties, the maximum tensile stress was located at the two bottom corners of the finite element wall panel. The maximum compressive stress was also located in the bottom row of brick solid elements of the wall panel. A similar stress pattern was found in the wall panel with the ASTM Type K mortar material properties. The difference in tensile stress between the finite element wall panels with the SANS and ASTM mortar was ranging at 10 MPa, whereas the maximum compressive stress was far less at 2 MPa difference. A distinct difference of stress in the brick and mortar solid elements was visible for both the SANS and ASTM mortar material properties.

The finite element wall panels with the second mesh refinement showed a significant decrease in overall stress compared to the finite element wall panel with the first mesh refinement. The maximum tensile stress was located in the central area of the top row of brick solid elements for both the SANS and ASTM finite element wall panels. The tensile stress for the SANS wall panel reached an upper limit at just under 9 MPa, where the maximum tensile stress in the ASTM finite element wall panel was half that of the SANS. The maximum compressive stress was in close range, differing with 3 MPa.

In the finite element wall panel with the third mesh refinement, the maximum tensile stress for both the SANS and ASTM wall panels was similar to those of the second mesh refinement. The same could be said about the maximum compressive stress in both wall panels. The maximum tensile stress in the SANS finite element wall panel with the fourth mesh refinement was approximately 9 MPa, whereas the ASTM wall panel had a tensile stress of half that of the SANS. The difference in maximum compressive stress between the SANS and ASTM remained almost the same as in the finite element wall panel with mesh refinement three. In the wall panel with mesh refinement five, the maximum tensile and compressive stress was near to identical to the wall panel of the fourth mesh refinement.

In all the finite element wall panels, the wall panels with the SANS mortar material properties showed a stress almost twice as high compared to the ASTM mortar material properties. This indicated that when a mortar mix with a higher Young’s modulus was used, the overall stress in a wall panel increased. When a mortar with a much lower Young’s modulus was used, the overall stress in the wall panel decreased. This analysis concurred with the results of the tests conducted on the physical experimental wall panels, where a higher Young’s modulus resulted in a more rigid masonry wall panel, compared to the lower Young’s modulus wall panel. Table 5.5 shows the performance of the different finite element wall panels with different mortar material properties:

Table 5.5: Performance of the finite element wall panel using different mortar material properties

Model Name	SANS no-lime mortar material properties	ASTM K mortar material properties
Finite element wall panel with mesh refinement 1	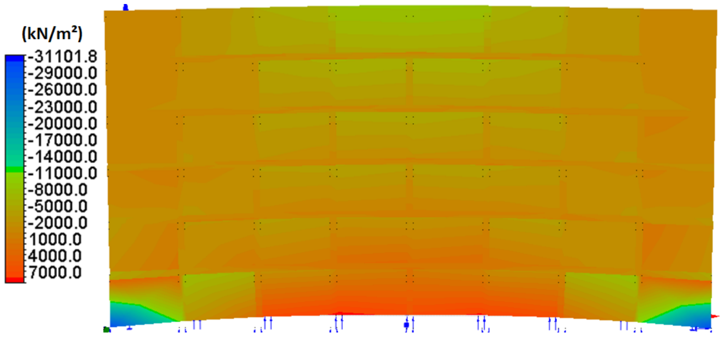	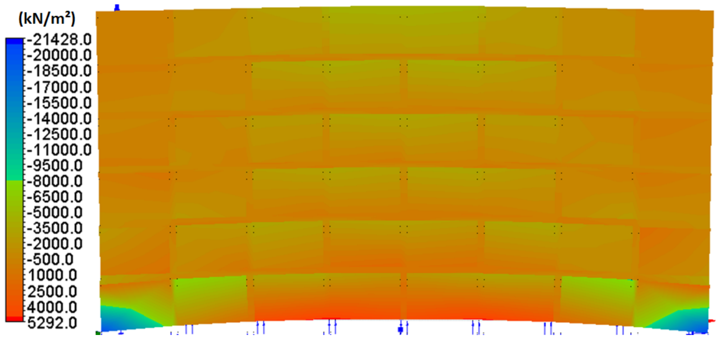
Finite element wall panel with mesh refinement 2	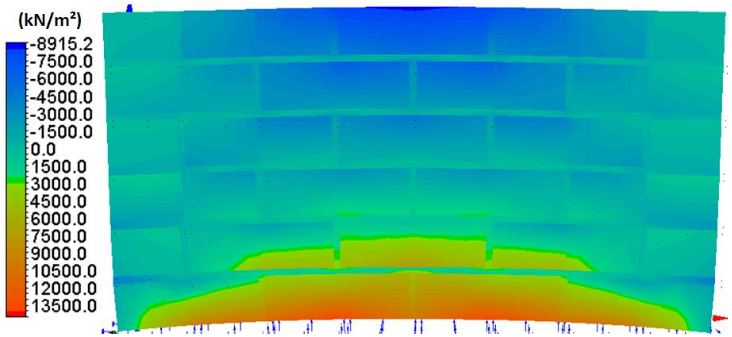	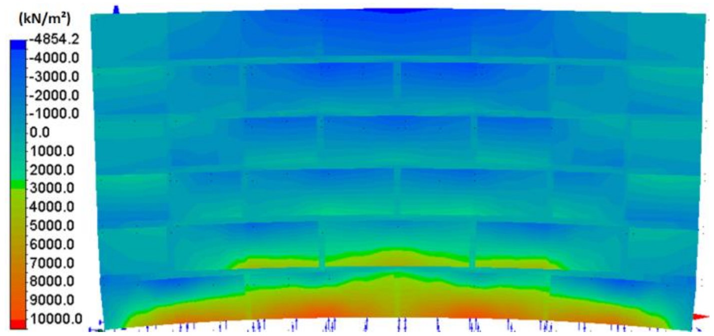
Finite element wall panel with mesh refinement 3	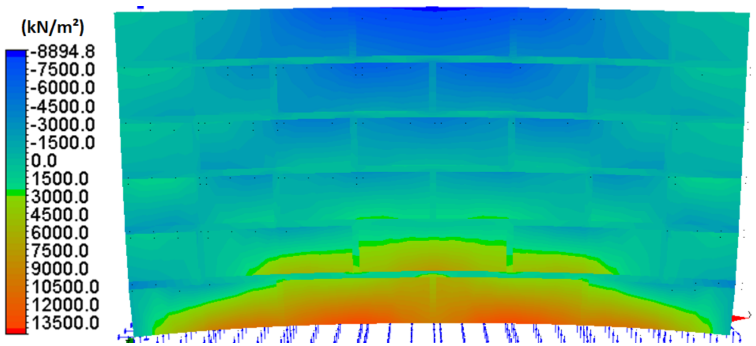	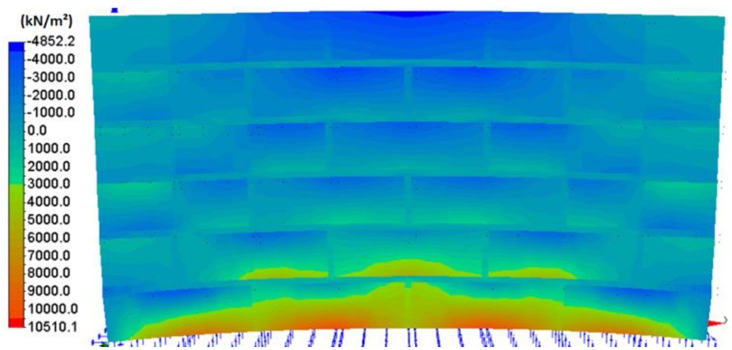

<table>
<tr><th>Model Name</th><th>SANS no-lime mortar material properties</th><th>ASTM K mortar material properties</th></tr>
<tr><td>Finite element wall panel with mesh refinement 4</td><td>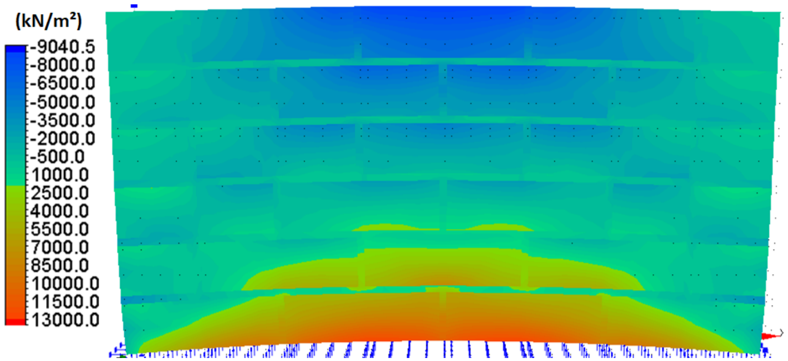
</td><td>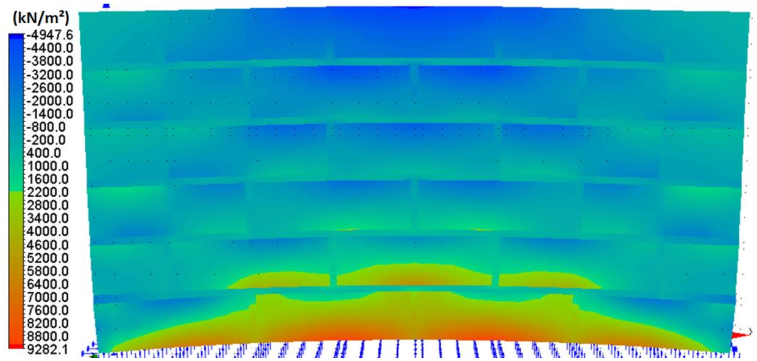
</td></tr>
<tr><td>Finite element wall panel with mesh refinement 5</td><td>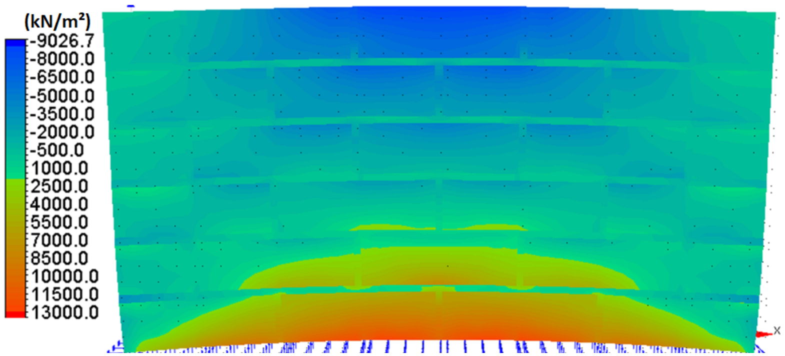
</td><td>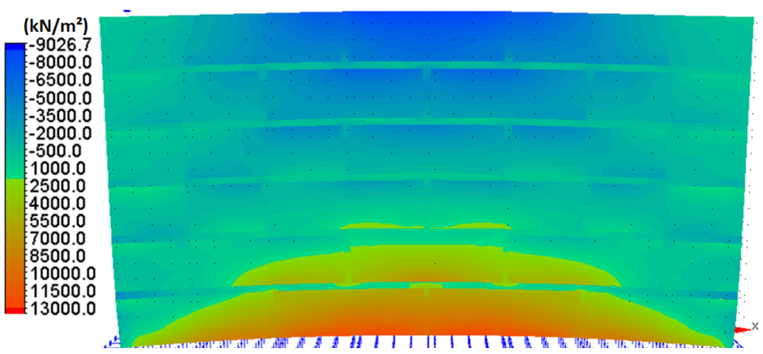
</td></tr>
</table>

5.4.2 6 × 8 Finite element wall panel

In the 6 × 8 finite element wall panel and first mesh refinement, the maximum tensile stress was in the central area of the top row of brick solid elements. The maximum compressive stress was in the bottom row of brick solid elements. The overall stress ranged from a maximum compressive stress of 8 MPa to a maximum tensile stress in proximity of 7 MPa. The difference in stress between the brick and mortar solid elements is highly visible throughout the entire wall panel. In the wall panel with the ASTM mortar material properties, the stresses were half those found in the SANS wall panel. The overall stress in the wall panel is much lower and the difference in stresses between the brick and mortar solid elements is visible throughout the entire wall panel.

In the wall panel with the second mesh refinement and SANS mortar material properties, the location of the maximum tensile and compressive stresses was similar to that of the first mesh refinement. The maximum tensile stress in the brick solid elements of the second refinement was also similar to that of the first refinement. The compressive stresses differed by just over 0.1 MPa from the first mesh refinement. In the finite element wall panel with the second mesh refinement and ASTM mortar material properties, the maximum tensile stress was in the same range as the tensile stress in the first refinement. The maximum compressive stress in the second refinement differed from that of the first refinement.

In the finite element wall panel with the third refinement, the stresses were identical to those of the second refinement. Little difference in stress in the finite element wall panels was found between the two refinements. Similar stresses were found in the finite element wall panels with the fourth and fifth refinements. The overall magnitude of tensile and compressive stress in these two refinements differed from the first, second and third refinements.

The overall stress in all the 6 × 8 finite element wall panels was markedly lower compared to those in the 4 × 6 finite element wall panels. This is to be expected because the 1mm deflection was applied over a shorter distance, so the deflection per unit wall length was higher. In this analysis, the size of the finite element wall panels had an effect on the magnitude of stress found in each wall panel. In both the 4 × 6 and 6 × 8 finite element wall panels, there were significant similarities between certain refinements. However, the wall panels with the fourth and fifth refinements showed the most consistent results. Table 5.6 shows the performance of the 6 × 8 finite element wall panels with different mortar material properties:

Table 5.6: Performance of the 6 × 8 finite element wall panel with different mortar material properties

Model Name	SANS no-lime mortar material properties	ASTM K mortar material properties
6 × 8 finite element wall panel with mesh refinement 1	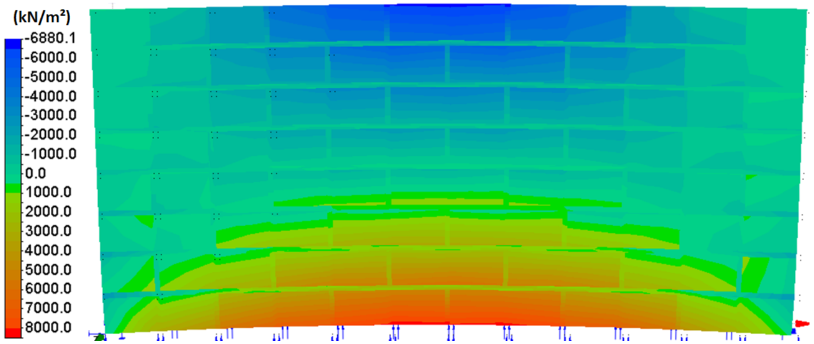	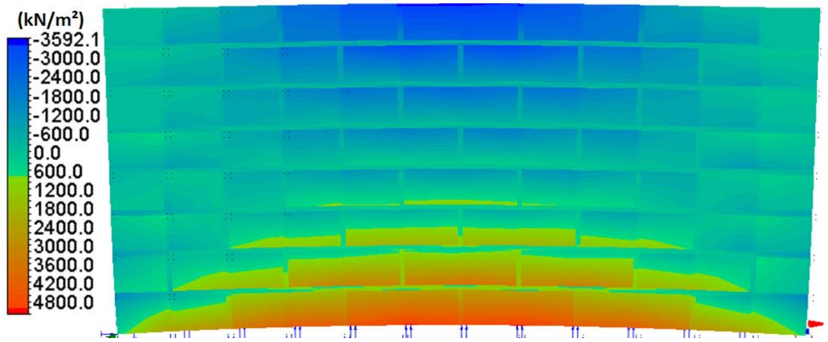
6 × 8 finite element wall panel with mesh refinement 2	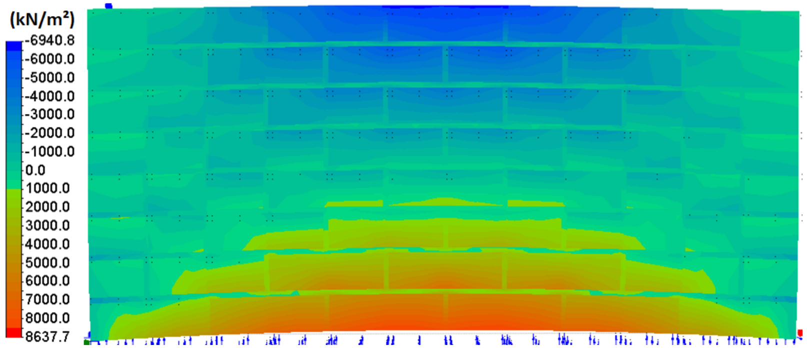	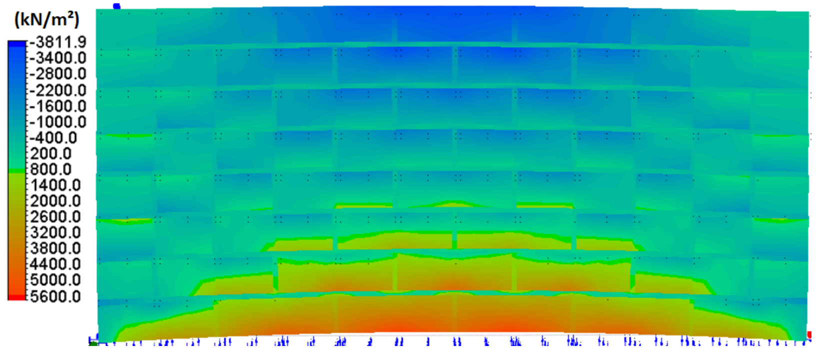

<table>
<tr><th>Model Name</th><th>SANS no-lime mortar material properties</th><th>ASTM K mortar material properties</th></tr>
<tr><td>6 × 8 finite element wall panel with mesh refinement 3</td><td>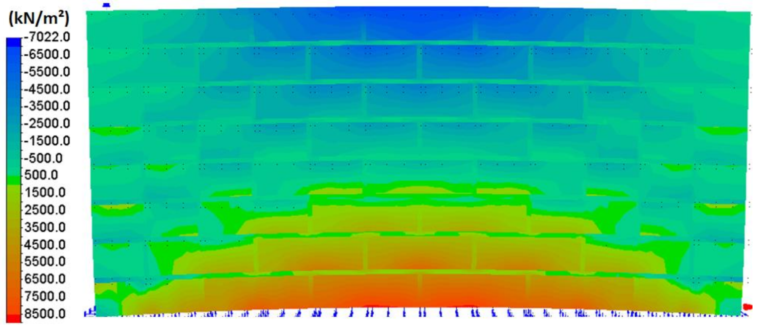</td><td>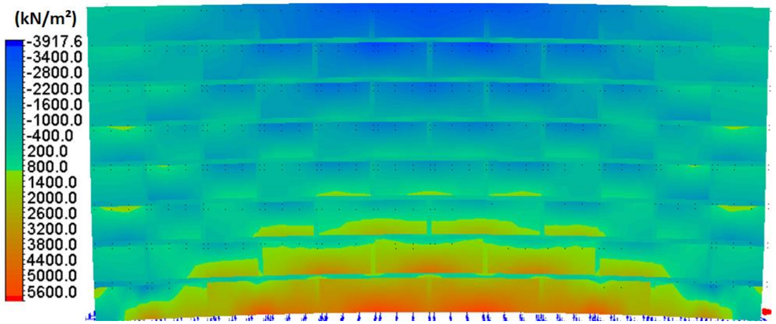</td></tr>
<tr><td>6 × 8 finite element wall panel with mesh refinement 4</td><td>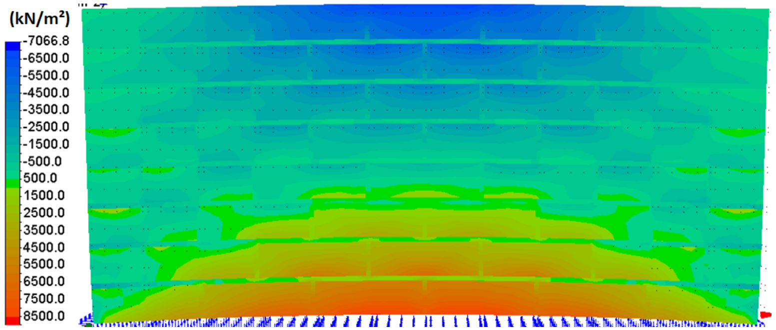</td><td>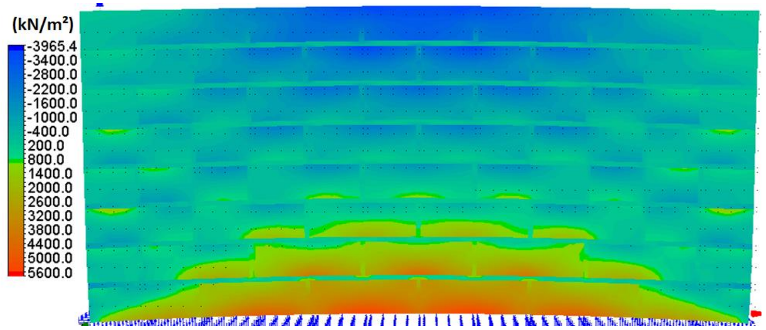</td></tr>
<tr><td>6 × 8 finite element wall panel with mesh refinement 5</td><td>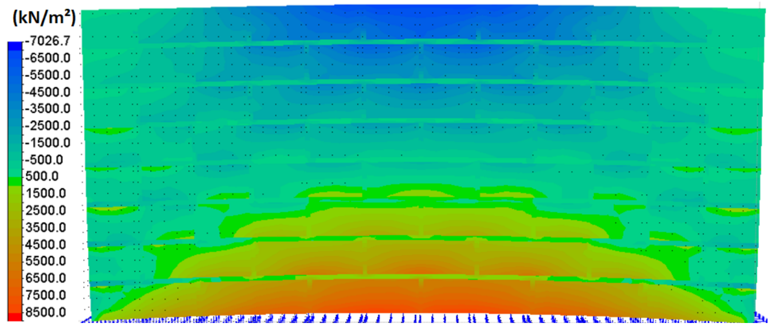</td><td>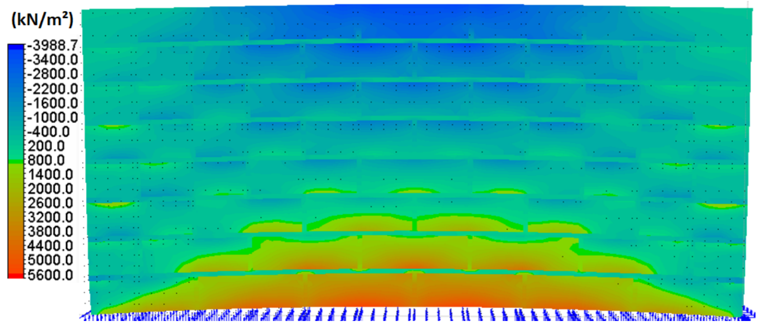</td></tr>
</table>

5.5 Analysis 3: Performance of material properties using selected finite element wall panel

In the third analysis, the performance of the material properties of a standard cement brick and four types of different mortar mixes was analysed. A selected finite element wall panel with dimensions of 8 × 10 was used in this analysis. This selected wall panel had the same dimensions as the physical experimental wall panel of 8 × 10 bricks where eight bricks were placed horizontally, ten courses high. For the finite element wall panel to truly reflect the performance of the material properties of the standard cement brick and different mortar solid elements, the same parameters as applied to the physical wall panel were applied to the finite element wall panel. In the 8 × 10 finite element wall panel, the support conditions had to be completely different to the panels analysed above since the above tests were intended to simulate performance on a soil dome with the self-weight of a wall panel being sufficient to restrain the wall from lifting. However, with current conditions and apparatus availability, the walls required different restraining conditions to still simulate the wall pressing down and resisting from lifting when deformation is applied. The four corners were restrained, leading to a very different stress pattern. A deformation of 1 mm was applied to the central brick and mortar solid elements in the bottom row. The performance of the 8 × 10 finite element wall panel was first analysed using the five refinements.

5.5.1 8 × 10 Finite element wall panel

The performance of the standard cement brick and two different mortar mix material properties was analysed in the 8 × 10 finite element wall panel. The material properties of the SANS no-lime mortar mix and ASTM Type K mortar mix were used in this analysis. In the 8 × 10 finite element wall panel with the first refinement and SANS no-lime mortar material properties, the maximum tensile stress was located in the central area of the top row of brick and mortar solid elements. Because the wall panel was now restrained from movement at the two top corners, maximum compressive stress was located at these two corners as well as in the central area of the brick and mortar solid elements in the bottom row. A maximum tensile stress of approximately 4.5 MPa was found as well as a maximum compressive stress of

14.5 MPa. In the 8 × 10 finite element wall panel with the first refinement and ASTM Type K mortar material properties, the amount of tensile stress and compressive stress was half the stress found in the SANS no-lime wall panel. The area where the maximum tensile and compressive stress was located was similar to that of the SANS no-lime wall panel. For the 8 × 10 finite element wall panel and second refinement, the overall stress in the wall panel was a little higher compared to the first refinement. The stress difference between the SANS no-lime and ASTM Type K for the second refinement followed the same trend where the ASTM Type K mortar material properties resulted in stress levels of almost half the amount as in the wall panel with the SANS no-lime mortar material properties. This pattern was followed in the wall panel with the third refinement as well.

However, the three wall panels with three different refinements all had different stress levels and were not consistent. In the 8 × 10 finite element wall panel and fourth refinement, the location of the maximum tensile and compressive stresses was the same as in the previous refinements. The magnitude of the tensile and compressive stress in the fourth refinement wall panel ranged from 4.5 MPa to 22 MPa for the SANS no-lime mortar material properties. The wall panel with the ASTM Type K mortar material properties and fourth refinement ranged from 2.5 MPa to 15 MPa. The range in stresses was similar to those found in the wall panel with the fifth refinement. This showed that the stresses in the wall panel with the fourth and fifth refinement were reasonably consistent. The range of stresses between the other refinements was not consistent and the stresses indicated that these refinement levels were inadequate. Table 5.7 shows the performance of the 8 × 10 finite element wall panel with two different mortar material properties:

Table 5.7: Performance of the 8 × 10 finite element wall panel with two different mortar material properties

Model Name	SANS no-lime mortar material properties	ASTM K mortar material properties
8 × 10 finite element wall panel with mesh refinement 1	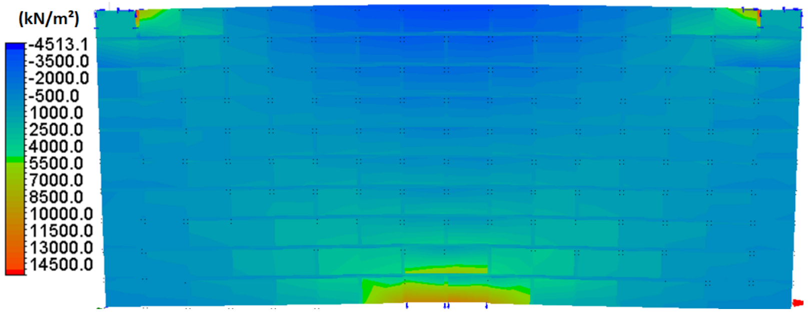	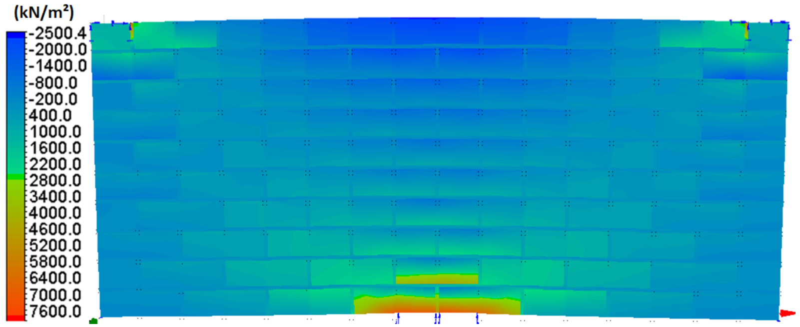
8 × 10 finite element wall panel with mesh refinement 2	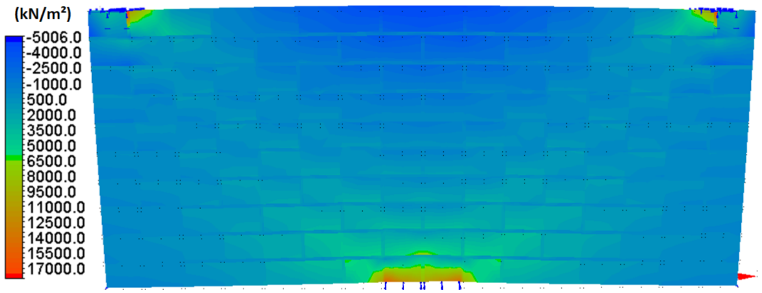	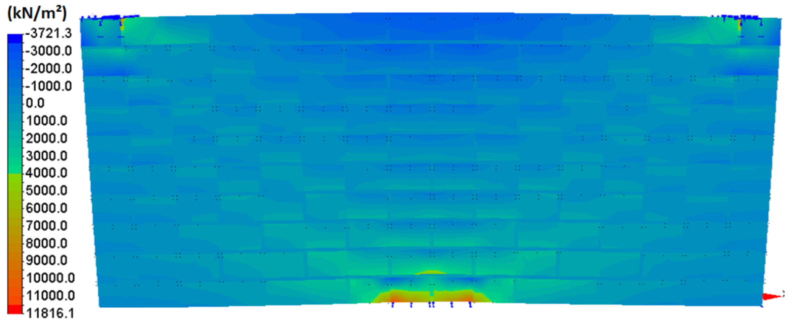
8 × 10 finite element wall panel with mesh refinement 3	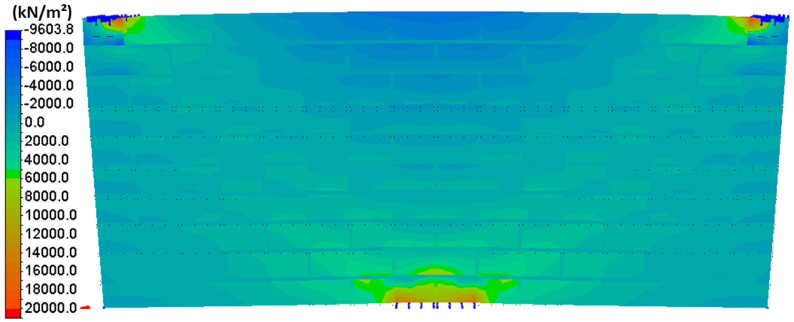	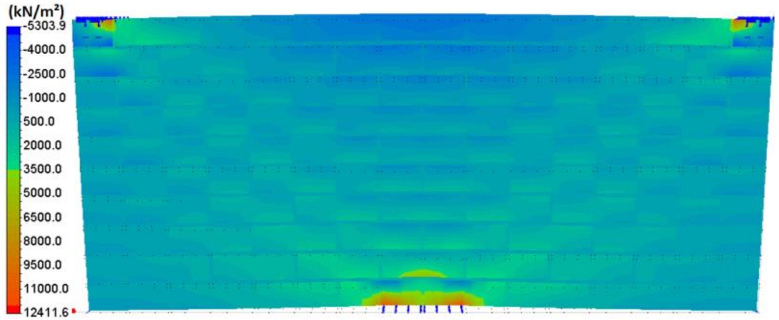

Model Name	SANS no-lime mortar material properties	ASTM K mortar material properties
8 × 10 finite element wall panel with mesh refinement 4	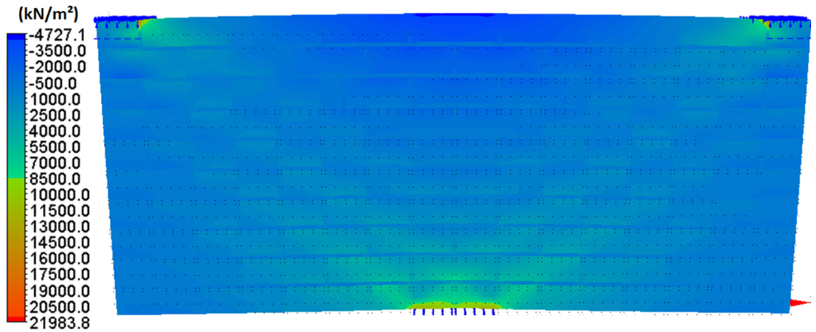	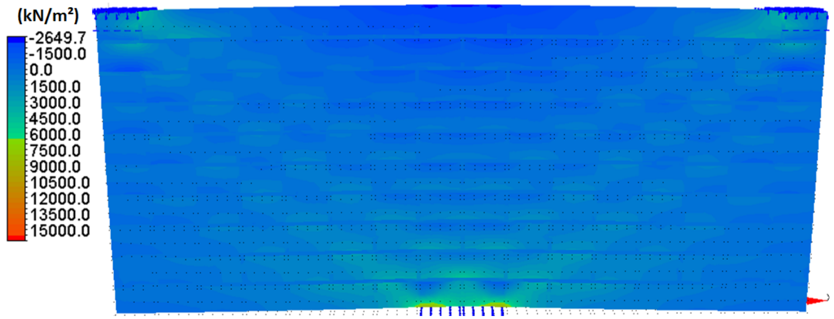
8 × 10 finite element wall panel with mesh refinement 5	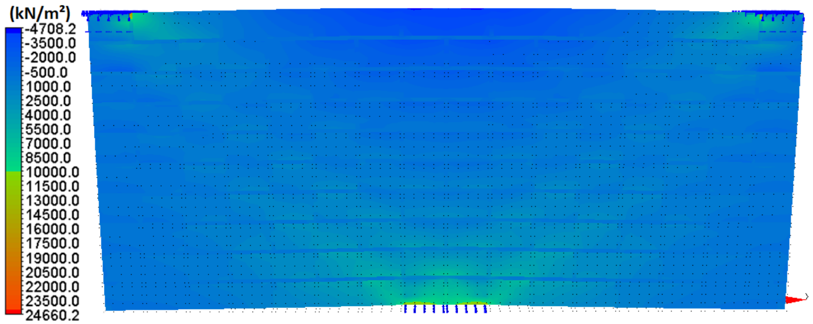	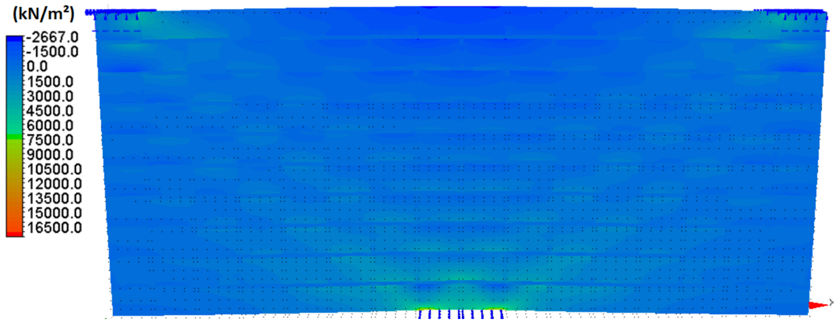

5.5.2 Performance of Costigan's mortar material properties

Two different mortar mixes were sourced from a study conducted by Costigan et al. in 2015. (Costigan, Pavía, and Kinnane, (2015b) performed a study in which they investigated the mechanical behaviour of lime-mortar masonry under applied compressive forces. There were two mortar compositions, namely the M6 (cement-mortar) mortar mix and the CL90 (lime-mortar) mortar mix. The M6 mortar mix consisted of one part cement, half part building lime and four parts sand, while the CL90 mortar mix consisted of only one part hydrated lime and three parts sand with no cement.

Each of the two different mortar mix material properties was used in the 8 × 10 finite element wall panel with fifth refinement, together with the material properties of the standard cement brick. A deformation of 1 mm was applied to the central bottom brick and mortar elements. The two top corners of the finite element wall panel were restrained from movement. The performance of the two different mortar mixes was analysed and compared using the minimum and maximum stress in each finite element wall panel, as well as the overall stress distribution.

The maximum tensile stress in the 8 × 10 finite element wall panel with the M6 (cement-mortar) mortar material properties was in the top central brick solid elements. The magnitude of the tensile stress in this wall panel was just passing 3.5 MPa and the maximum compressive stress at 21 MPa. The maximum compressive stress was located in the two top corners of the wall panel and the central area of the bottom row of brick and mortar solid elements. In the CL90 (lime-mortar) mortar material properties, the overall compressive stress in the wall panel was approximately half that of the M6 wall panel. The tensile stress in CL90 wall panel was similar to the tensile stress in the M6. Overall, the magnitude of stress in the CL90 was much lower as this mortar mix contained no cement and only hydrated lime and sand. The M6 mortar contained cement with little hydraulic lime and sand. Table 5.8 shows the performance of the M6 and CL90 mortar mixes in the 8 × 10 finite element wall panel and fifth refinement:

Table 5.8: Performance of the M6 and CL90 mortar mixes and standard cement brick material properties in the 8 × 10 finite element wall panel and fifth refinement

Mortar mix	View of performance of material properties (kPa)
M6 (1:0.5:4)	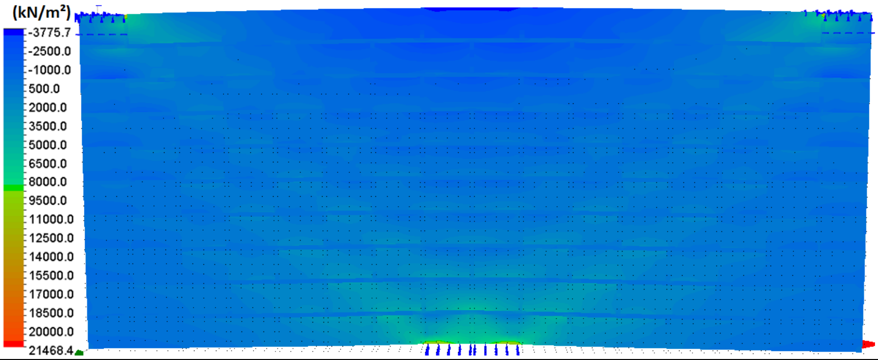
CL90 (0:1:3)	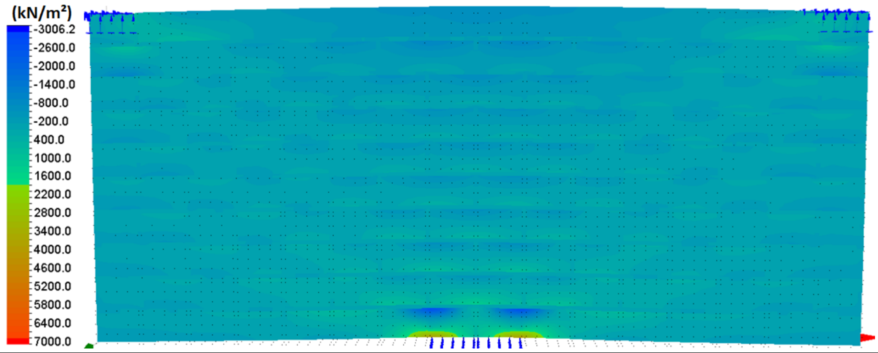

5.6 Conclusion

After conducting the analysis on the finite element wall panels designed using the five refinements, one refinement was selected that would potentially determine the most consistent stress analysis pattern found in a masonry wall panel. After applying the 1 mm deformation to each finite element wall panel, it was clearly visible that the finite element wall panel with the higher strength mortar having a higher Young's modulus value showed higher stresses for a given deformation compared to the wall panels with the weaker mortar having lower Young's modulus with much lower stress. This compares well with the behaviour of the experimental walls, where the walls made with low Young's modulus mortar absorbed more deformation and experienced less stress per unit of distortion with higher flexibility. This gives some level of confidence that the effect of heaving soil could be modelled using the Prokon software package as a tool to predict probable responses to different mortar mixes.

CHAPTER 6: DISCUSSION AND CONCLUSION

6.1 Introduction

Masonry remains one of the most widespread structural material types used particularly for the construction of light masonry structures. Because many light masonry constructions are for residences and for small commercial enterprises, they must comply with the specific safety regulatory standards of the South African Bureau of Standards (SABS). In the ever-changing living and business world, new technologies are constantly being developed, leading to new approaches to masonry material choices. Therefore, the introduction of new materials and material combinations needs to be tested prior to their use in construction to ensure the minimum safety limits. However, the performance of physical experiments and tests is time consuming, labour intensive and may be prohibitively expensive (Abdulla et al., 2017; Bui et al., 2017; Rodič, 2017). This study was thus undertaken to ascertain whether a finite element model could be employed to assist in the analysis of choice of materials, according to the SANS 10164-1, for an unreinforced light masonry structure constructed on heaving clay. Therefore, a series of finite element mesh refinement models was designed in the finite element analysis computer package, Prokon, developed in South Africa by Eschberger and Pienaar in 1989. These models were then assessed using a set of parameters to ascertain which mesh refinement model would be most adequate in interpreting the performance of various brick and mortar material properties.

Although the employment of new technological developments in the simulation of physical experiments has only recently received attention, some studies have provided new insights to the body of knowledge in simulating physical experiments. Also under consideration are the physical experiments conducted on masonry walls or wallettes to determine the maximum compression and maximum shear of those walls. andMiccoli, Garofano, Fontana, & Müller, (2015) conducted a study whereby a finite element model was designed to determine the maximum compressive strength of a wall panel until failure occurred. Another example of a study conducted to determine the maximum compressive strength of a brick prism was performed by (Yang et al., 2019).

Physical experiments to determine the shear strength of masonry included physical experiments conducted on masonry triplets using the bond wrench test (S. Sharma et al., 2021). Borri, Castori, and Corradi, (2012) also conducted various shear strength tests on physical masonry wall panels using the diagonal compression test and by applying inductive transducers to a wall panel to exercise shear strength on a wall panel. All the analyses and procedures performed in previous works focus on the strength characteristics of masonry walls. Strength is rarely a limiting factor for small light masonry structures for example single-storey houses in South Africa. These single-storey houses typically fail because of applied deformation caused by heaving clay and not because of applied loading from the roof.

6.2 Major Findings of this Study

In this study the focus is on the response to applied deformation, rather than the response to loads. The aim is to gain insight into how to cope with deformation applied to small light masonry structures caused by heaving clays. The experiments conducted on the five different mortar mixes showed that as the strength of the mortar increased, the Young's modulus increased as well. This was visible in the cases whereas the strength of the mortar decreased, the Young's modulus also decreased. The higher Young's modulus impacted the flexibility of a physical wall panel when it was subjected to deformation. The SANS no-lime mortar mix had the highest Young's modulus, which resulted in the wall panel failing at an applied deformation of only 0.35 mm. The ASTM Type K mortar had the lowest Young's modulus and highest content of lime, resulting in a wall panel that could withstand a deformation of up to 1.15 mm before failure occurred. This shows that as the lime content in a mortar mix increases, the flexibility coefficient increases as well, resulting in a mortar with higher flexibility. In the 8 × 10 finite element wall panel analysis, the material properties of the two mortar mixes with the highest and lowest Young's modulus were analysed. In this analysis, the SANS no-lime mortar mix had a high Young's modulus and was shown to have the highest stress pattern visible in the finite element wall panel. The material properties of the ASTM Type K with the low Young's modulus were also applied and showed a remarkably lower stress pattern in the finite element wall panel. This difference in stress between the SANS no-lime and the ASTM Type K was also visible in the 4 × 6 and the 6 × 8 finite element wall panels.

6.3 Concluding Remarks

In this study, a finite element model was successfully designed in the Prokon software package as a method for analysing the performance of masonry material properties in experimental wall panels subjected to soil deformation. Although the study was conducted on a limited number of different mortar mixes and one brick type, the outcome firstly showed an increasing flexibility pattern. This pattern indicated that the lower the lime and sand content in a mortar mix, the more rigid and linear the masonry with little to no flexibility. The higher the lime and sand content in a mortar mix, the higher the flexibility and more non-linear the behaviour of the materials. The higher flexibility potential in wall panels, the higher the potential of the masonry to accommodate deformation caused by expansive clays. Secondly, the finite element wall panel designed using the fifth mesh refinement had reasonable consistency, suggesting probable adequacy of the refinement.

The selected mesh refinement could potentially determine the response of the materials used in masonry construction when applied to various soil deformations and should be further investigated. This model also pointed out the issue of material choices in masonry construction. Masonry subjected to soil deformation needs to be flexible enough to absorb the maximum deformation before failing. Premature failure of a masonry structure on expansive soil will occur if the mortar is of a higher strength as indicated. A lower strength mortar could potentially have a higher flexibility coefficient and absorb considerably more deformation of the heaving soil before failure would occur.

In the future, the expense of constructing full size masonry wall panels, as well as the size of constructing a single storey masonry building, propose if the modelling of small-scale physical models would be best. The results of this study give confidence perceiving to larger models.

REFERENCES

A & E Television Networks. (2019). *The Colosseum : A Grand Amphitheatre*. [Internet]. National Geographic. New York. Available from: https://www.history.com/author/history. [Accessed: 07 December 2020]

Abdulla, K. F., Cunningham, L. S., & Gillie, M. (2017). Simulating masonry wall behaviour using a simplified micro-model approach. *Engineering Structures*, *151*(August), 349–365.

AEM. (2018). *Applied Element Method*. [Internet]. AEM. Available from: https://www.appliedelementmethod.org. [Accessed: 04 March 2021]

Agarwal, D. M., Basutkar, S. M., Madhavi, K., Devi, M. V. R., & Jagadish, K. S. (2021). Influence of surface reinforcement on the strength of brick masonry wall. *Materials Today: Proceedings*, *46*(10), 5112–5117.

Aguilar, R., Noel, M. F., & Ramos, L. F. (2019). Integration of reverse engineering and non-linear numerical analysis for the seismic assessment of historical adobe buildings. *Automation in Construction*, *98*(November 2018), 1–15.

Ahmed, A., & Shahzada, K. (2020). Seismic vulnerability assessment of confined masonry structures by macro-modeling approach. *Structures*, *27*(June), 639–649.

Al-Hadhrami, L. M., & Ahmad, A. (2009). Assessment of thermal performance of different types of masonry bricks used in Saudi Arabia. *Applied Thermal Engineering*, *29*(June), 1123–1130.

Alonso-Santurde, R., Coz, A., Viguri, J. R., & Andrés, A. (2012). Recycling of foundry by-products in the ceramic industry: Green and core sand in clay bricks. *Construction and Building Materials*, *27*(August), 97–106.

Andreotti, G., Graziotti, F., & Magenes, G. (2019). Expansion of mortar joints in direct shear tests of masonry samples: implications on shear strength and experimental characterization of dilatancy. *Materials and Structures/Materiaux et Constructions*, *52*(4), 1–22.

Aneke, I., Hassan, M., & Moubarak, A. (2019). Shear strength behavior of stabilized unsaturated expansive subgrade soils for highway backfill. In: eds. *Bituminous Mixtures and Pavements VII- Proceedings of the 7th International*

Conference on Bituminous Mixtures and Pavements, ICONFBMP 2019, *June*, 111–122.

ANSYS. (1970). *ANSYS*. ANSYS.

Apostolaki, C., Agioutantis, Z., Perdikatsis, V., & Markopoulos, T. (2009). Preliminary investigation of the in-plane shear behaviour of masonry structures. *3rd AMIREG International Conference*, *September*, 6–10.

Association of Australia. (2001). Bond strength in masonry construction. In *Cement and Concrete* (Vol. 65, Issue May).

Asteris, P. G., & Tzamtzis, A. D. (2015). Non-linear analysis of masonry shear walls. *Proceedings of the Sixth International Masonry Conference*, *October*, 1–6.

ASTM C1825-19. (n.d.). *Standard guide for developing specifications for masonry units*. ASTM International.

Australian Standards: BD-004. (2020). Masonry Structures. In *Australian Standards*.

Bergami, A. V, & Nuti, C. (2015). Compression tests on masonry walls realized with a single or double masonry panel. *Journal of Civil Engineering and Architecture Research*, *2*(July), 802–809.

Bester, D. (2017). The Determination of Moisture Variation Patterns in Clay Soils Under a Light Structure House. Published M. Eng., Civil Engineering, Central University of Technology, Bloemfontein, South Africa.

Binici, H., Aksogan, O., & Shah, T. (2005). Investigation of fibre reinforced mud brick as a building material. *Construction and Building Materials*, *19*(July), 313–318.

Borri, A., Castori, G., & Corradi, M. (2012). Evaluation of shear strength of masonry panels through different experimental analyses. *14th Structural Faults and Repair*, *July* 1–13.

Brick Industry Association. (2006). Technical notes on brick construction: Manufacturing of Brick. [Internet]. Brick Industry Association, Reston, Virginia. Available from: https://www.gobrick.com/docs/default-source/read-research-documents/technicalnotes/9-manufacturing-of-brick.pdf?sfvrsn=0. (Accessed: 03 March 2020]

Bui, T. T., Limam, A., & Sarhosis, V. (2019). Failure analysis of masonry wall panels subjected to in-plane and out-of-plane loading using the discrete element method. *European Journal of Environmental and Civil Engineering*, *10*(November), 1–17.

Bui, T. T., Limam, A., Sarhosis, V., & Hjiaj, M. (2017). Discrete element modelling of the in-plane and out-of-plane behaviour of dry-joint masonry wall constructions. *Engineering Structures*, *136*, 277–294.

Building Solutions. (2015). *Masonry Past, Present, and Future Early Masonry was the Ultimate Green Design Masonry Today: An Industry in Evolution*. [Internet]. CRH Americas Inc. Available from: https://www.buildingsolutions.com/industry-insights/masonry-past-present-and-future. [Accessed: 05 March 2020]

Cartwright, M. (2018). *Colosseum*. Ancient History Encyclopedia. https://www.ancient.eu/Colosseum/

Case, J., Chilver, L., & Ross, C. T. F. (1964). *Strength of Materials and Structures* (Fourth). John Wiley & Sons Inc.

Cervenka Consulting. (n.d.). *ATENA* (5.7). Cervenka Consulting.

CIDB. (2007). *The building and construction materials sector, challenges, and opportunities*.

Colefield, N. (2018). *History of Brick Masonry*. [Internet]. Sullivan Engineering. Available from: https://sullivanengineeringllc.com/2018/02/28/history-brick-masonry/. [Accessed: 16 February 2021]

Costigan, A., PavÃa, S., & Mazzolani, F. M. (2009). Compressive, flexural and bond strength of brick/lime mortar masonry. *Proceedings of PROHITEC 09*, *1993*, 1609–1615.

Costigan, A., Pavía, S., & Kinnane, O. (2015a). An experimental evaluation of prediction models for the mechanical behavior of unreinforced, lime-mortar masonry under compression. *Journal of Building Engineering*, *4*(October), 283–294.

Costigan, A., Pavía, S., & Kinnane, O. (2015b). An experimental evaluation of prediction models for the mechanical behavior of unreinforced, lime-mortar masonry under compression. *Journal of Building Engineering*, *4*, 283–294.

Crofts, F. S., & Lane, J. W. (2000). Masonry for low cost housing in South Africa. *9th Canadian Masonry Symposium*.

Cuffari, B. (2019). *The applications of mortar in construction* (pp. 1–3).

Dassault Systems. (2013). *Abaqus Unified FEA* (p. 1).

De Villiers, W., Boshoff, W. P., & Fourie, J. (2019). *Numerical modelling of alternative masonry units*. *November*.

Del Zoppo, M., Di Ludovico, M., Balsamo, A., & Prota, A. (2020). Diagonal compression testing of masonry panels with irregular texture strengthened with inorganic composites. *Materials and Structures/Materiaux et Constructions*, *53*(4), 1–17.

Demir, I., Baspinar, M. S., & Orhan, M. (2005). Utilization of kraft pulp production residues in clay brick production. *Building and Environment*, *40*(November), 1533–1537.

DIANA FEA BV. (2003). *DIANA FEA*.

Dinesh, M. R., Singh, V. P., Begum, M. S., Kenneth, F. H. T., Jairaj, V., & Khalid, K. (2015). Construction of a three-dimensional finite element model of maxillary first molar and it's supporting structures. *Journal of Pharmacy and Bioallied Sciences*, *7*(August), S443–S450.

Dizhur, D., Jiang, X., Chengliang, Q., Almesfer, N., & Ingham, J. (2015). Historical development and observed earthquake performance of unreinforced clay brick masonry cavity-walls. *Structural Engineering Society Journal - SESOC*, *28*(January), 55–67.

Domaneschi, M., Pellecchia, C., De Iuliis, E., Cimellaro, G., Morgese, M., Khalil, A., & Ansari, F. (2020). Collapse analysis of the Polcevera viaduct by the applied element method. *Engineering Structures*, *214*(April), 110659.

Drougkas, A., Roca, P., & Molins, C. (2015). Numerical prediction of the behaviour, strength, and elasticity of masonry in compression. *Engineering Structures*, *90*(February), 15–28.

Encyclopaedia Britannica. (1998). History of Masonry Construction. [Internet]. Britannica. Available from: https://www.britannica.com/technology/masonry. [Accessed: 05 March 2020]

Encyclopaedia Britannica. (1998). MASONRY. [Internet]. Britannica. Available from: https://www.britannica.com/technology/masonry. [Accessed: 05 March 2020]

Eschberger, K., & Pienaar, J. (1989). *Prokon structural analysis & design*. Prokon.

Eslami, A., Ronagh, H. R., Mahini, S. S., & Morshed, R. (2012). Experimental investigation and nonlinear FE analysis of historical masonry buildings - A case study. *Construction and Building Materials*, *35*(October), 251–260.

European Union. (2011). *Eurocode 6 - Design of masonry structures - Part 1-1: General rules of reinforced and unreinforced masonry structures* (Vol. 1, Issue 2005). European Standards.

Fix My Brick. (2018). *The history of masonry & notable masonry structures – Part 1*. [Internet]. Fix My Brick. Available from: https://fixmybrick.ca/the-history-of-masonry-notable-masonry-structures-part-1/. [Accessed: 16 February 2021]

Gabor, A., Ferrier, E., Jacquelin, E., & Hamelin, P. (2006). Analysis and modelling of the in-plane shear behaviour of hollow brick masonry panels. *Construction and Building Materials*, *20*(July), 308–321.

Geyer, P. (2012). Systems modelling for sustainable building design. *Advanced Engineering Informatics*, *26*(June), 656–668.

Gohel, V., Patel, P. V, & Joshi, D. (2013). Analysis of Frame using Applied Element Method (AEM). *Procedia Engineering*, *51*(NUiCONE 2012), 176–183.

Goossens, P. (2017). *Industry 4.0 and the power of the Digital Twin*. Maple Soft.

Gumaste, K. S., Nanjunda Rao, K. S., Venkatarama Reddy, B. v, & Jagadish, K. S. (2007). Strength and elasticity of brick masonry prisms and wallettes under compression. *Materials and Structures/Materiaux et Constructions*, *40*(July), 241–253.

Gupta, M. (2018). *Everything about mortar in construction*. [Internet]. Go Smart Bricks. Available from: http://gosmartbricks.com/everything-about-mortar-in-construction/. [Accessed: 17 February 2021].

Hallissey, T. (2018). *The history of masonry construction in 3 minutes or Less*. [Internet]. ContractorsInsurance.Org. Available from: https://contractorsinsurance.org/masonry-construction/. [Accessed 17 February 2021].

Hamer, K., & Karius, V. (2002). Brick production with dredged harbour sediments. An industrial-scale experiment. *Waste Management*, *22*(July), 521–530.

Haseltine, B. (2012). the Evolution of the design and construction of masonry buildings in the Uk. *Gestão & Tecnologia de Projetos*, *7*(November), 20–26.

Hendry, E. A. W. (2001). Masonry walls: Materials and construction. *Construction and Building Materials*, *15*(June), 323–330.

Hernández-Zaragoza, J. B., López-Lara, T., Horta-Rangel, J., López-Cajún, C., Rojas-González, E., García-Rodríguez, F. J., & Adue, J. (2013). Cellular concrete bricks with recycled expanded polystyrene aggregate. *Advances in Materials Science and Engineering*, *2013*(December), 1–5.

Kadir, A. A., Mohajerani, A., Roddick, F., & Buckeridge, J. (2009). Density, Strength , Thermal Conductivity and Leachate Characteristics of Light-Weight Fired Clay Bricks Incorporating Cigarette Butts. *International Journal of Materials and Metallurgical Engineering*, *3*(5), 1035–1040.

Kunal, S. R. (2016). Utilization of industrial by-products and natural ashes in mortar and concrete: development of sustainable construction materials. In K. A. Harries & B. Sharma (Eds.), *Nonconventional and Venacular Construction Materials* (2nd ed., pp. 159–196). Elsevier Science & Technology.

Kunal, S. R., & Rajor, A. (2012). Use of cement kiln dust in cement concrete and its leachate characteristics. *Recources, Conservation and Recycling*, *61*(January), 59–68.

Lakshani, M. M. T., Jayathilaka, T. K. G. A., & Thamboo, J. A. (2020). Experimental investigation of the unconfined compressive strength characteristics of masonry mortars. *Journal of Building Engineering*, *32*(April), 101558.

Lancaster LimeWorks. (2020). *Very Brief Overview of Mortars and Mortar History*. Lancaster LimeWorks. https://www.lancasterlimeworks.com/about-us/brief-history-of-mortar-and-mortars/

Lawrence, S. J., Sugo, H. O., & Page, A. W. (2008). Masonry bond strength and the effects of supplementary cementitious materials. *Australian Journal of Structural Engineers*, *8*(2), 101–115.

London Damp Company. (2018). *The Cavity Wall: A Brief History*. [Internet]. London Damp Company. Available from:

https://www.londondampcompany.co.uk/the-cavity-wall-a-brief-history/. [Accessed: 17 February 2021].

Lotfy, E. M., Mohamadien, H. A., & Hassan, H. M. (2015). Flexural and Shear Strength of Reinforced Perforated Clay Brick Masonry Members. *International Journal of Engineering and Technical Research*, *3*(January), 81–84.

Lourenço, P. B. (1998). Experimental and numerical issues in the modelling of the mechanical behaviour of masonry. *Structural Analysis of Historical Constructions II*, *January*, 57–91.

LS-DYNA. (n.d.). *LS-DYNA*. ANSYS LST.

Luo, Q., Zheng, Q., & Yu, A. (2017). From micro to macro: A comparative study of DEM and FEM in modelling hopper flow. *Proceedings of the 7th International Conference on Discrete Element Methods*, *188*, 977–985.

Maas, R. (2013). *Masonry Construction: Then and Now*. [Internet]. Mason Contractors Association of America. Available from: www.masoncontractors.org. [Accessed: 18 February 2021].

Maldonado, N. G., Martin, P., del Sol, G. G., & Domizio, M. (2016). Historic Masonry. *IntechOpen*, *Tourism*, 19.

Mark, E. (2015). *Great Wall of China*. [Internet]. Ancient History Encyclopaedia. Available from: https://www.ancient.eu/Great_Wall_of_China/. [Accessed: 18 February 2021].

Matthews, F. L., Davies, G. A. O., Hitchings, D., & Soutis, C. (2000). *Finite element modelling of composite materials and structures* (1st ed.). Woodhead Publishing Limited.

Menezes, R. R., Ferreira, H. S., Neves, G. A., Helio de Lira, L., & Ferreira, F. C. (2005). Use of granite sawing wastes in the production of ceramic bricks and tiles. *Journal of the European Ceramic Society*, *25*(July), 1149–1158.

Miccoli, L., Garofano, A., Fontana, P., & Müller, U. (2015). Experimental testing and finite element modelling of earth block masonry. *Engineering Structures*, *104*, 80–94.

Milling, A., Mwasha, A., & Martin, H. (2020). Exploring the full replacement of cement with expanded polystyrene (EPS) waste in mortars used for masonry construction. *Construction and Building Materials*, *253*(April), 119–158.

MiMeTICS Engineering. (n.d.). *LMGC90*. MiMeTics Engineering.

Mineral Economics. (2008). *Overview of South Africa'S Clay Brick Industry*.

Moayedian, S. M., & Hejazi, M. (2021). Effect of Scale on Compressive Strength of Brick Masonry with Gypsum Mortar. *Measurement*, *172*(July), 108932.

Multiphysics Cyclopaedia. (2016). *Finite element mesh refinement*. [Internet]. Multiphysics. Available from: https://www.comsol.com/multiphysics/mesh-refinement. [Accessed: 19 February 2020].

Murthi, P., Akib, M., Imran, M., Ahmed, S., & Prasanna, V. (2021). Studies on the strength variation of brick masonry using novel blended masonry mortar mixes and mortar thickness. *Materials Today: Proceedings*, *126-130*(39), 1.

Murthi, P., Bhavani, M., Musthaq, S., Jauhar, O., & Devi, V. R. (2021). Development of relationship between compressive strength of brick masonry and brick strength. *Materials Today: Proceedings*, *258-262*(39), 1.

Nalon, G. H., Santos, C. F. R., Pedroti, L. G., Ribeiro, J. C., Verissimo, G. S., & Ferreira, F. A. (2020). Strength and failure mechanisms of masonry prisms under compression, flexure and shear : Components ' mechanical properties as design constraints. *Journal of Building Engineering*, *28*(April), 101038.

Nodargi, N. A., & Bisegna, P. (2020). A unifying computational approach for the lower-bound limit analysis of systems of masonry arches and buttresses. *Engineering Structures*, *221*(June), 110999.

Oliveira, R. A., Silva, F. A. N., Sobrinho, C. W. A. P., Azevedo, A. C., Delgado, J. M. P. Q., & Guimarães, A. S. (2018). Structural performance of unreinforced masonry elements made with concrete and horizontally perforated ceramic blocks – Laboratory tests. *Construction and Building Materials*, *182*(June), 20–34.

Onion, A., Sullivan, M., & Mullen, M. (2019). Great wall of China. *Notes and Queries*, *s2-V*(121), 342–343. https://doi.org/10.1093/nq/s2-V.121.342-d

Ozer, M., Ulusay, R., & Isik, N. (2012). Evaluation of damage to light structures erected on a fill material rich in expansive soil. *Bulletin of Engineering Geology and the Environment*, *71*(1), 21–36. https://doi.org/10.1007/s10064-011-0395-2

Pachta, V., Stefanidou, M., Konopisi, S., & Papayianni, I. (2014). Technological Evolution of Historic Structural Mortars. *Journal of Civil Engineering and Architecture*, *8*(July), 846–854.

Page, A. (2012). the Evolution of the Design and Construction of Masonry Buildings in Australia. *Gestão & Tecnologia de Projetos*, *7*(December), 27–34.

Parisi, F., & Augenti, N. (2012). A Shear Response Surface for the Characterization of Unit-Mortar Interfaces. *15th International Brick and Block Masonry Conference*, *October*.

Pigeon, J. (1980). A Comparison of Existing Methods for the Design of Stiffened Raft Foundations on Expansive Soil. Council for Scientific and Industrial Research National Building Research Institute. Pidgeon, J.T., 1980. *7th Regional Conference for Africa on Soil Mechanics and Foundation Engineering*, 1980.

Pirsaheb, H., Moradi, J. M., & Milani, G. (2020). A Multi-Pier MP procedure for the non-linear analysis of in-plane loaded masonry walls. *Engineering Structures*, *212*(March), 110534.

Prakash, P. R., Azenha, M., Pereira, J. M., & Lourenço, P. B. (2020). Finite element based micro modelling of masonry walls subjected to fire exposure: Framework validation and structural implications. *Engineering Structures*, *213*(April), 110545.

Prasad, R. B. K., Nasir, O. B., & Amarnath, K. (2014). Size Effect in Brick Masonry Wallets. *International Journal of Research in Engineering and Technology*, *03*(May), 15–18.

Prokon Software Consultants. (2010). *PROKON User' s Guide* (Issue March).

Research and Markets. (2019). *South Africa clay and concrete bricks manufacturing market report 2019 with profiles of 28 companies*. [Internet]. Cision PR Newswire. Available from: https://www.prnewswire.com/news-releases/. [Accessed: 19 February 2020].

Resketi, N. A., & Toufigh, V. (2019). Enhancement of brick-mortar shear bond strength using environmental friendly mortars. *Construction and Building Materials*, *195*(November), 28–40.

Rodič, B. (2017). Industry 4.0 and the new simulation modelling paradigm. *Organizacija*, *50*(3), 193–207.

Saloustros, S., Pelà, L., Cervera, M., & Roca, P. (2017). An enhanced finite element macro-model for the realistic simulation of localized cracks in masonry structures: A large-scale application. *International Journal of Architectural Heritage*, *12*(August), 432–447.

SANS 0164: Part 1. (1980). *Unreinforced masonry walling* (p. 74).

SANS 10400. (1990). *SABS code of practice for the application of the national building regulations*. *1977*(31084), 34–35.

SANS Edu. (2019). *Numerical list of South African National Standards* (pp. 1–1219). SABS.

Shadlou, M., Ahmadi, E., & Kashani, M. M. (2020). Micromechanical modelling of mortar joints and brick-mortar interfaces in masonry Structures: A review of recent developments. *Structures*, *23*(August), 831–844.

Shakir, A. A., & Mohammed, A. A. (2013). Manufacturing of Bricks in the Past, in the Present and in the Future: A state of the Art Review. *International Journal of Advances in Applied Sciences*, *2*(September), 145–156.

Sharma, N., Telang, D., & Rath, B. (2017). A Review on Strength of Clay Brick Masonry. *International Journal for Research in Applied Science & Engineering Technology (IJRASET)*, *5*(December), 2620–2626.

Sharma, S., Graziotti, F., & Magenes, G. (2021). Torsional shear strength of unreinforced brick masonry bed joints. *Construction and Building Materials*, *275*(December), 122053.

Silva, R. V., De Brito, J., & Dhir, R. K. (2016). Performance of cementitious renderings and masonry mortars containing recycled aggregates from construction and demolition wastes. *Construction and Building Materials*, *105*(December), 400–415.

Singh, S. B., & Munjal, P. (2017). Bond strength and compressive stress-strain characteristics of brick masonry. *Journal of Building Engineering*, *9*(June), 10–16.

Staten, M. L., & J, N. L. (1997). Local refinement of three-dimensional finite element meshes. *Engineering with Computers*, 165–174.

Stats SA. (2020). *Key findings: P3041.2 - Manufacturing: Production and sales, December 2020*. [Internet]. Department: Statistics South Africa. Available from: http://www.statssa.gov.za/. [Accessed: 19 February 2020]

Stott, P. R. (2017). Identification and assessment of problematic expansive soils. Published Ph.D., Civil Engineering, *Central University of Technology*, Bloemfontein, South Africa.

Stott, P., & Theron, E. (2015). Some shortcomings in the standard South African testing procedures for assessing heaving clay. *Journal of the South African Institution of Civil Engineering*, *57*(2), 36–44.

Sugo, H. O., Page, A. W., & Moghtaderi, B. (2004). A comparative study of the thermal performance of cavity and brick veneer construction. *13th International Brick and Block Masonry Conference - IBMAC*, *January*, 767–776.

Thamboo, J. A., Dhanasekar, M., & Yan, C. (2013). Flexural and shear bond characteristics of thin layer polymer cement mortared concrete masonry. *Construction and Building Materials*, *46*(May), 104–113.

The Concrete Centre. (2010). Gypsum mortar. [Internet]. Sustainable Concrete. Available from: https://www.sustainableconcrete.org.uk. [Accessed: 05 March 2020]

Thompson, J. J. (2008). Masonry design and construction. In E. G. Nawy (Ed.), *Concrete Construction Engineering Handbook* (2nd ed., Issue January, pp. 1127–1198). Taylor & Francis.

Turner, D. P., & Paige-Green, P. (2007). The preliminary identification of problem soils for infrastructure projects. *Researchgate*, *January*.

UNESCO. (n.d.). Taj Mahal. [Internet]. World Heritage Convention. Available from: https://brill.com/view/book/edcoll/9789047444541/Bej.9789004180048.i-962_127.xml. [Accessed: 16 February 2021]

Veazey, D. (2010). *History of Masonry*. Mason Contractors Association of America.

Venkatarama Reddy, B. V, & Uday Vyas, C. V. (2008). Influence of shear bond strength on compressive strength and stress-strain characteristics of masonry. *Materials and Structures/Materiaux et Constructions*, *41*(10), 1697–1712.

Ventra, G. J. (1998). Life cycle analysis of Brick and Mortar products. In *ATHENA Sustainable Materials Institute*.

Viana, C. E., Dias, D. P., de Holanda, J. N. F., & Paranhos da Rocha, R. P. (2009). The use of submerged-arc welding flux slag as raw material for the fabrication of multiple-use mortars and bricks. *Soldagem e Inspecao*, *14*(July), 257–262.

Vorwerk, S., Cameron, D., & Keppel, G. (2015). Clay Soil in Suburban Environments: Movement and Stabilization through Vegetation. In *Ground Improvement Case Histories: Chemical, Electrokinetic, Thermal and Bioengineering Methods* (pp. 655–682).

Wahby, W. S. (2004). Ancient masonry work in Egypt, China, and Rome: a comparative study. *Proceedings of the 13th Int. Brick and Block Masonry Conference*, 1–10.

Walker, R. T., & Swinney, A. T. H. (2011). Taj Mahal. [Internet]. A & E Television Networks. Available from: https://www.history.com/topics/india/taj-mahal. [Accessed: 21 February 2020]

Watermeyer, R. (2016). Withdrawal of SANS 1200 and SANS 10120 as a South African national standard. *Civil Engineering*, *March*, 31–34.

Wu, F., Gang, L., Hong-Nan, L., & Jin-Qing, J. (2013). Strength and stress – strain characteristics of traditional adobe block and masonry. *Materials and Structures/Materiaux et Constructions*, *46*(2013), 1449–1457.

Wu, J., Bai, G. L., Zhao, H. Y., & Li, X. (2015). Mechanical and thermal tests of an innovative environment-friendly hollow block as self-insulation wall materials. *Construction and Building Materials*, *93*(June), 342–349.

Yang, K. H., Lee, Y., & Hwang, Y. H. (2019). A stress-strain model for brick prism under uniaxial compression. *Advances in Civil Engineering*, *2019*(April), 10.